Effect of Large Mountain Ranges on Atmospheric Flow Patterns as Seen from TIROS Satellites

By
E. R. Reiter, D. W. Beran, J. D. Mahlman, G. Wooldridge

Final Report
Contract Cwb-108789
With United States Department of Commerce
Weather Bureau

Project Leader: Elmar R. Reiter
Professor, Department of Atmospheric Science
Colorado State University
Fort Collins, Colorado

The Research Period Covered by the Report is
15 June 1964 to 31 August 1965

Atmospheric Science Technical Paper No. 60
September 1965

Colorado State University

Department of Atmospheric Science

Paper No. 69

Effect of Large Mountain Ranges on Atmospheric Flow Patterns as Seen from TIROS Satellites

by

E. R. Reiter, D. W. Beran, J. D. Mahlman, and G. Wooldridge

Final Report

Contract No. Cwb - 10879

with United States Department of Commerce,

Weather Bureau

Project Leader: Elmar R. Reiter
Professor, Department of Atmospheric Science
Colorado State University
Fort Collins, Colorado

The Research Period Covered by this Report is
15 June,1964 to 31 August,1965

Atmospheric Science Technical Paper No. 69
September 1965

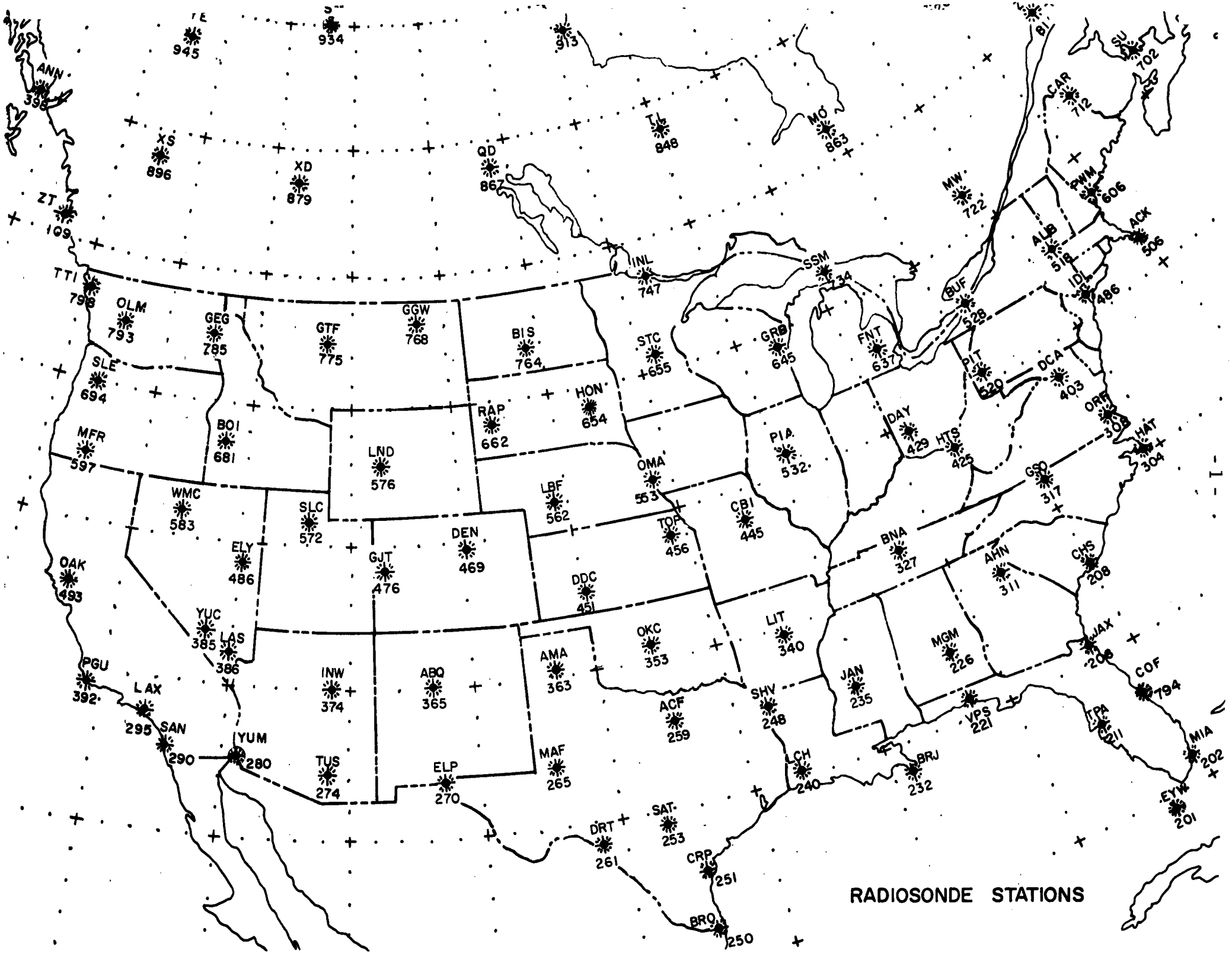
RADIOSONDE STATIONS
ANN 398
945
934
913
XS 896
XD 879
QD 867
TL 848
MO 863
BI
SU 702
CAR 712
ZT 109
TTI 798
OLM 793
GEG 785
GTF 775
GGW 768
BIS 764
INL 747
STC 655
SSM 734
MW 722
PWM 606
ACK 506
ALB 518
IDL 486
BUF 528
GRB 645
FNT 637
PIT 529
DCA 403
SLE 694
MFR 597
BOI 681
RAP 662
HON 654
LND 576
PIA 532
IDAY 429
HTS 425
ORF 308
HAT 304
OMA 553
LBF 562
WMC 583
SLC 572
DEN 469
GJT 476
TOP 456
CBI 445
GSO 317
BNA 327
AHN 311
CHS 208
ELY 486
OAK 493
DDC 451
YUC 385
LAS 386
PGU 392
LAX 295
SAN 290
YUM 280
INW 374
ABQ 365
AMA 363
OKC 353
LIT 340
MGM 226
JAX 206
COF 794
JAN 235
SHV 248
ACF 259
VPS 221
TPA 211
MIA 202
TUS 274
ELP 270
MAF 265
CH 240
BRJ 232
EYW 201
DRT 261
SAT 253
CRP 251
BRO 250

Abstract

A survey is given of case studies of TIROS cloud patterns conducted under the provisions of the present research contract with the U. S. Weather Bureau. Detailed investigations were made, or are in progress, of a chinook period in the Colorado region; of a macro- and meso-scale wave-cloud pattern over North Platte; of a baroclinic wave formation along a cold front east of the Rocky Mountains; of the association of an observed cloud band with the jet stream; of the flow pattern around a cyclone over Minnesota; and of the flow in two merging jet streams. This report contains only a summary of results. More details will be given in forthcoming project reports.

I. Introduction:

In general, atmospheric flow phenomena may be considered as consisting of a steady, mean current, upon which perturbations of a variety of scales, ranging from small-scale isotropic turbulence to large planetary waves, are superimposed. The fluctuations in atmospheric flow may be treated with the statistical tools outlined in modern turbulence theory. From such treatment we may obtain an indication as to the relative importance of various scale ranges in contributing to the energy of large and small-scale turbulence.

Measurements of atmospheric flow characteristics over a wide spectrum range do not present a major problem near the ground. Here the spectrum range is limited at high frequencies by the sensitivity of the instrument, and by the length of available record on the low-frequency end. In the free atmosphere experimental conditions are not as simple. There are no stable and stationary platforms available yet, which would allow continuous measurements of speed and temperature fluctuations. Information on the characteristics of flow in the free atmosphere, therefore, has to be pieced together from many different sources of measurement.

While statistical treatment of atmospheric flow characteristics gives valuable results in terms of average energy levels associated with atmospheric disturbances, they neither indicate the source nor the physical nature of these disturbances. The purpose of the present investigation was to explore in a preliminary way these two aspects of perturbations in atmospheric flow. Specifically the orographic influence of the Rocky Mountains was to be studied in detail. Mountain ranges have been recognized in many previous studies as an important input region where disturbances may form, ranging from clear-air turbulence (Colson, 1963) to wave-cloud formation (Harrison, 1956, 1957; Kuettner, 1959) to planetary waves (Bolin, 1950).

In exploring the physical nature of disturbances in the vicinity of this mountain region, extensive use has been made of TIROS cloud photographs. Detailed case studies--part of them still in progress--helped to establish correlations between cloud distribution as seen from TIROS and the dynamics of large and small-scale flow patterns.

In the following, an outline is given of the cases under investigation. More detailed results will be published in individual reports.

II. The Structure of Flow in the Free Atmosphere:

From 15 to 22 June,1965 the principal investigator participated in the "International Colloquium on the Fine-Scale Structure of the Atmosphere" which was held at the University of Moscow. This colloquium yielded interesting results, especially on clear-air turbulence (CAT) (Reiter and Burns, 1965; Reiter, 1965 a; Vinnichenko, Pinus, and Shur, 1965). From these investigations, together with those conducted by Kao and Woods (1964), we may arrive at the composite diagram of "turbulence" spectra in the free atmosphere shown in Fig. 1, and ranging from wave lengths of about 60 m to ca. 6000 km. The sources of information and the spectrum characteristics are identified in Table I.

It has been argued by Reiter and Burns (1965) that in the wave-length range of ca. 300 to ca. 1200 m a significant amount of energy is made available to the CAT region (roughly at wave lengths 10-200 m) by unstable gravity waves which break up into isotropic turbulence, following the Kolmogorov-Obukhov "-5/3" slope of the spectrum curve, characteristic of the inertial subrange (Spectra Nos. 2 to 4). This energy input is shown by a "hump" in the spectrum curves, whose shape strongly depends on flight direction.

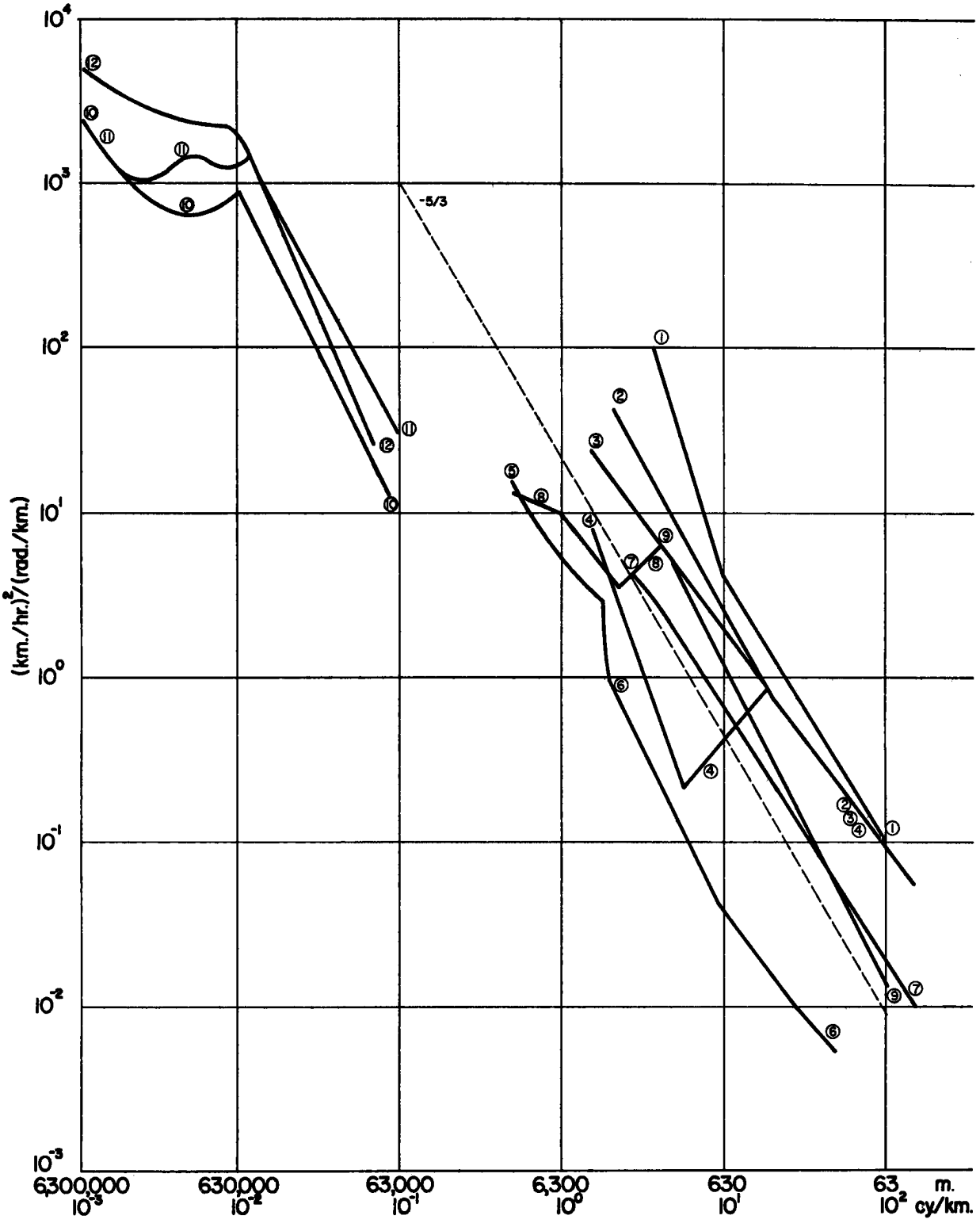

Fig. 1: Schematic presentation of spectral density, $(\frac{km}{hr})^2 / \frac{rad}{km}$ as a function of wave number (cycles/ km), or wave length (m) for turbulence in the free atmosphere. Data sources of spectra are identified in Table I.

Table I. Spectra of Turbulence in the Free Atmosphere

Spectrum No.	Source	Characteristics (turbulence components given with respect to course of aircraft)
1	Vinnichenko, Pinus and Shur, 1965	w-component, severe CAT, near jet stream level, stable stratification
2	Reiter and Burns, 1965	u, v- components, moderate CAT, jet stream level, stable stratification
3	Reiter and Burns, 1965	w-component, flight parallel to wind, moderate CAT, jet-stream level, stable stratification
4	Reiter and Burns, 1965	w-component, flight nearly normal to wind, moderate CAT, jet-stream level, stable stratification
5	Vinnichenko, Pinus and Shur, 1965	u-component, no CAT, near jet-stream level, stable stratification
6	Vinnichenko, Pinus and Shur, 1965	w-component, no CAT, near jet-stream level, stable stratification
7	Reiter and Burns, 1965	u, v, w- components, light turbulence at 100 m altitude, unstable stratification
8	Vinnichenko, Pinus and Shur, 1965	u-component, light turbulence at 1000 m altitude, unstable stratification
9	Vinnichenko, Pinus and Shur, 1965	w-component, light turbulence at 1000 m altitude, unstable stratification
10	Kao and Woods, 1964	u-component, at jet stream level, flight parallel to jet stream
11	Kao and Woods, 1964	v-component, at jet stream level, flight parallel to jet stream
12	Kao and Woods, 1964	u, v- components at jet stream level, flight normal to jet stream

A hump at slightly longer waves (ca. 1 to 2 km) appears in Russian turbulence measurements at low levels (Spectra Nos. 8 and 9), suggesting the effect of convective bubbles in the superadiabatic mixing layer as main energy source.

There is a gap of data in the meso-scale range from approximately 10 to 60 km. At longer waves, data obtained by Kao and Woods suggest an energy input near a scale of ca. 600 km, characteristic of the jet stream. The "striated" jet stream flow becomes apparent from the discrepancies between spectra measured across (No. 12) and along (Nos. 10 and 11) the upper flow. A similar "striation" is suggested by a comparison between Spectra Nos. 4 and 3 in the gravity-wave range. From the case shown in Fig. 1 we may deduce that the gravity waves leading to CAT were oriented with their crests at a relatively large angle across the direction of flow.

One may speculate that in bridging the meso-scale data gap mentioned above one should find another input region of turbulent energy. In this range cloud observations (Conover, 1960) give some indication of existing structure. One such case will be described later in this report.

The average resolution offered by TIROS photographs covers the range of perturbations with wave lengths > ca. 15 km. If only standard radiosonde data are available, quantitative estimates of spectral densities are unreliable for waves < ca. 1000 km. TIROS data may, however, serve as very useful qualitative indications of atmospheric disturbances in the region of the data gap shown in Fig. 1.

Large mountain ranges, such as the Rocky Mountains, are expected to contribute energy in all input regions that may be defined from Fig. 1. They are known to affect the formation of planetary waves (L > 6000 km). The input region found by Kao and Woods near 600 km would suggest the existence of inertial waves.

Newton (1959) has identified jet maxima as a quasi-inertial phenomenon. Intensification and re-formation of jet maxima is frequently found over and to the lee of the Rockies. Frequent observations of low-level jet streams in this region (see for instance Reiter and Mahlman, 1964) may offer a contribution in this scale range. Also the splitting of jet streams associated with flow over mountain barriers (Reiter, 1963, 1965 b) generates characteristic scale lengths of this order. Persistent anomalies in accurately measured vertical wind profiles (Stinson, Weinstein, and Reiter, 1964; Weinstein, Reiter and Scoggins, 1965), identifiable for several hours, may qualify in this scale range, as they suggest the existence of inertial motions. No information is available as yet on the horizontal extent of these anomalies.

In the scale range between 10 and 60 km orographic lee waves suggest a direct action of mountains on upper flow patterns. A case study incorporating the development of strong chinook winds in the Colorado area will be considered later.

Gravity waves of wave lengths from 10^2 to 10^3 m have been observed to be frequently associated with lee waves of larger scale. They appear visibly as waves on cirrus-cloud decks, but their presence has to be assumed on "dry" stable interfaces as well. Some evidence of "breaking" gravity waves has been produced from cloud photographs (Reiter and Hayman, 1962). It has been suggested that such breaking waves lead to CAT formation (Reiter, 1965 a). They occur within stable stratification in the presence of vertical wind shears.

Studies by Colson (1963) indicate that CAT shows a frequency maximum over the Rocky Mountain region. But also smaller hills may--under favorable conditions of atmospheric structure and flow--generate enough perturbation energy to show frequency maxima of CAT occurrence (Clodman, Morgan, and Ball, 1961).

CAT data available in connection with TIROS photographs usually consist of subjective pilot reports (Wiegman, 1965; Reiter and Whitney, 1965). From Fig. 2 it appears that even such crude data may yield useful results in terms of energy estimates of turbulent motion. In this diagram, a subjective CAT intensity index has been plotted on a logarithmic scale against the logarithm of spectral density obtained from Fig. 1. Two regression lines have been drawn, one for spectral density at 315 m, the other at 160 m wave length. Even though the subjective intensity scale is very crude (1 = no turbulence, 2 = light CAT, 3 = light to moderate CAT, 4 = moderate CAT, 5 = severe CAT), and aircraft of different types have been used in the measurements, straight line approximations are suggested by the data points. One may, therefore, assume an empirical relation of the form

$$\log E(k) = a \log (I) + \log b(k) \qquad (1)$$

or

$$E(k) = b(k) \cdot I^{a} \qquad (2)$$

Where E (k) is spectral density, I is the subjective CAT index mentioned above, b (k) is a constant depending on wave number k, and a is a constant determining the slope of the curves in Fig. 2, and depending on the choice of CAT index. A different index, proposed by Panofsky and McLean (1964), which is evaluated from radiosonde data, might possibly be adapted for use in Eqn. (2).

This equation may be used to "quantify" the vast amount of subjective statistical information available on CAT occurrence. Since a "-5/3 slope" seems to hold in the spectra of Fig. 1 for much longer waves than affect jet aircraft of conventional design as CAT, one might attempt estimates on gust load expectancies for faster aircraft. No such attempts have been made as yet under the present research contract.

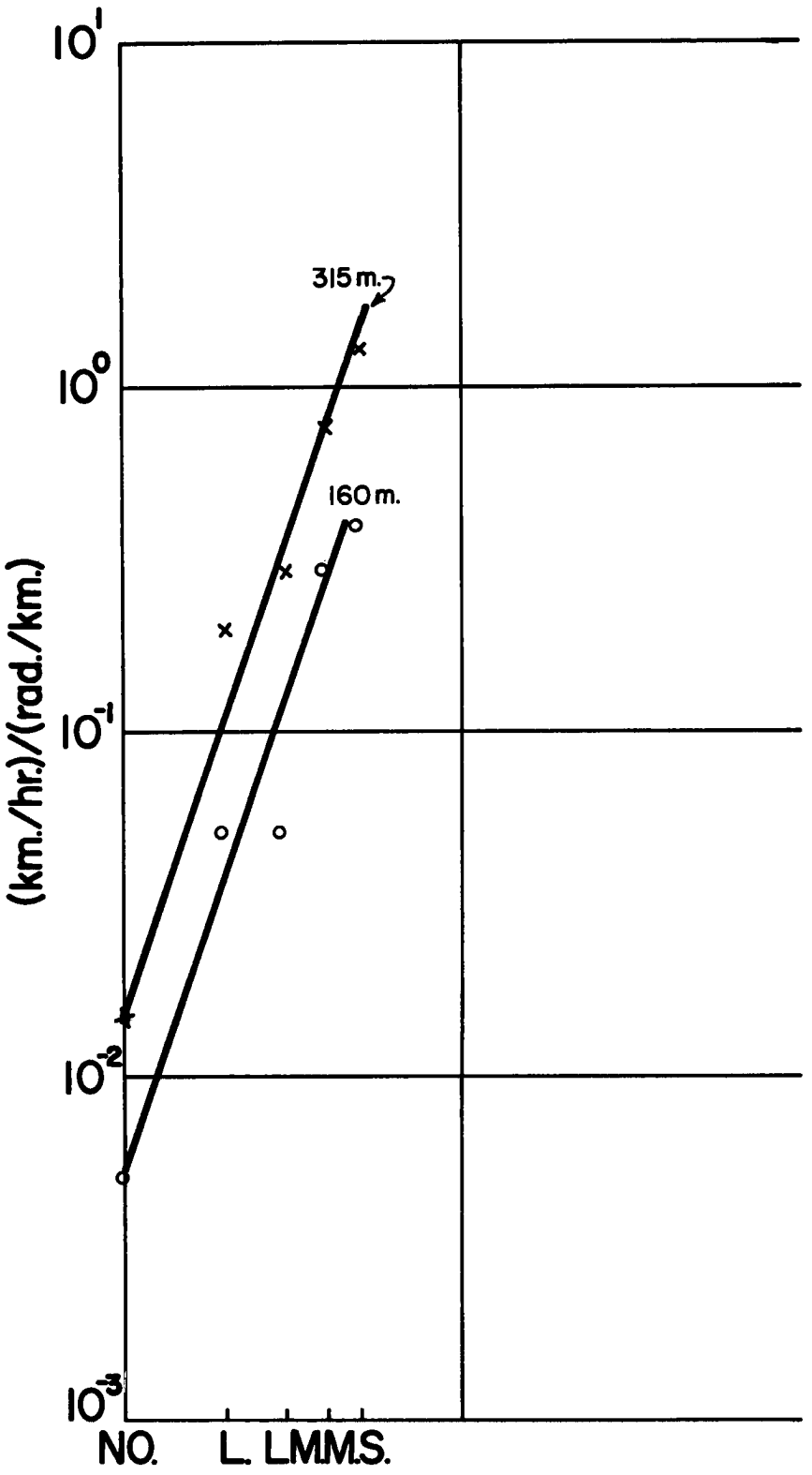

Fig. 2: Logarithm of spectral densities, $(km/hr^2)/$ rad/km, at wave lengths of 315 m and 160 m, as a function of the logarithm of CAT intensity [No turbulence (NO) = 1, light CAT (L) = 2, light to moderate CAT (LM) = 3, moderate CAT (M) = 4, severe CAT (S) = 5].

Attempts at establishing direct correlations between cloud patterns visible from TIROS photographs and CAT occurrence have not been too successful (Wiegman, 1965). Fig. 1 offers at least a partial explanation for this: the energy input region for CAT, mainly consisting of breaking gravity waves of approximately 1 km wave length, is far removed in scale from meso-structural wave patterns and flow details that may be detected by TIROS. The energy transformation in this meso-scale range may be rather complicated. In any case, one should not expect a simple one-to-one correlation between meso- and micro-scale.

Some encouragement may be found in the fact that spectral density levels seem to increase even at wave lengths of > 6 km for increasing intensity of CAT measured at much shorter wave lengths. Some, yet unknown, mechanism might therefore feed energy from the meso-scale into the range of breaking gravity waves, thus exerting a certain control on the micro-scale.

III. TIROS Case Studies of Atmospheric Meso- and Macro-Structure:

In the following a short description will be given of the case studies undertaken within the provisions of the present research contract. Some are completed and others have begun and are continuing under Weather Bureau Grant WBG - 59. Since most of the studies involve a large amount of detailed analysis work, only a selection of diagrams will be presented in this Final Report, together with some of the major conclusions reached from these studies. More detailed results and analytical evidence are published in a series of technical reports as each task is completed.

(1) General Procedure and Selection of Cases.

As outlined in the Progress Report (Reiter, 1964), a large number of photographs from orbits of TIROS IV, V, VI, and VII were viewed for possible case selection. Case studies of the following periods have been prepared, or are still in progress:

(a) Chinook case with "foehn wall" or "barrier" clouds in the Colorado region: TIROS V, orbit 4363 T, 19 April, 1963.

(b) Macro- and meso-scale wave cloud over North Platte: TIROS V, orbits 4363 T and 4349 T, 18-19 April, 1963.

(c) Baroclinic wave formation along cold front in the lee of the Rocky Mountains: TIROS VI, orbit 3070 T, 16 April, 1963.

(d) Comparison between cloud bands and jet stream, east of the mountains: TIROS V, orbit 4349 T, 18 April, 1963.

(e) Structure of a cyclone developing east of the Rocky Mountains: TIROS V and VI, orbits 4347 D, 4363 D, 3084 D, 4349 T, 4363 T, and 3070 T, 16, 17, 18, 19 April, 1963.

(f) Flow patterns in the region of merging jet streams: TIROS V and VI, orbits 2209 and 0922, 20 November, 1962 (based on a study by Oliver et al., 1964).

Rectification procedures followed outlines given by Fujita (1961, 1963, 1964), with small modifications especially suited for TIROS coverage over regions with well-established landmarks. A review report on rectification procedures adopted for this project has been prepared by Wooldridge (1965).

Two main difficulties, also recognized by other investigators, were encountered in the interpretation of TIROS data. One was the similarity between snow and cloud cover in mountainous terrain. Especially with orographic cloud formation the appearance of distinct dark valleys on the photographs cannot be taken as conclusive indication of snow rather than cloud observations. As additional criteria in the distinction between the two phenomena, lack of time continuity in the observed patterns between successive orbits speaks in favor of cloud formations, so does the appearance of meso-scale striations along particle trajectories. Dendritic patterns,on the other hand, speak in favor of snow cover reaching down to a certain height above mean sea level, and not spreading over the valley floors. Another difficulty arose from the fact that TIROS

is unable to see thin clouds. In the case of broken cloudiness a gray haze appears on TIROS photographs if the individual cloud patches are smaller than the resolution of the television system.

In several of the case studies outlined below isentropic analysis techniques have been employed. Since a large number of soundings had to be plotted as preparatory step for these analyses, and Montgomery stream-function values had to be computed accurately, electronic computer programs were developed jointly for this research project and for a project under the sponsorship of the U. S. Atomic Energy Commission. The programs are listed and described in an Appendix to this report.

In the computation of isentropic trajectories investigators so far have tried to stay away from regions in which condensation processes invalidated the dry-adiabatic assumption. In tracing particle motions through cloud regions seen by TIROS this was no longer possible. Attempts have been made, therefore, to include moist-adiabatic processes into the trajectory calculations. Although these experiments still have to be considered preliminary, results were encouraging. Some details will be reported farther below.

(2) Chinook in the Colorado Region.

Figs. 3 and 4 show TIROS V pictures of orbit 4349 (Tape), Frame 14, 18 April, 1963; 1955 GMT and of orbit 4363 (Tape), Frame 18, 19 April 1963, 1921 GMT. In each photograph latitude-longitude grids have been entered together with the letter designations of several Weather Bureau stations. Marked changes in the shape and size of the high-albedo region west and south of Denver within the 24-hour period between the two photographs may be noted. Furthermore, on April 18 a striated pattern appeared between Denver and Albuquerque (ABQ) with the streaks approximately parallel to the wind direction in the middle troposphere. From this evidence we may conclude that the photographs, especially Fig. 3, actually show cloud patterns rather than snow fields. Even on

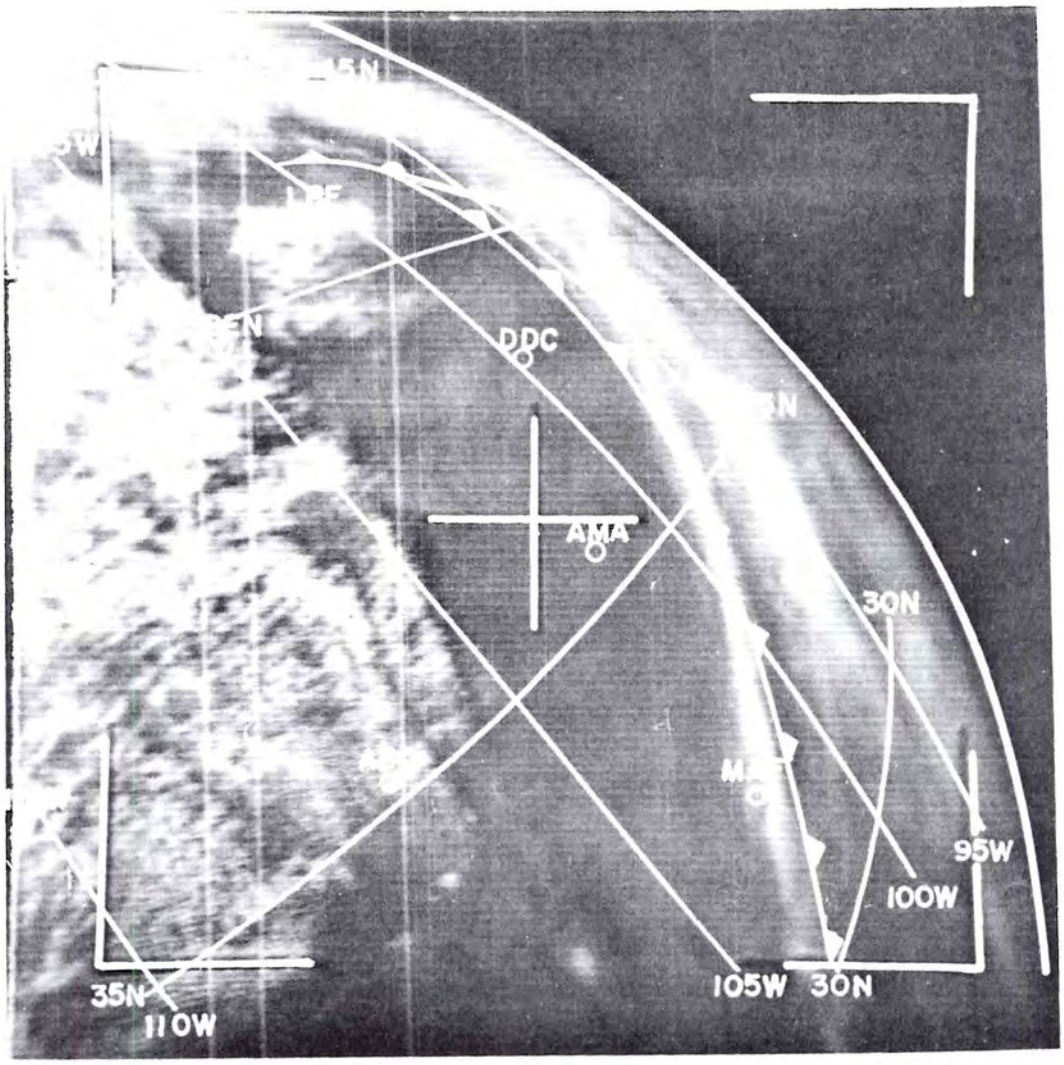

Fig. 3: Cloud photograph, TIROS V orbit 4349 (tape) Frame 14, 18 April, 1963, 1955 GMT, showing cloud formations over the Rocky Mountains in the Colorado region (DEN = Denver, LBF = North Platte, DDC = Dodge City, AMA = Amarillo, ABQ = Albuquerque, MAF = Midland).

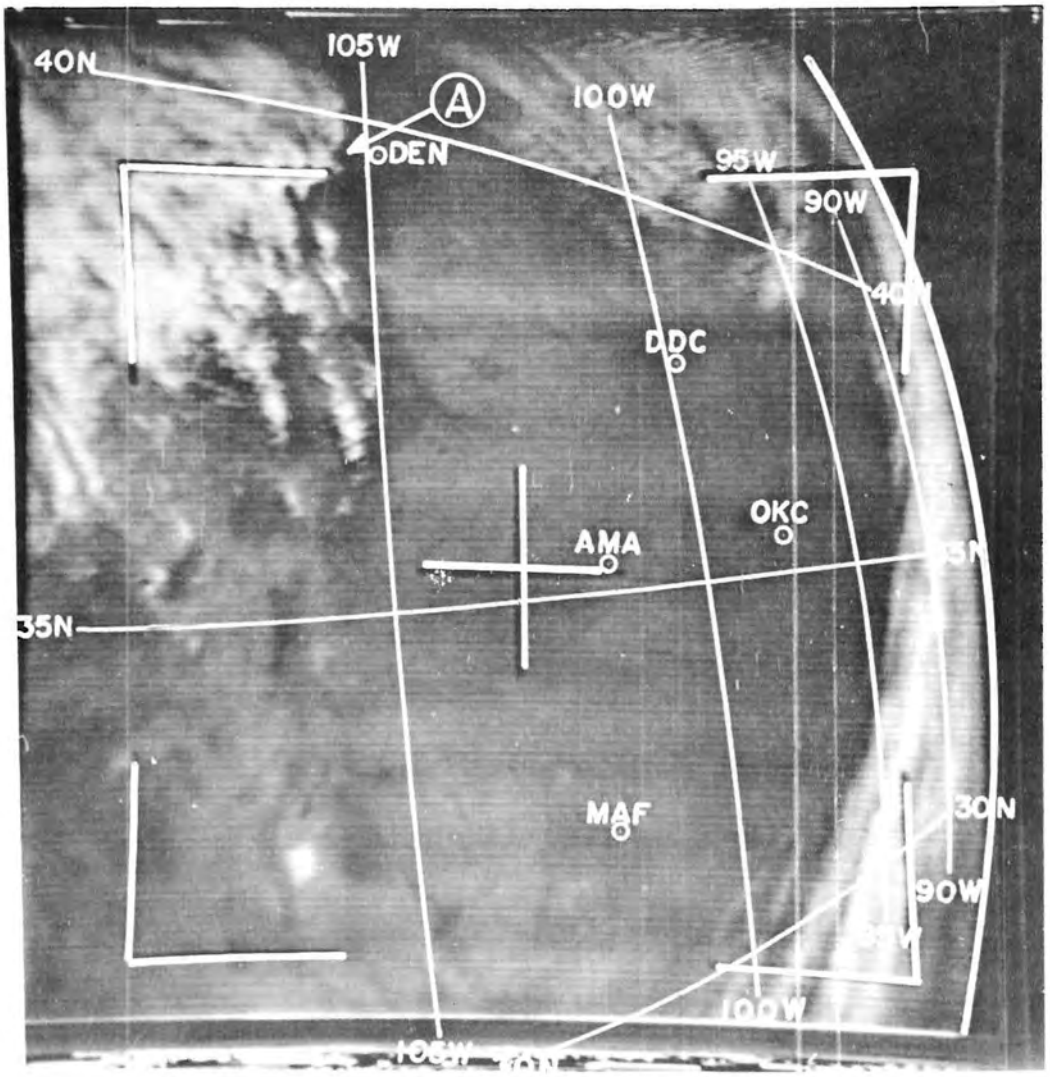

Fig. 4: Cloud photograph TIROS V orbit 4363 (tape) Frame 18, 19 April 1963, 1921 GMT (OKC = Oklahoma City. For other station identifications see legend to Fig. 3).

19 April, certain sharp features in the Denver region (indicated by letter A in Fig. 4) appear in the photograph which cannot be identified on the previous day. This justifies the assumption that during the latter of the two orbits a "foehn wall" of clouds was still present over and to the west of the Continental Divide in the Denver region, with nearly clear skies east of the mountains (Table II).

A number of details appear in the cloud field between Denver and Albuquerque on 18 April which coincide with orographic features. The Rio Grande Valley, the Alamosa Basin and the San Juan River Valley may be distinguished clearly as areas with relatively little cloud cover. By 19 April the cloud cover south of Denver (DEN) has decreased. Correlation between clouds and terrain features is still evident, however.

The upper air flow patterns near the jet-stream level may be seen from Fig. 5 which gives a sample of 250 mb isotachs and isotherms of 17, 18, and 19 April 00 GMT. The map of 19 April 00 GMT (Fig. 5 c) shows three parallel branches of a southwesterly jet stream over the central United States. A cyclonic vortex overlies the northern Rocky Mountain states, with southeasterly flow in the region shown by the upper left corner of Fig. 3 which was taken approximately 4 hours before observation time in Fig. 5 c.

Figs. 6 to 9 contain analysis of "steady wind" speeds and stream lines, as well as peak gust velocities and dew point spread (i. e. the temperature difference between dry- and wet-bulb thermometers in ^{o}F) at the ground for 18 April 1800 GMT and 19 April 1900 GMT, respectively. The center branch of the jet stream shown in Fig. 5 b overlies a region of strong and gusty winds at the surface with extremely dry conditions.

Another branch of dry and gusty winds from a northwesterly direction appears over and to the north of Denver (Figs. 6 and 8). These winds undergo considerable adiabatic descent as they cross the

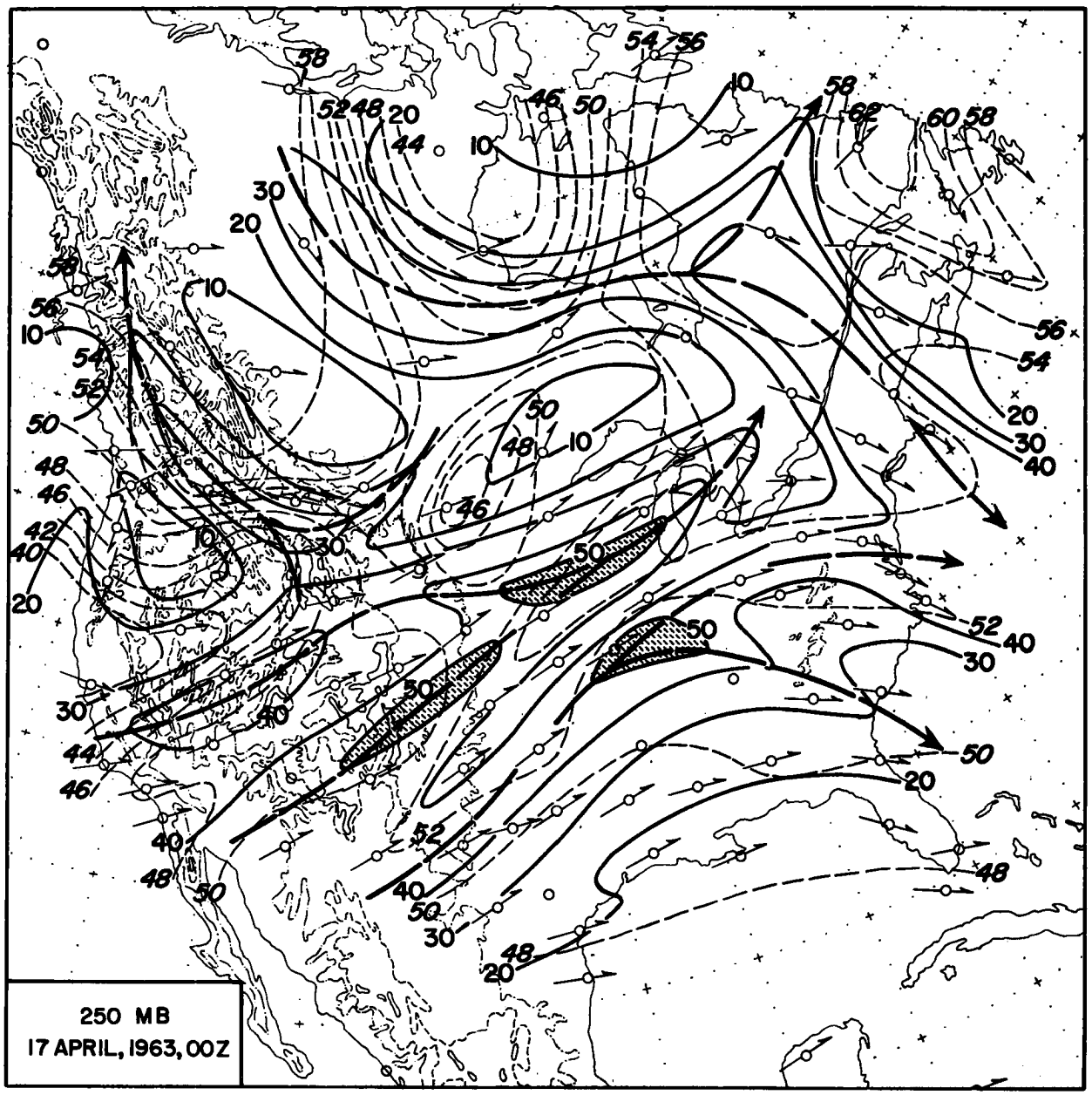

Fig. 5 a: 250-mb isotachs (solid lines, mps, vertical numbers, areas > 50 mps are shaded) and isotherms (thin dashed lines, °C, slanting numbers, minus signs omitted) for dates and observation times as indicated. Jet axes are marked by heavy dashed lines with arrows.

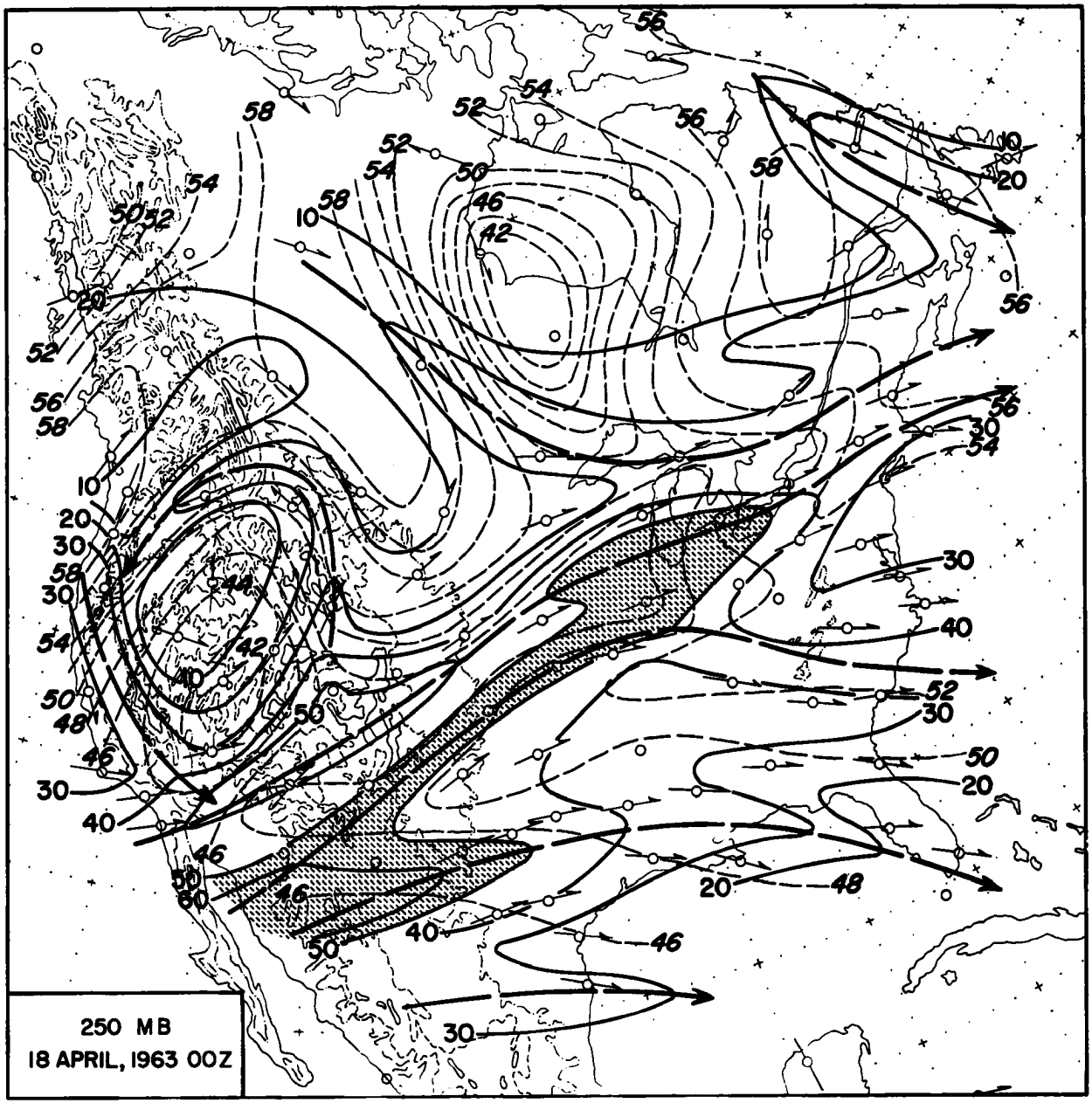

Fig. 5 b: 250-mb isotachs (solid lines, mps, vertical numbers, areas > 50 mps are shaded) and isotherms (thin dashed lines, °C, slanting numbers, minus signs omitted) for dates and observation times as indicated. Jet axes are marked by heavy dashed lines with arrows.

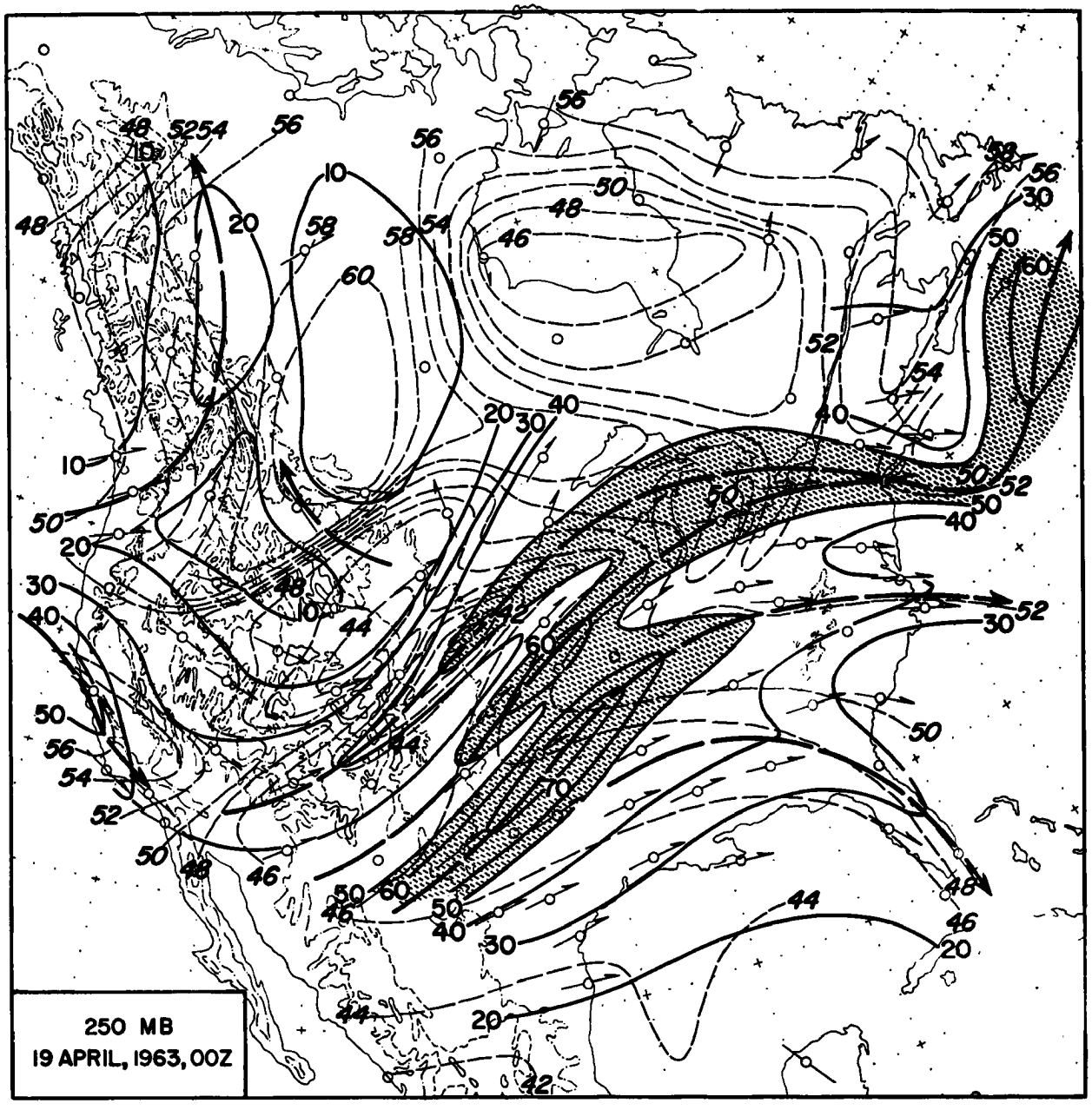

Fig. 5 c: 250-mb isotachs (solid lines, mps, vertical numbers, areas > 50 mps are shaded) and isotherms (thin dashed lines, °C, slanting numbers minus signs omitted) for dates and observation times as indicated. Jet axes are marked by heavy dashed lines with arrows.

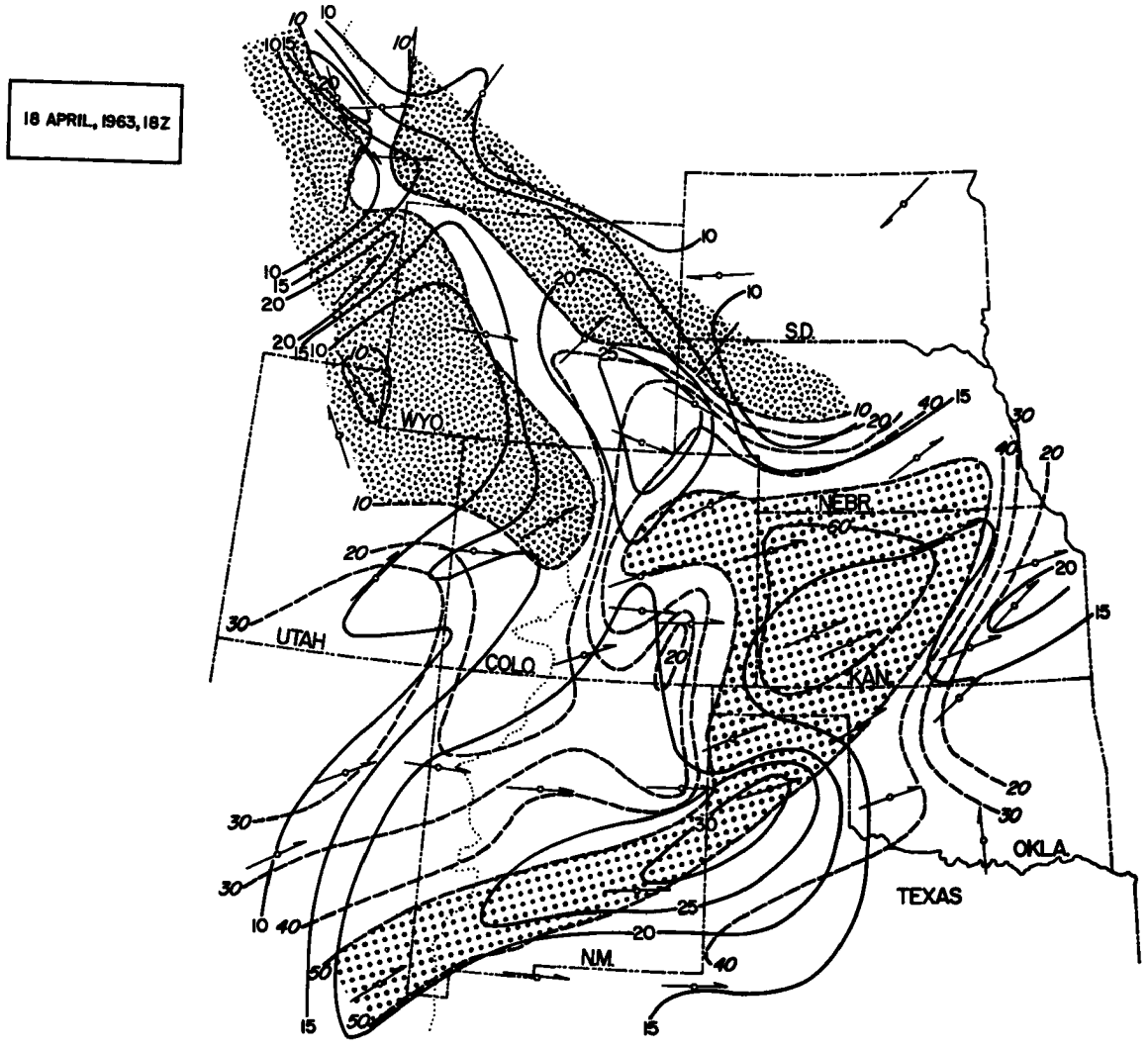

Fig. 6 : Dew point spread (i. e., difference between dry- and wet-bulb thermometer, ^{o}F, dashed lines, slanting numbers) and "steady" surface winds (averaged over 2 minutes at observation time, knots, solid lines, vertical numbers). Dry ($\Delta T \geq 50^{o}$ F) and moist regions ($\Delta T \leq 10^{o}$ F) indicated by different shading. Dates and observation times as indicated by shading and small arrows and dots, respectively.

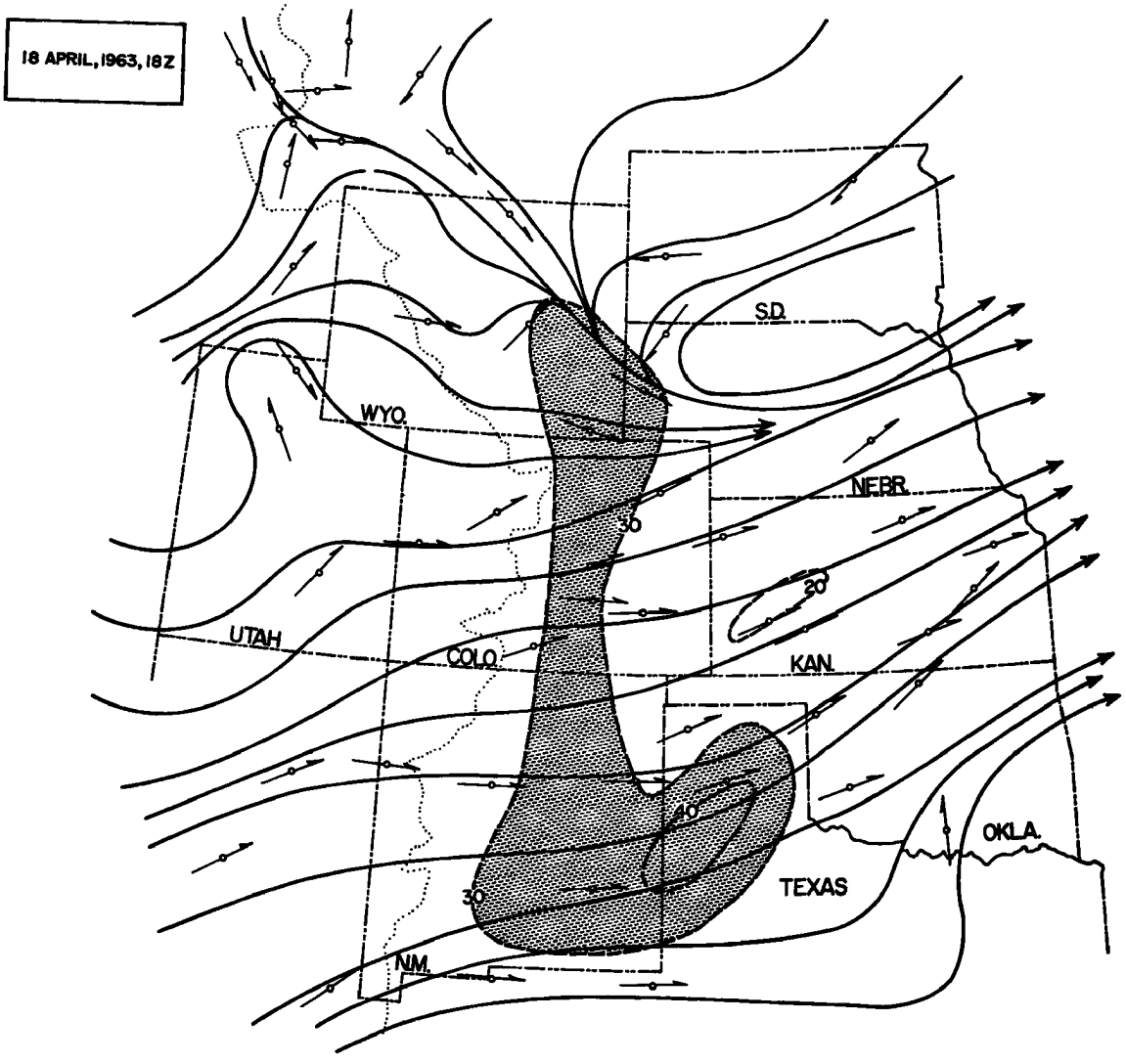

Fig. 7.: Surface stream lines (solid lines) and peak gusts (during seven-minute interval prior to observation time, knots, dashed lines). Areas with gusts > 30 knots are shaded. Dates and observation times as indicated.

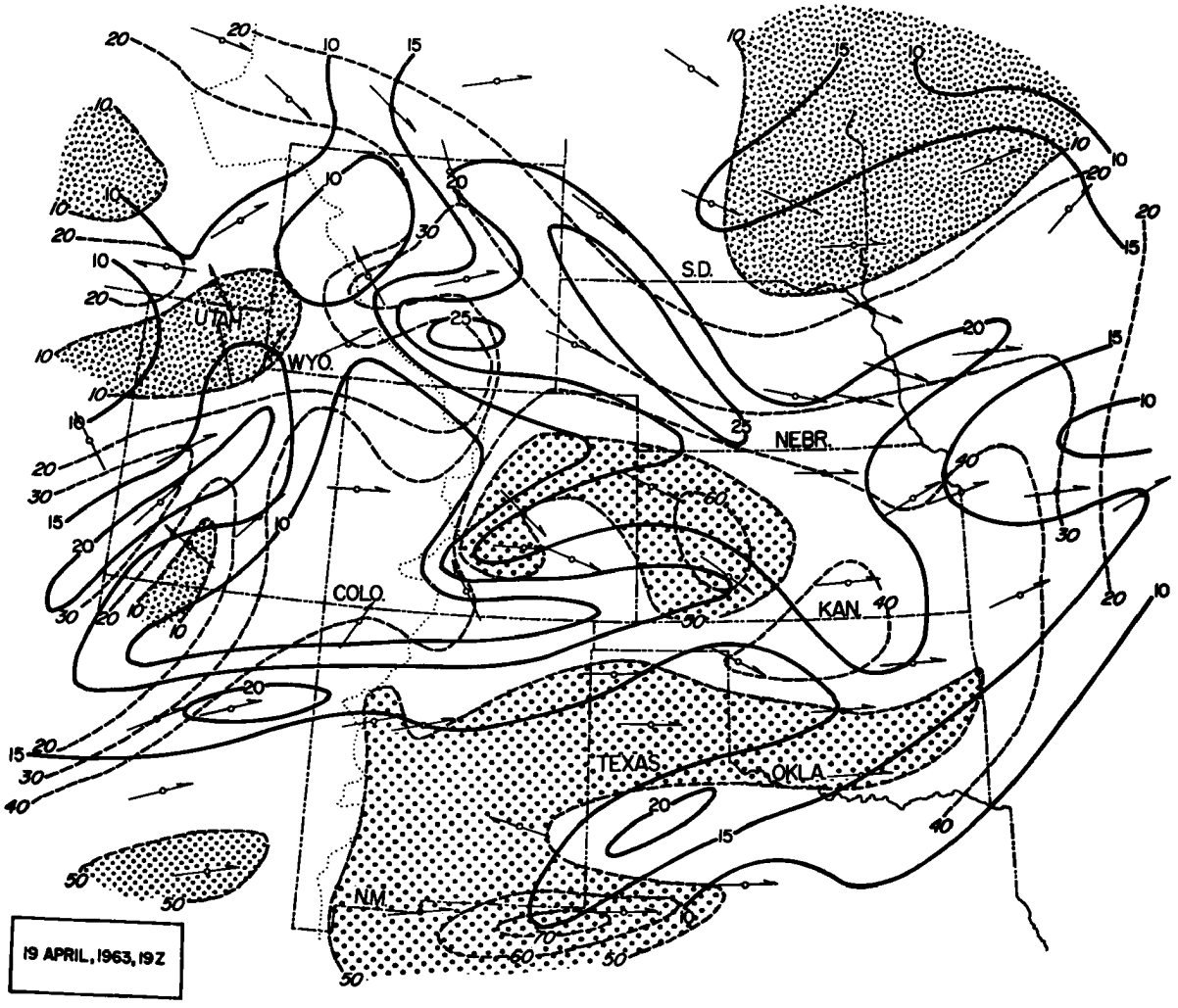

Fig. 8: Dew point spread (i. e., difference between dry- and wet-bulb thermometer, ^{o}F, dashed lines, slanting numbers) and "steady" surface winds (averaged over 2 minutes at observation time, knots, solid lines, vertical numbers). Dry ($\Delta T \geq 50^{o}$ F) and moist regions ($\Delta T \leq 10^{o}$ F) indicated by different shading. Dates and observation times as indicated by shading and small arrows and dots, respectively.

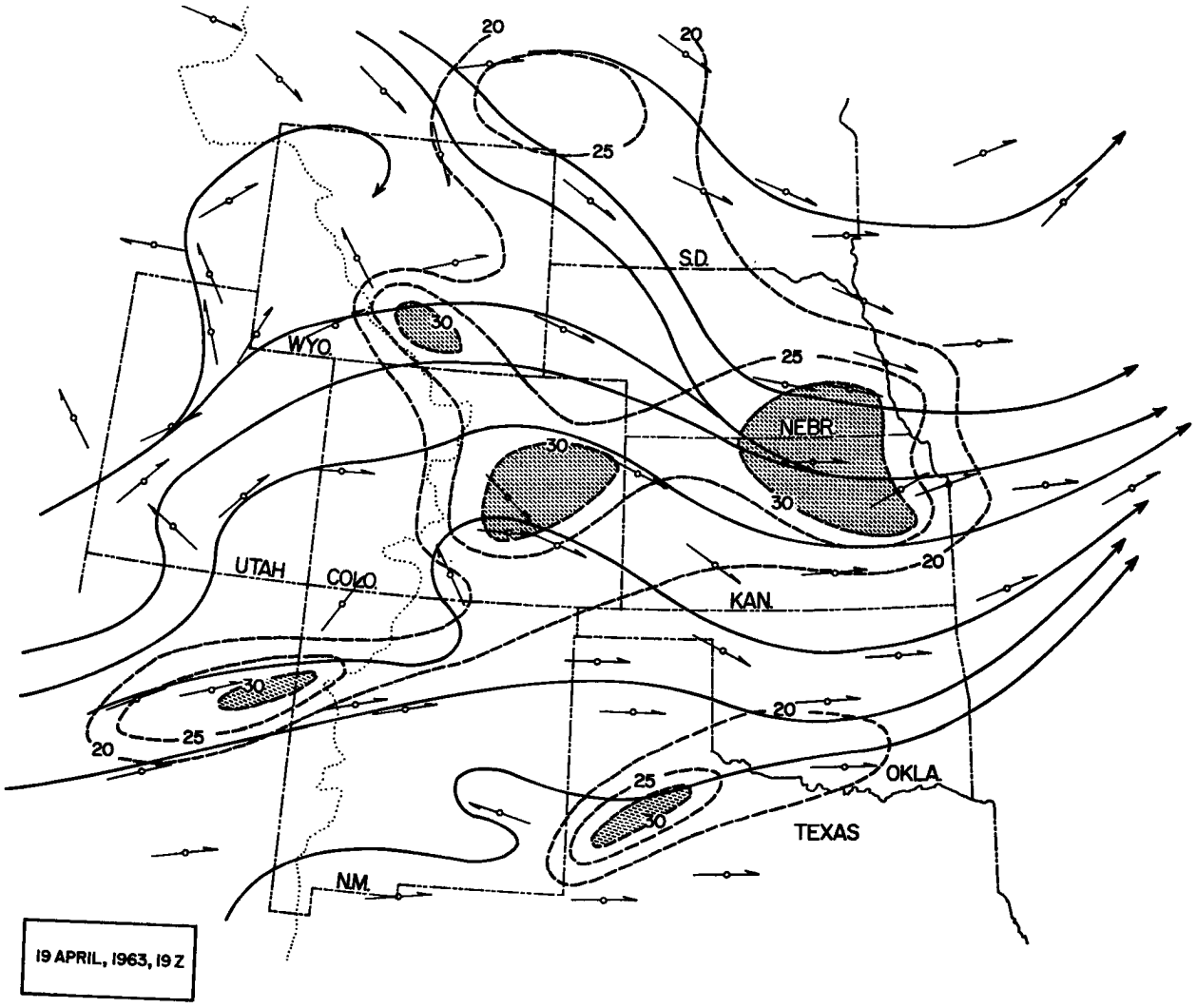

Fig. 9: Surface stream lines (solid lines) and peak gusts (during seven-minute interval prior to observation time, knots, dashed lines). Areas with gusts > 30 knots are shaded. Dates and observation times as indicated.

TABLE II

AVIATION WEATHER CLOUD REPORTS

DENVER (DEN), COLORADO

DATE	TIME (GMT)	CLOUD HEIGHT (feet)	CLOUD AMOUNT	COMMENTS
18 April,1963	1600		CLR	HIR MTNS OBSCD W-NW
"	1700		CLR	HIR MTNS OBSCD W-NW
"	1800	9000	⌀	HIR MTNS OBSCD W-NW
"	1900	9000	⌀	SNOW SHOWERS INTENSITY UNK OBSCG HIR MTNS SW-NW
"	2000	8000	⌀	SNOW SHOWERS INTENSITY UNK OBSCG HIR MTNS SW-NW
19 April,1963	1600	18000	⌀	CLDS TPG HIR MTNS
"	1700	18000 Higher	-⌀ -⌀	CLDS TPG HIR MTNS
"	1800		CLR	CLDS TPG HIR MTNS
"	1900		CLR	CLDS OBSCG TPS HIR MTNS
"	2000		CLR	CLDS OBSCG TPS HIR MTNS W-NW

TABLE III

AVIATION WEATHER CLOUD REPORTS
for
Akron, Colo. (AKO), Scottsbluff, Nebr. (BFF),
and
North Platte, Nebr. (LBF)

STATION AND DATE	TIME (GMT)	CLOUD HEIGHT (feet)	CLOUD AMOUNT	COMMENTS
LBF 18 April,1963	1800	6000	◐	
LBF 18 April,1963	1900	6000	◐	
LBF 18 April,1963	2000	Est. 9000 Higher	● ●	
LBF 18 April,1963	2100	Est. 8000 Higher	● ⊕	BINOVC VIRGA ALQOS TCU NW-NE
BFF 18 April,1963	1800	HIGHER	◐	
BFF 18 April,1963	1900	HIGHER	◐	
BFF 18 April,1963	2000	HIGHER	◐	
BFF 18 April, 1963	2100	HIGHER	◐	
AKO 18 April,1963	1800	6000	◐	
AKO 18 April,1963	1900	Est. 4000	●	
AKO 18 April,1963	2000	Est. 4000	●	
AKO 18 April,1963	2100	Est. 4000	●	SNOW WITH PARTIAL OBSCURATION

main range of the Rocky Mountains. This also accounts for the dryness of the air in the lee of the mountains. On the westward side humidity conditions are close to saturation in the northern part of the chinook region with some rain and snow falling there (Fig. 10). The descent on the lee side causes relative humidities as low as 8% near the ground. A dry-adiabatic layer is observed over Denver, extending from the ground to nearly 400 mb on 19 April 00 GMT (Fig. 11).

Above this adiabatic layer there is a stable region which, as the sections shown in Figs. 12 and 13 suggest, may be identified as a "jet stream front", using terminology introduced by Endlich and McLean (1957). The chinook in the Denver region thus transports air from close to the jet stream level towards the ground (see Cook and Topil, 1952; McClain, 1952). This is also evident from the isentropic chart of the 300 K surface shown in Fig. 14. The steep pressure gradient on this isentropic surface, which appears near the Continental Divide, indicates a front-like slope of the stable layer. No fronts, however, have been indicated in this region on the surface map. The surface cold front runs much farther to the east in the area in which the 300K isentropic surface is grounded.

The cloudy regions of Fig. 3 have been entered schematically in Fig. 14. The clouds seem to be confined to the left-hand side of the zone of strong pressure gradient (shows baroclinicity). The cloud-free tongue slightly east of Denver (DEN) is orographically produced by chinook winds. Only near Albuquerque (ABQ) do the clouds cross the baroclinic zone. From Fig. 5 c we see that this is the region where the axis of the northern-most jet branch crosses the mountains. This jet branch coincides closely with the baroclinic zone indicated in Fig. 14. Thus, a close correlation between jet-stream and cloud patterns, such as the "foehn wall" exists, at least in the present case.

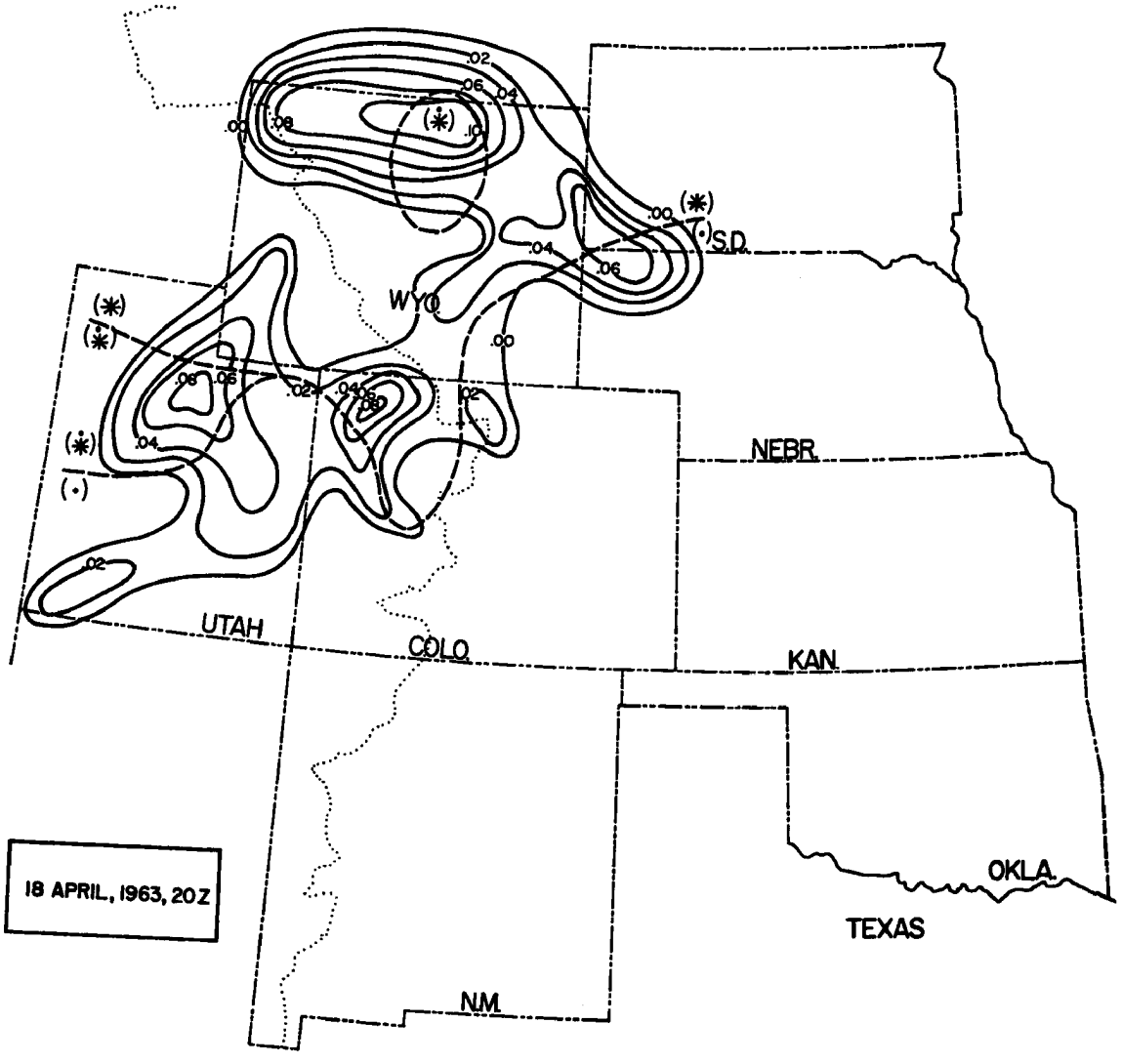

Fig. 10: Precipitation (inches) within 4 hours prior to observation time. Dashed lines indicate boundaries between snow, rain and snow mixed, and rain.

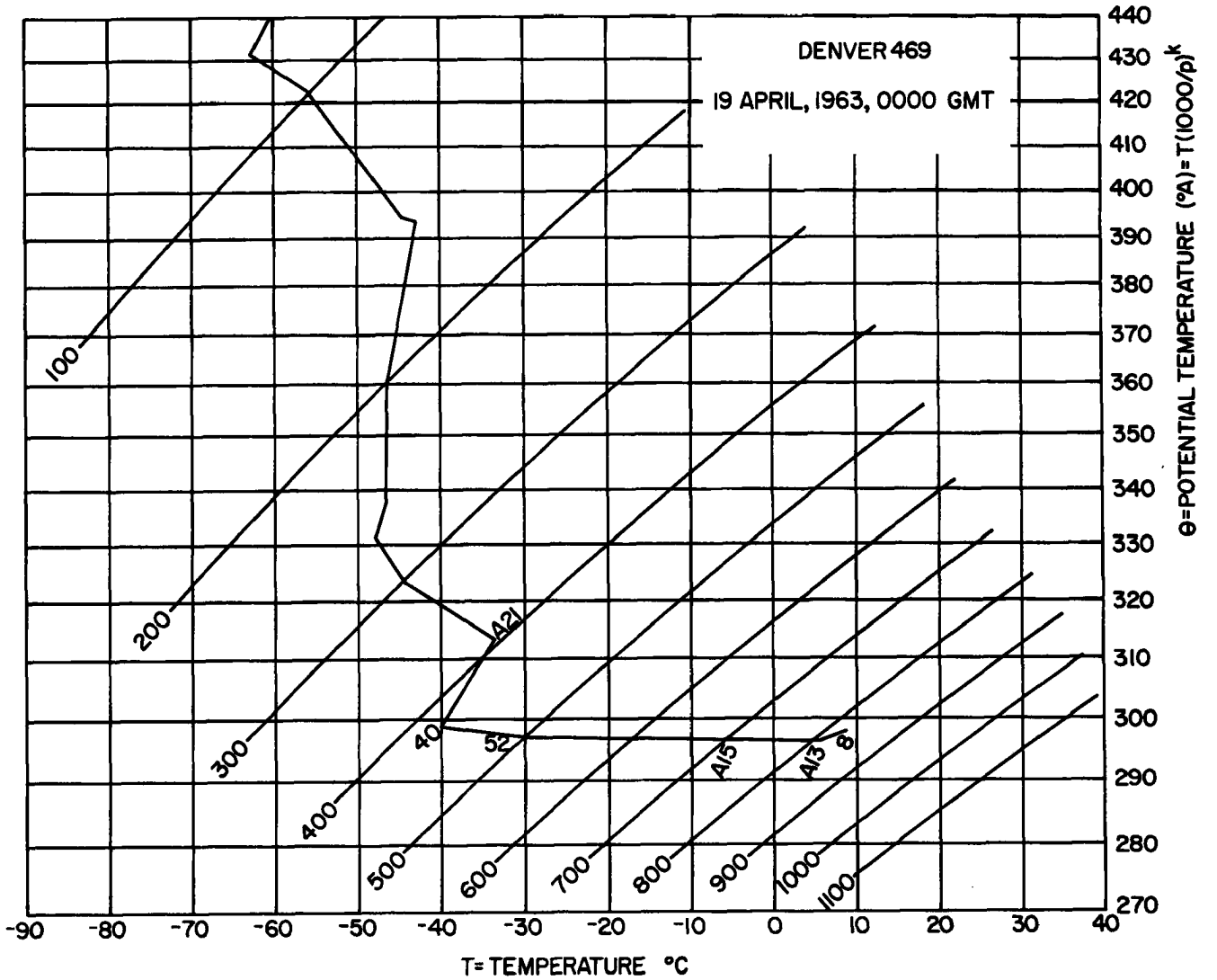

Fig. 11: Sounding for Denver (DEN), Colorado, 19 April, 1963, 00 GMT, plotted on a tephigram. Relative humidities, wind speeds and directions are given numerically along the sounding.

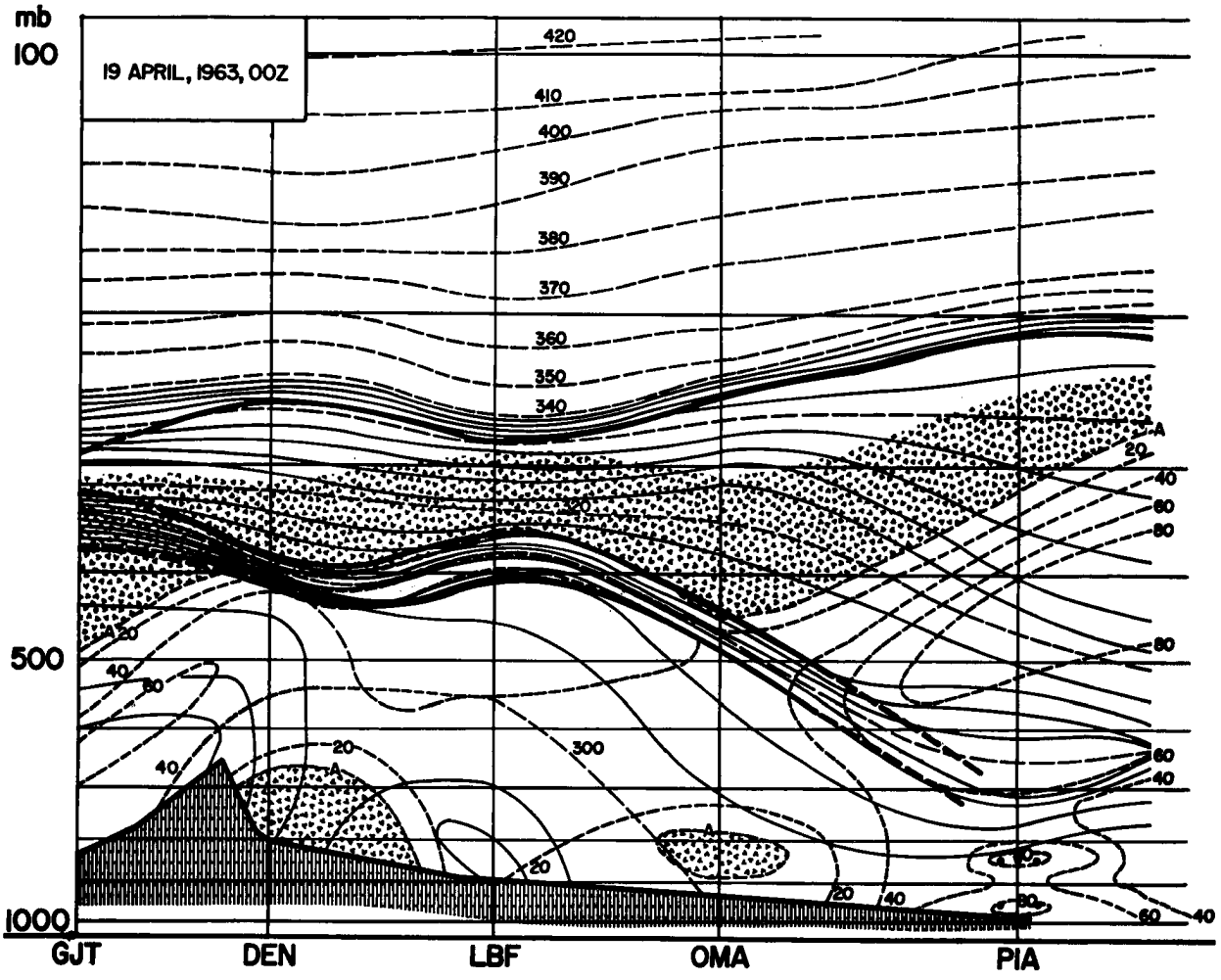

Fig. 12: Cross section through the atmosphere from Grand Junction (GJT), Colorado, through Denver (DEN), Colorado, North Platte (LBF), Nebraska, Omaha (OMA), Nebraska, to Peoria (PIA), Illinois: Potential temperature (solid and long-dashed lines) and relative humidities (per cent, short-dashed lines, "A" indicates "motor-boating"). Stable layers and tropopause are marked by heavy dashed and solid lines.

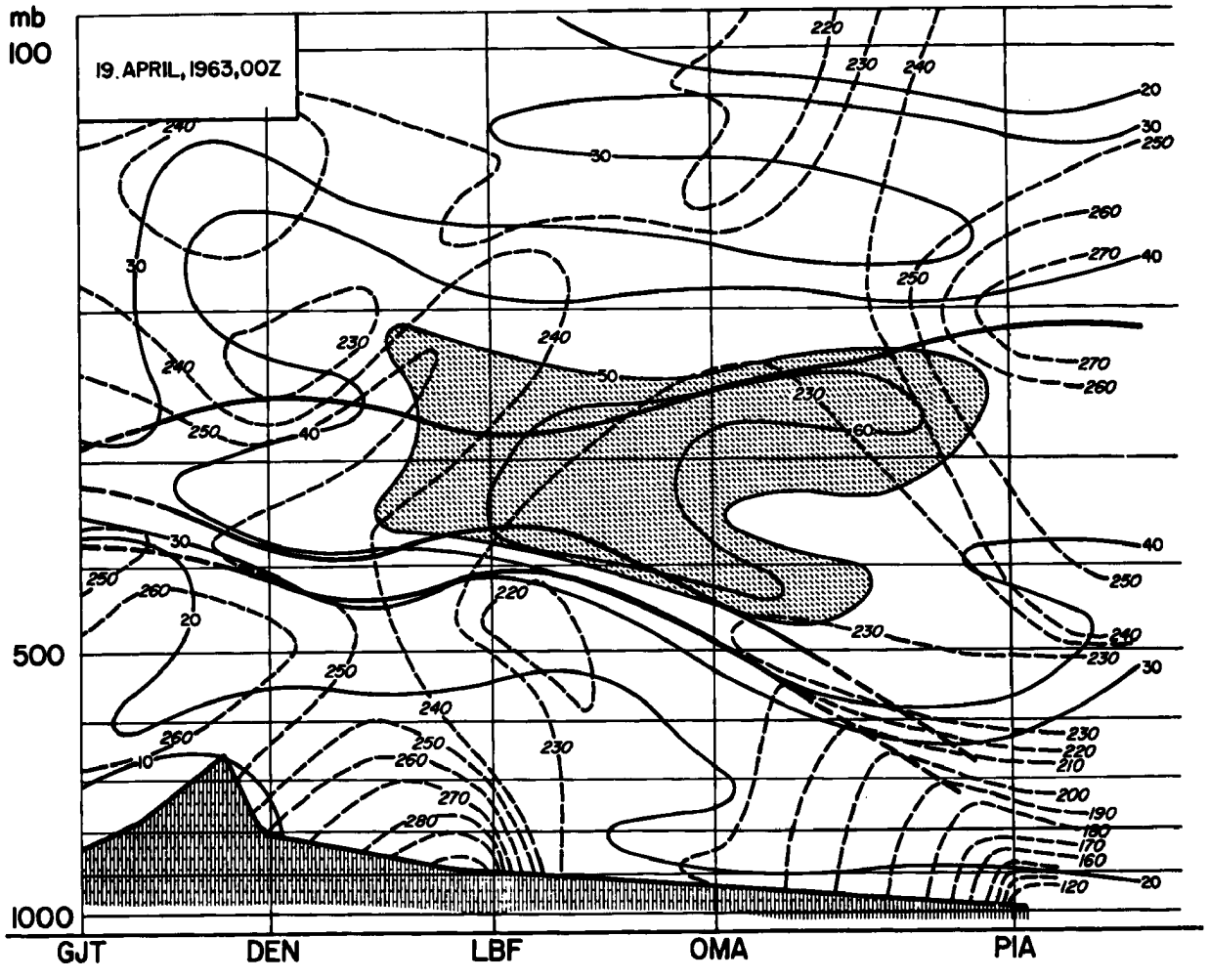

Fig. 13: Cross section through the atmosphere from Grand Junction (GJT), Colorado, through Denver (DEN), Colorado, North Platte (LBF), Nebraska, Omaha (OMA), Nebraska, to Peoria (PIA), Illinois: Wind speeds (mps, solid lines) and wind directions (degrees, dashed lines).

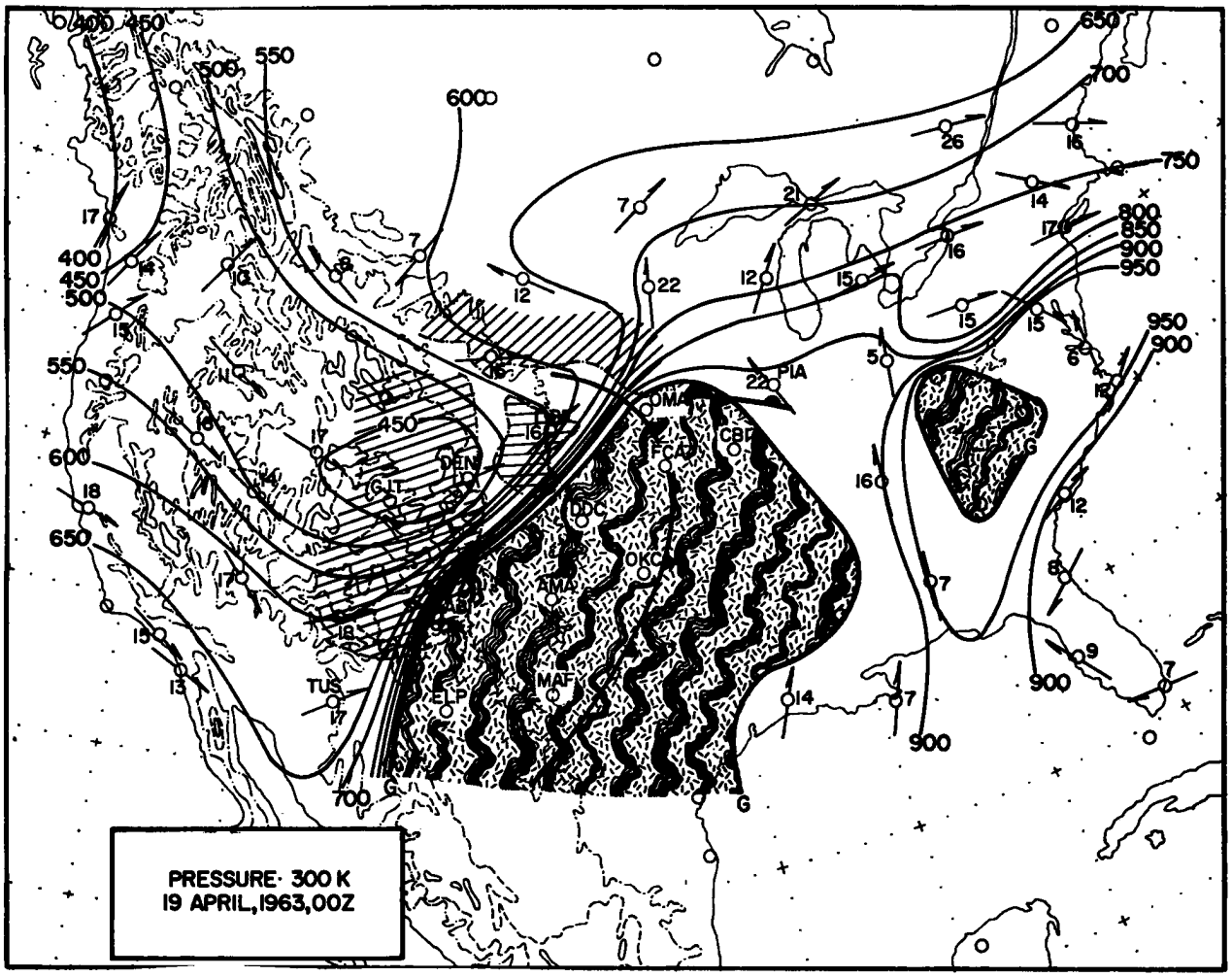

Fig. 14: Pressure (mb) on 300 K isentropic surface, 19 April, 1963, 00 GMT. Wind speeds (mps) indicated numerically. Irregularly shaded area is where 300 K surface is grounded. Cloud cover from Fig. 3 is schematically indicated by hatching. Frontal positions entered for 18 April 21 GMT.

Since large vertical transport processes of air are involved in chinook situations such as the one analyzed in the present case study, similar weather patterns may be of importance in regionally confined downward transport of radioactively contaminated air. No quantitative studies of this problem have been undertaken as yet.

As has been shown in Fig. 10, precipitation is not associated with the entire flow crossing the Rocky Mountains. The striated cloud patterns between Denver and Albuquerque, shown in Fig. 3, do not produce precipitation due to the barrier effect of the mountains. Precipitation sets in west-south-west of Denver on the windward side of the mountains where cloud patterns in the TIROS photograph appear more diffuse and show less detail. Analysis of additional case studies of similar nature will have to help decide whether or not the presence or lack of detail in orographic cloud patterns may be used in distinguishing between regions without or with precipitation.

Furthermore, one should learn from such studies whether or not the distribution of orographic clouds relative to the location of the jet stream, as described above, may be considered typical.

More details on the flow and cloud patterns in chinook weather situations will be given in a forthcoming report on an investigation which is presently in progress.

(3) Waves East of the Mountains.

From Fig. 3, and even more so from Fig. 15 (TIROS V, orbit 4349 (Tape), Frame 10), a cloud region is evident in the vicinity of North Platte (LBF) on 18 April 1963, 1957 GMT. The Aviation Weather Reports from this region are given in Table III. The cloud bases at satellite observation time were estimated at 9000 ft.

Fig. 16 shows surface cloud observations of 18 April 21 GMT approximately one hour past satellite observation time. According to these data, the bright cloud area over and to the west of North Platte

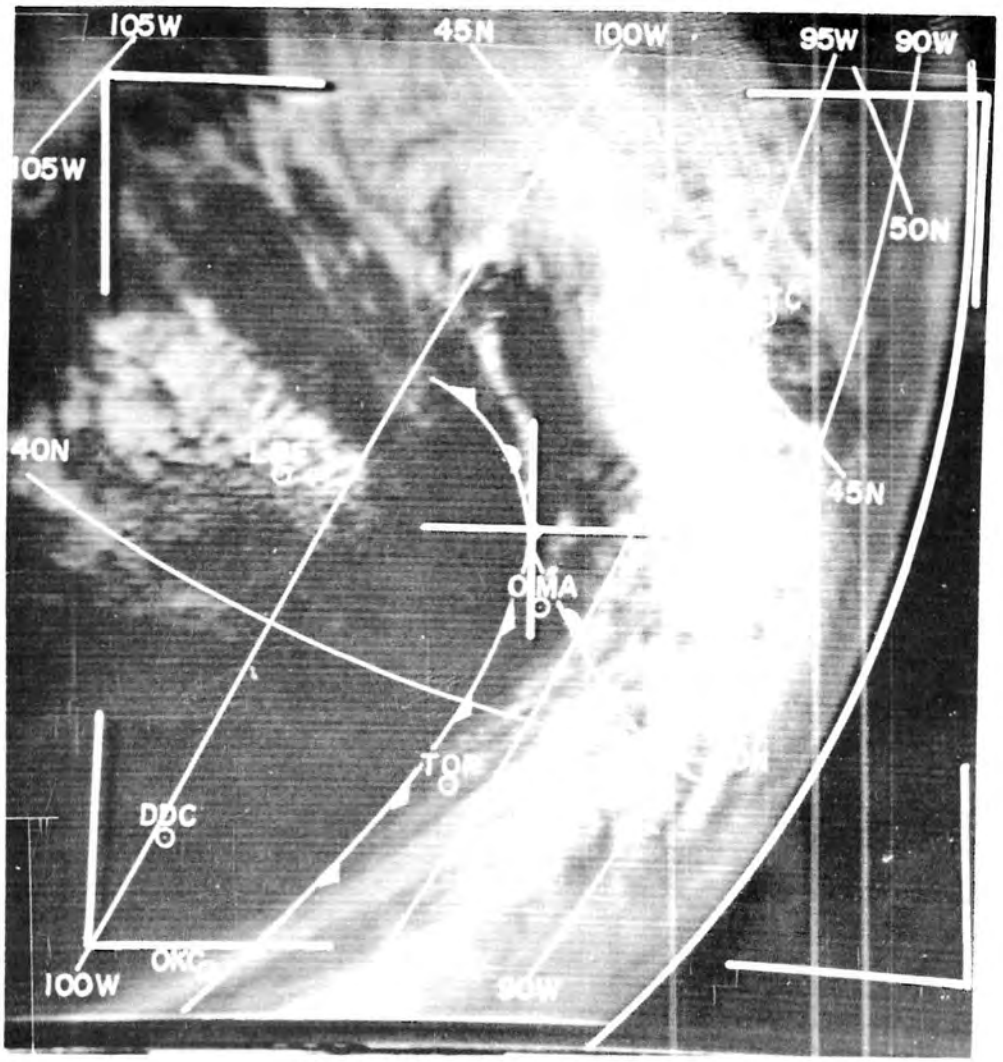

Fig. 15: Cloud photograph, TIROS V orbit 4349 (tape) Frame 10, 18 April, 1963, 19:57 GMT.

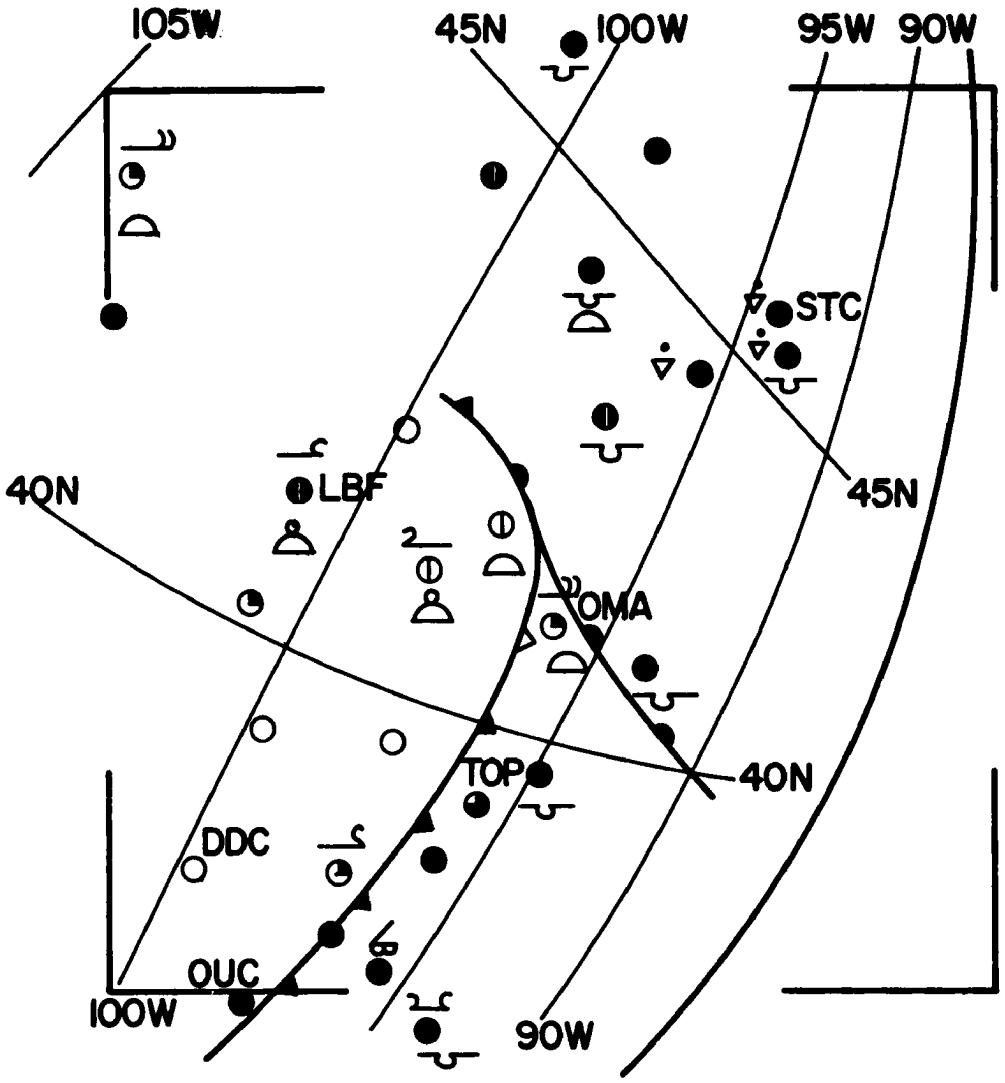

Fig. 16: Cloud reports from surface observation stations, 18 April, 1963, 21 GMT, plotted to scale of TIROS photograph, Fig. 15.

seems to be mainly broken cumulus congestus and some cirrus, the latter probably associated with the stable layer near 400 mb (Fig. 12). This layer is also expected to act as a "lid" on convective activity.

The convective clouds reported between North Platte and the cold front farther east obviously are below the resolution of TIROS photographs. Less than 1/10 sky cover is observed in this region.

According to Fig. 15, the cumulus clouds near North Platte reveal a "wavelike" pattern. The cloud rows are oriented along directions of approximately 180° to 200°. (A slight veering of the directions of orientation is observed as one proceeds from west to east in this area.) This wave alignment conforms approximately to the direction of the mean shear vector in the tropospheric convective layer underneath the stable layer whose bottom is found at 400 mb (6997 m) over North Platte on 19 April 00 GMT (Figs. 17 and 18).

A similar parallel alignment of convective clouds to the east of the Continental Divide is quite frequently observed in the Colorado region, especially during the hail season. On such occasions the region in the immediate lee of the mountains is either cloud free (as it appears to be on the TIROS photographs of Figs. 3 and 15), or experiences cirrus clouds which are advected from the windward side of the Continental Divide. At a distance of 50 to 100 miles east of the Divide a row of cumulonimbi may frequently be observed.

The parallel alignment of convective clouds which often develop east of the Rocky Mountains during the hail season suggests the presence of a gravity-wave effect, possibly produced by the terrain. The lines of cumulus congestus observed near North Platte (Figs. 3 and 15) may be of similar origin. The distance between the cloud rows may be measured from the TIROS photographs. It is 28 km (4 rows to a distance equivalent to 1° lat.). By assuming that the wave pattern causing the observed cloud alignment is either

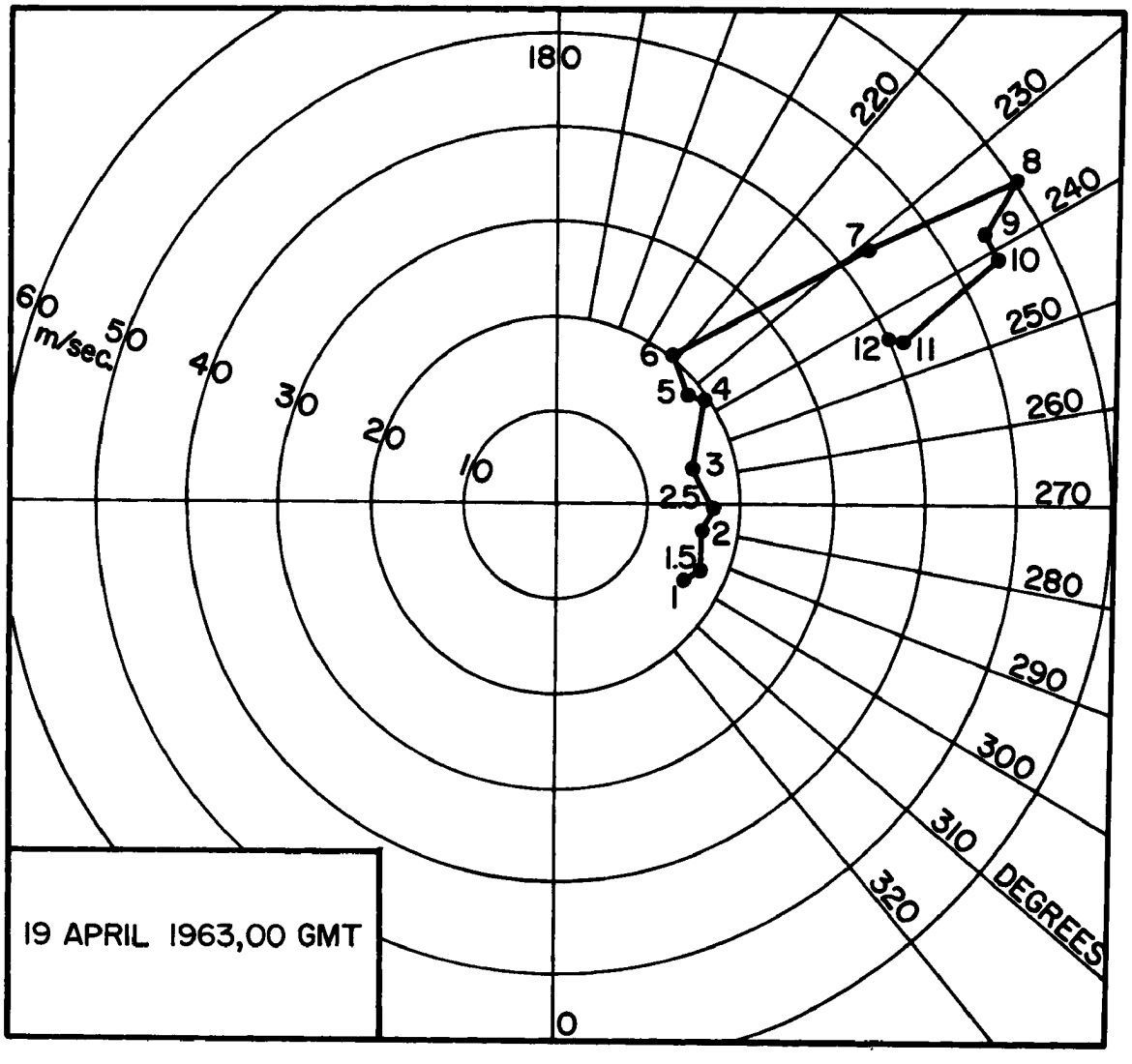

Fig. 17: Hodograph, North Platte, 19 April, 1963, 00 GMT.
Numbers by dots indicate levels in kilometers.

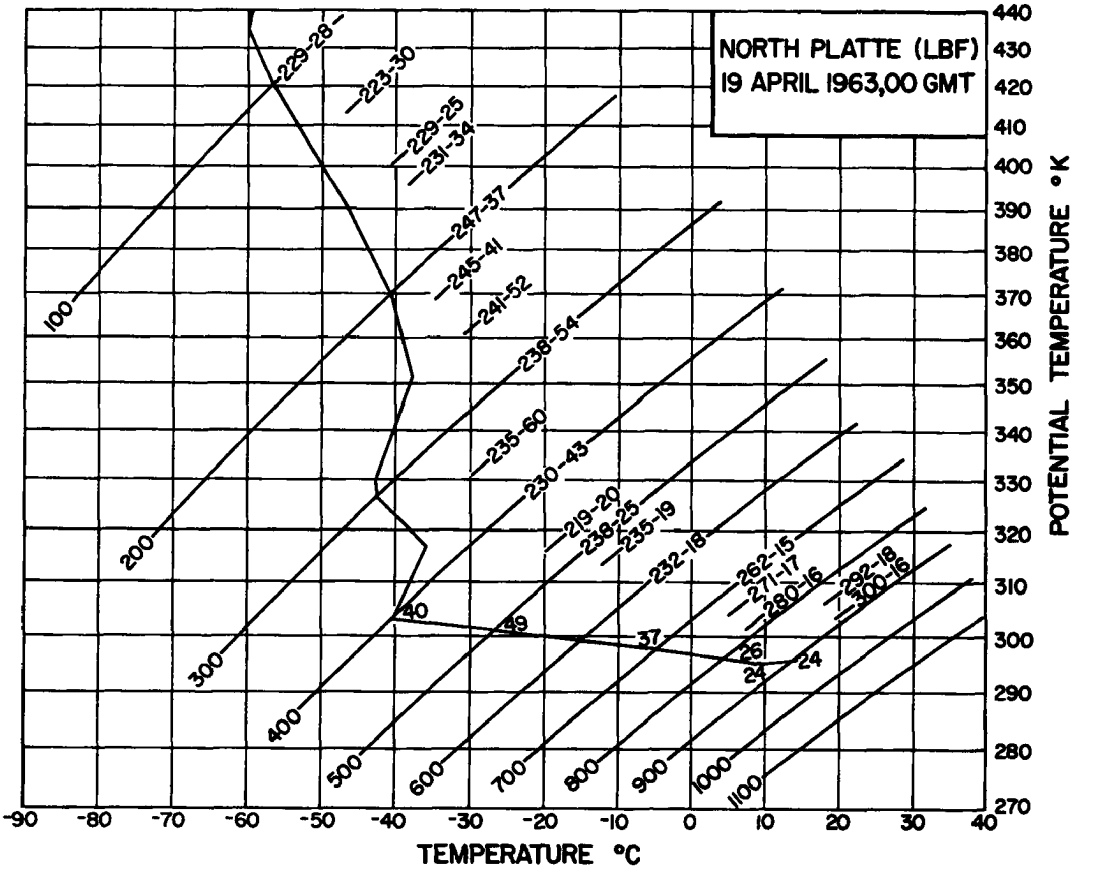

Fig. 18 : Temperature sounding for North Platte (LBF), 19 April,1963, 00 GMT, plotted on a tephigram. Relative humidities, wind directions, and wind speeds are given numerically along the sounding. Prefix "A" indicates a "motorboating" humidity value (after Reiter and Mahlman, 1965).

stationary,or moves only slowly as compared with the mean wind of the convection layer, one may attempt to compare the "wave length" in the cloud pattern with lee wave theory. According to this theory, the wave development is controlled by layers in which Lyra's parameter

$$\ell^2 = \frac{g}{\theta} \frac{\partial \theta}{\partial z} / V^2 \qquad (3)$$

shows a minimum. Scorer (for references see Reiter, 1963) has introduced an additional term $\frac{1}{V} \frac{\partial^2 V}{\partial z^2}$ which contains the curvature of the vertical wind profile and which is subtracted from the right-hand side of Eqn. 3. Since this term is difficult to evaluate in view of the rather crude wind measurements available from rawinsondes, it is usually neglected and the simplified form of Eqn. 3 is used for lee-wave estimates. It should be pointed out that ℓ is the vertical wave number, indicating the vertical separation of nodal surfaces in the atmosphere. It may be considered, however, to be of the same order of magnitude as the horizontal wave number.

From the sounding of North Platte, taken at 19 April,1963, 00 GMT, a minimum wave number $\ell = 2.1 \times 10^{-4}\ m^{-1}$ is observed in the layer between 400 and 500 mb underneath the inversion. This corresponds to a vertical wave length, $L_z = \frac{2\pi}{\ell}$, of 30 km.

The layer of convective clouds near North Platte is expected to extend through the lower troposphere up to the bottom of the inversion layer. The latter is found at approximately 7 km above the terrain. This is in good agreement with $\frac{L_z}{4}$ computed from Lyra's parameter. (This represents the distance between the ground which corresponds to the level of zero wave amplitude and the first level at which maximum wave amplitude is reached.) This suggests that the parallel alignment of cumulus congestus observed near North Platte is possibly controlled by a gravity-wave phenomenon acting over a deep tropospheric layer below the inversion at 400 mb.

Even though the clouds observed in the present case are not lenticular or lee-wave (moazagotl) clouds, it is quite possible that vertical motions in the relatively deep convection layer are controlled by thermal structure and vertical wind shears in a fashion similar to the one described by lee-wave theory. In view of the strong backing of wind with height observed in the convection layer over North Platte (Fig. 17), the actual three-dimensional trajectory pattern will be more complex in this region that two-dimensional lee-wave theory might predict.

From Fig. 12 which contains a section through the atmosphere that follows approximately the course of a stream line between Denver (DEN) and North Platte (LBF) at 19 April 00 GMT an upward bulge of the isentropic surfaces in the inversion layer is evident. This bulge has a half-wave length of approximately 320 km (full wave length ca. 640 km), and thus exceeds the wave length of gravity waves by at least one order of magnitude. Above the inversion layer the isentropic surfaces show a downward dip over North Platte. This suggests that the inversion layer at 7 km above the terrain constitutes a nodal surface with respect to vertical motions of a scale larger than lee waves.

From isentropic analysis it was found that the cloud region near North Platte also appeared as a wave in quasi-horizontal planes between 18 April, 1963, 12 GMT and 19 April, 12 GMT with nearly the same wave length as indicated above. The quasi-stationary nature of this wave phenomenon strongly suggests an orographic control. Assuming that the main range of the Rocky Mountains gave rise to this wave formation, mainly by frictional effects on the tropospheric flow, we may compute the inertial wave length from the equation

$$L_{is} = \frac{2\pi}{f} \bar{u} \qquad (4)$$

Assuming $\bar{u}$ = 20 mps as mean speed of the tropospheric layer below the inversion, over which we may assume that frictional effects

showed their influence in the chinook region described earlier, we arrive at $L_{is} \tilde{=} 1340$ km. This is much longer than the values of L_{is} measured from the isentropic lines of the cross section in Fig. 12. If we substitute wind speeds at the inversion level for $\bar{u}$, we would arrive at even larger wave lengths. From these estimates it appears that the observed wave and cloud formation near North Platte cannot be regarded as a simple inertia phenomenon.

A mathematical treatment of inertial gravity waves on sloping interfaces is extremely complex. To obtain an order-of-magnitude estimate of wave lengths that may be observed in this spectrum region of atmospheric disturbances we may follow a rather crude approach, outlined by Godske et al. (1957, p. 343):

The frequency of inertial waves is given by

$$\nu_i^2 = f^2 \tag{5}$$

f being the Coriolis parameter. The imaginary frequency of short (gravitational) shearing waves may be expressed as

$$\nu_g^2 = -\frac{\pi^2}{L^2}(V - V')^2 \tag{6}$$

where V and V' stand for wind speeds on either side on the interface separating the shearing layer. It is assumed that a combination of both wave effects would produce a frequency

$$\nu^2 = \alpha_1 f^2 - \alpha_2 \frac{\pi^2}{L^2}(V - V')^2 \tag{7}$$

α_1 and α_2 being factors which depend on the kinematics of the fluid system. Assuming furthermore that $\frac{\alpha_1}{\alpha_2} \tilde{=} 1$ we may derive a critical wavelength for which $\nu = 0$

$$L_c = \frac{\pi (V' - V)}{f} \tag{8}$$

For an order-of-magnitude estimate we may consider the bottom of the inversion layer over North Platte on 19 April 00 GMT as a zero-order discontinuity in wind speeds. Taking the wind

speed below the inversion as 25 mps, the wind speed in the inversion layer as 45 mps (see Fig. 13), we arrive at L_c = 650 km. Although the assumptions underlying this estimate are very crude, it agrees with the large-scale wave length observed along isentropic surfaces in the cloud region near North Platte. As has been mentioned before, one may attribute the quasi-stationary character of this wave to orographic effects, produced by the passage of the stable layer over the Continental Divide, and by the strong vertical mixing in the troposphere underneath the inversion in the chinook conditions described earlier.

From the preliminary investigation conducted here it appears that several factors may have contributed to the observed cloud distribution near North Platte:

(a) Development of a wave of considerably shorter length than should be expected from a pure inertial wave.

(b) If a gravity-inertial wave mode may be held responsible for the observed large-scale wave development, characteristic vertical motion patterns are to be expected in the lower troposphere underneath the inversion. Ascending motions should occur to the west and over North Platte (LBF), according to the wave-configuration in Figs. 12 and 13. This is in excellent agreement with the observed cloud distribution of Figs. 3 and 15.

(c) Upward motion in this region should--for reasons of continuity--be associated with low-level convergence. According to Figs. 7 and 9, this condition is met in the area under consideration.

(d) Superimposed upon this synoptic-scale wave phenomenon are meso-scale "waves" of considerably smaller lengths (ca. 28 km). These "waves" are controlled by the stability and shear characteristics of the tropospheric layer below the inversion in which vertical mass and momentum exchange due to convective motions is present. These smaller waves appear to agree well with lee-wave theory, suggesting that the arrangement of convective clouds (cumulus congestus) may be controlled by a slow-moving (or standing) gravity-wave phenomenon. The observed changes of wind direction with height is expected to lead to a more complex trajectory pattern than the one suggested by two-dimensional lee-wave theory.

Further investigations of these and similar wave patterns appearing on TIROS photographs will have to be made in order to gain an insight into the

structure and dynamic properties of the atmosphere which cause the formation of such waves.

(4) Baroclinic Wave Formation.

Fig. 19 shows Frame No. 7 of orbit 3070 (Tape), TIROS VI, taken at 1819 GMT on 16 April, 1963. Frontal positions have been entered in this photograph. A weak cold front extends from Columbia (CBI), Missouri, to Oklahoma City (OKC), Oklahoma. According to the surface weather map of 18 GMT on the same day, there was no temperature gradient across the front near the earth's surface. Temperatures ranged in the low eighties (^{o}F) on either side of the front. Wind shifts associated with the passing front also were hardly noticeable. The air mass boundary was very well marked, however, in the dew-point spread (i. e. the difference in the air temperature and the dew point). The air between the eastern slopes of the Rocky Mountains and the cold front is very dry, especially to the southeast of the weak low-pressure system located over Colorado (Fig. 20). This moisture distribution is rather similar to the one described earlier in connection with chinook winds (see Figs. 6 to 9).

The cloud pattern in Fig. 19 shows a peculiar "bulge" which does not yet appear in the surface frontal position of 18 GMT on 16 April. A frontal wave is indicated, however, on the 21 GMT surface map of April 16, amplifying within the next 6 hours (Fig. 21).

From a comparison of the TIROS photograph (Fig. 19) with surface weather maps it appears that baroclinic wave formation in the tropospheric flow pattern precedes cyclogenesis near the earth's surface. This sequence of events is postulated by the "vorticity advection theory" of cyclone formation, whereby upper-tropospheric flow through a pronounced vorticity pattern causes a characteristic distribution of divergence and convergence areas which, in turn, result in surface pressure falls and rises. With a 12-hour spacing of upper-air information from radiosondes it is difficult, however, to substantiate a clear-cut "chain of events". With the time resolution of upper-air synoptic data the meteorologist can usually better establish simultaneous rather than sequential facts.

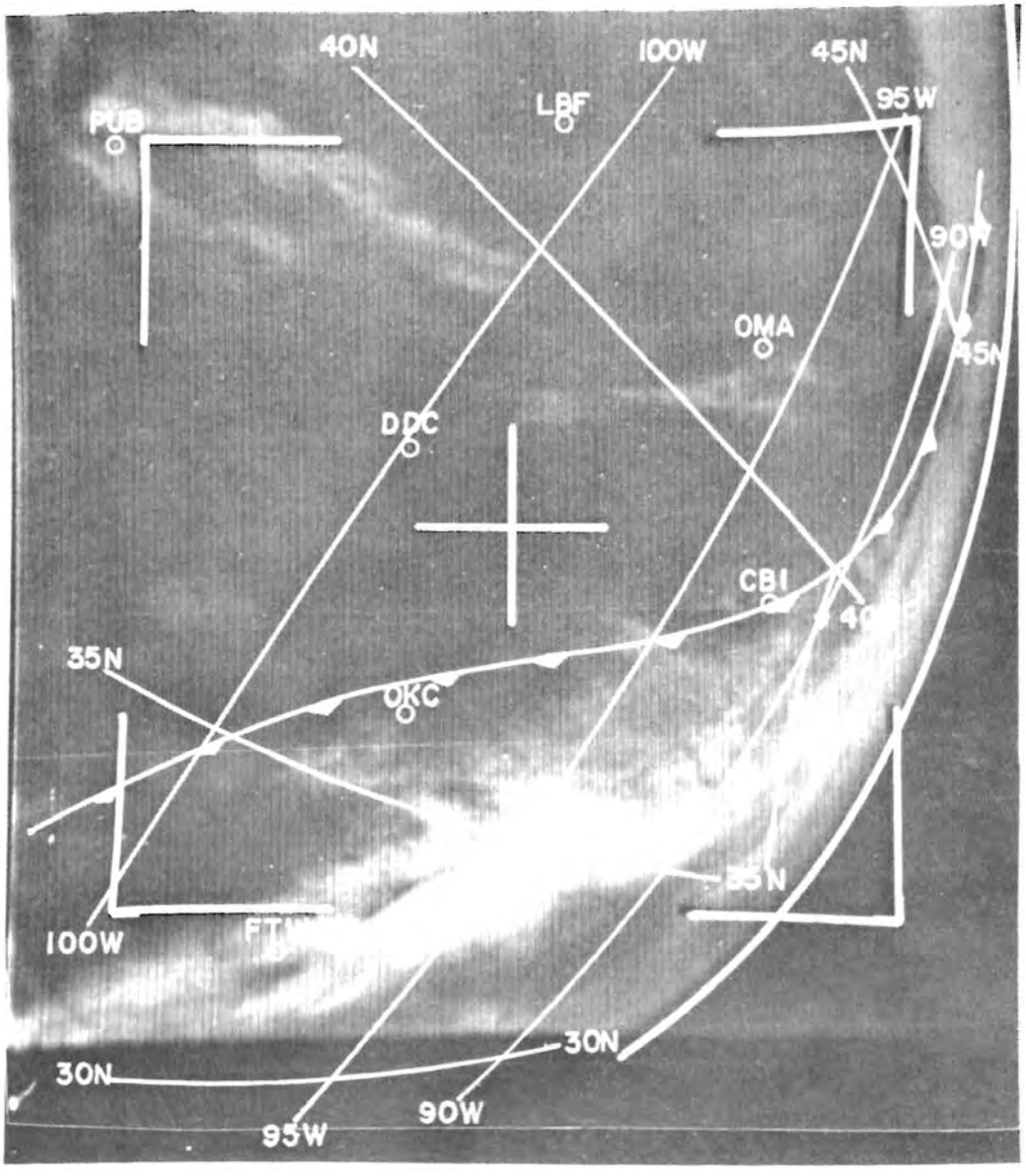

Fig. 19: Cloud photograph, TIROS VI orbit 3070 (Tape) Frame 7, 16 April, 1963, 1819 GMT.

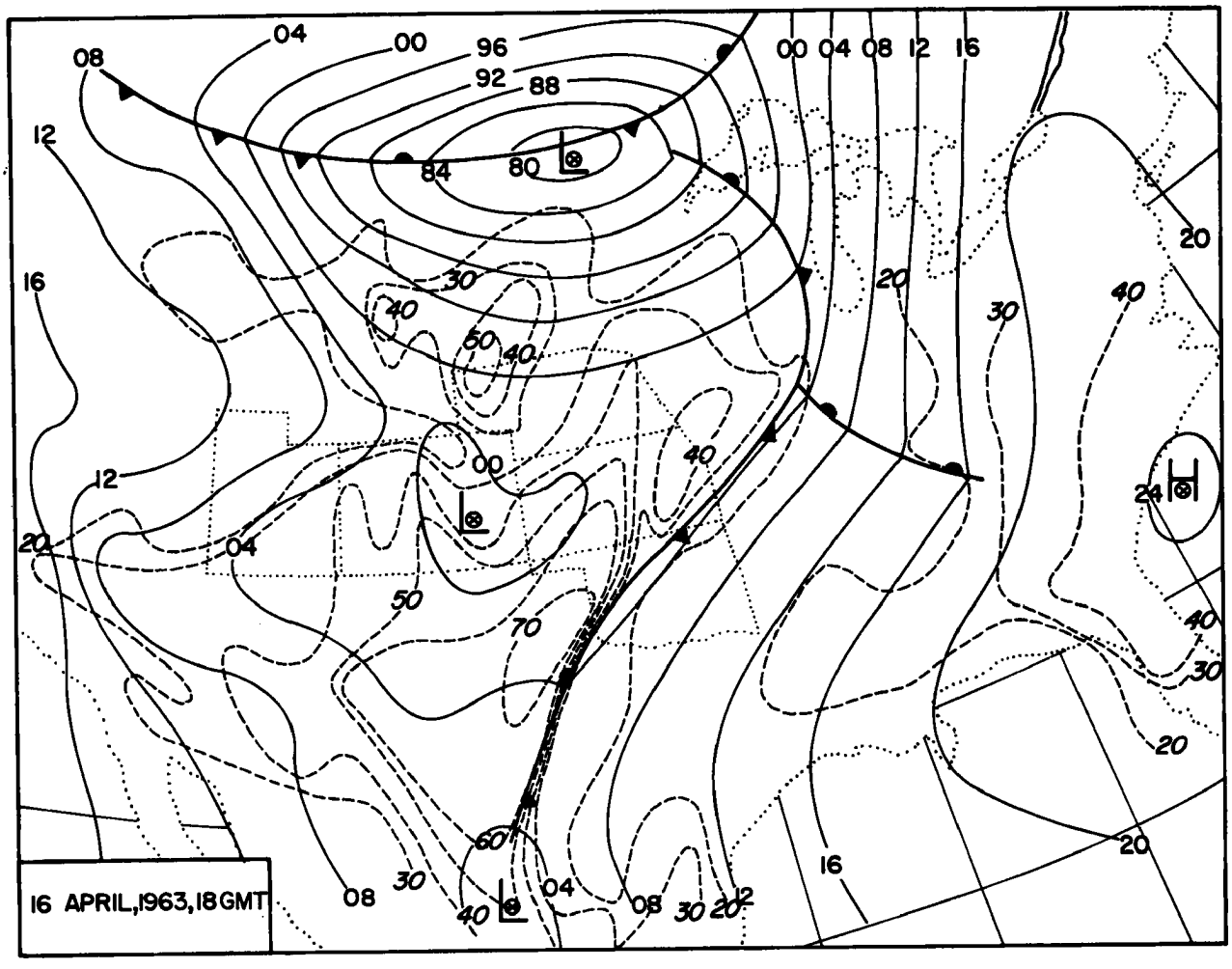

Fig. 20: Surface pressure distribution (mb, solid lines), frontal positions, and dew point spread (^{o} F, dashed lines) of 16 April, 1963, 18 GMT.

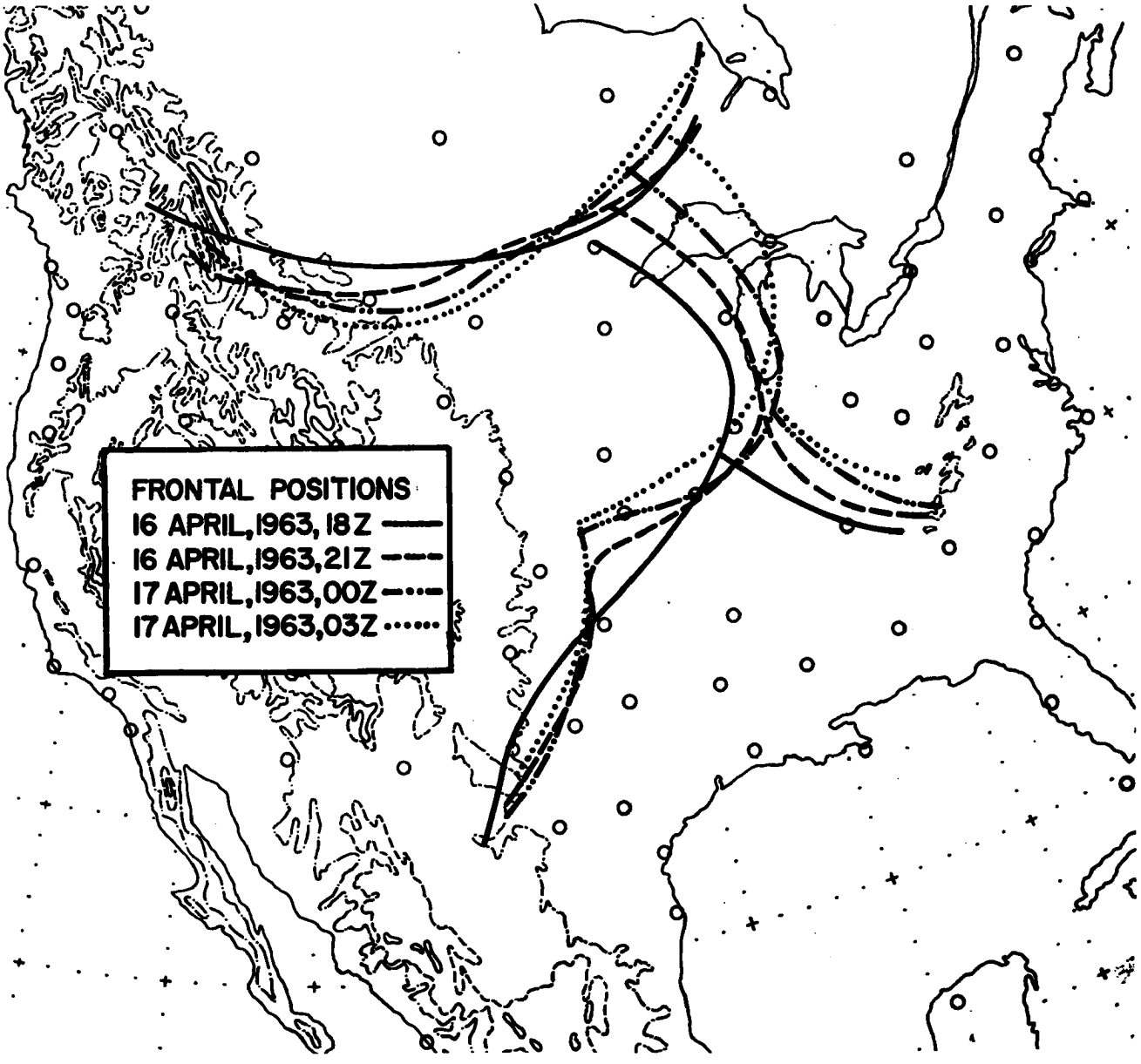

Fig. 21: Frontal positions for 3-hour intervals between 16 April, 1963, 18 GMT and 17 April, 1963, 13 GMT.

The incipient wave near Oklahoma City is associated with a rather complex high-tropospheric flow pattern. Fig. 5 a shows the 250-mb isotachs and isotherms of 17 April 00 GMT. Three distinct southwesterly jet-stream branches are evident from this analysis. An isotach analysis on the 330 K isentropic surface reveals a similar triple jet stream arrangement. This isentropic surface cuts through the cores of the southern two jet branches. The formation of a baroclinic wave seems to be associated with a wind-speed maximum along the southeastern-most jet branch. The dense clouds seen to the south of the cold front in the TIROS photograph of Fig. 19 are associated with this jet stream.

The center one of the three jet stream branches flows slightly poleward from the occlusion points of the two frontal waves appearing on the surface maps (Fig. 21). Cirrus clouds reported between Pueblo (PUB), Colorado, and Omaha (OMA), Nebraska, are located along this jet stream. Along the anticyclonic side of its axis they are dense enough to appear on the TIROS photograph of Fig. 19.

The cross section through the atmosphere from Lander (LND), Wyoming, to Burrwood (BRL), Louisiana, of 17 April,1963, 00 GMT (Figs. 22 a and 23 a) corroborates the multiple jet-stream structure seen on the 250-mb map. This cross-section also reveals the dry conditions behind the cold front. Dodge City (DDC), Kansas, reports "motorboating" of the humidity sensor (indicated by letter "A" in the cross section) above the 900-mb level.

The region south of Oklahoma City (OKC) shows two layers with relatively high humidities, one near 850 mb, and one near 500 mb. Aviation Weather Reports from OKC on 16 April. 18 GMT indicate scattered clouds at 3500 and 10000 ft, broken clouds at an unspecified higher level. The surface weather map at this observation time indicates stratocumulus over OKC. Broken clouds at 3000 ft are observed over Tulsa, Oklahoma, about 100 n. miles to the northeast of Oklahoma City, and overcast skies with cloud bases of 2300 ft are reported over Fort Smith, Arkansas. (ca. 150 n. miles east of OKC).

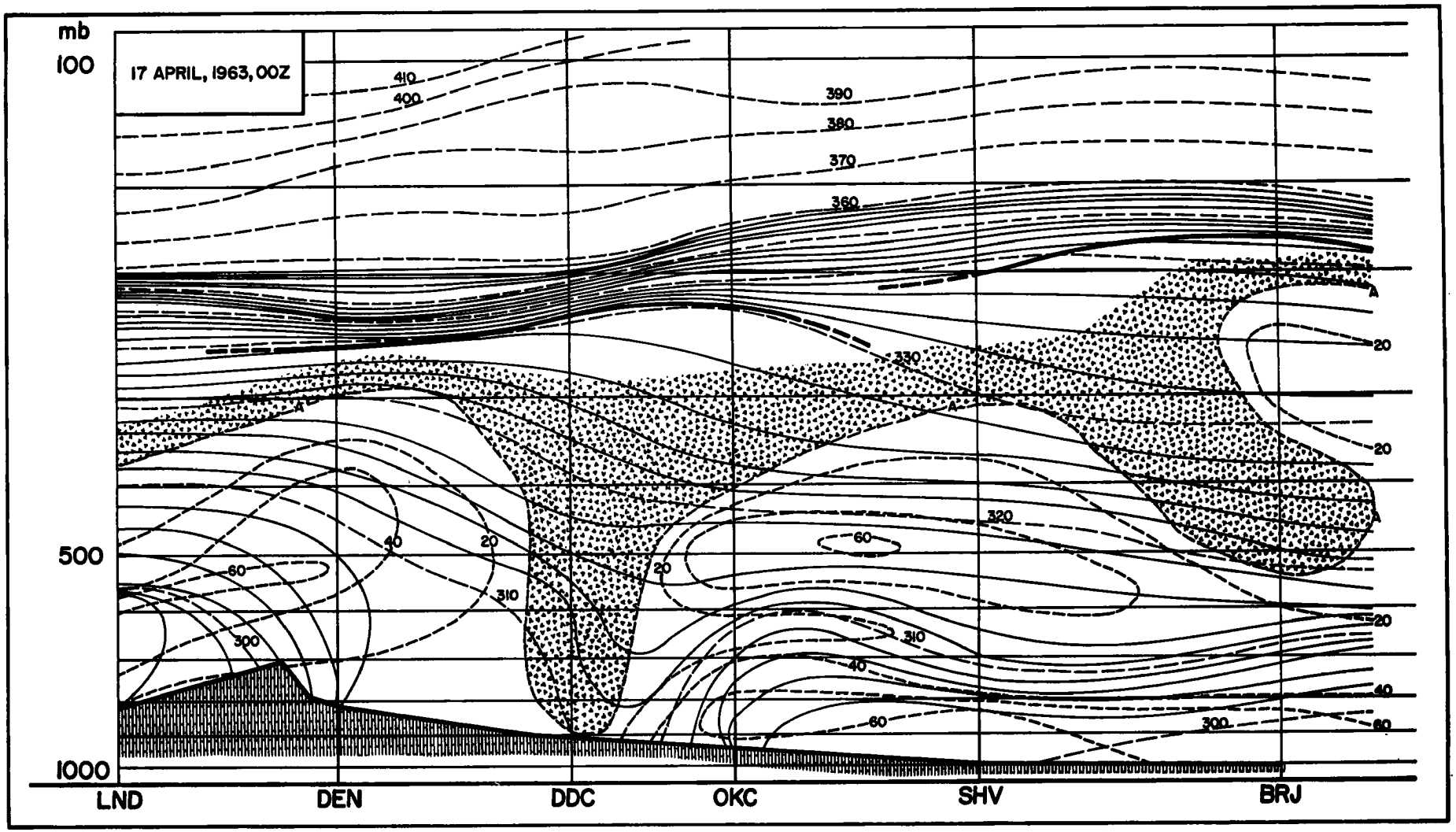

Fig. 22 a: Cross sections through the atmosphere, from Lander (LND), Wyoming, to Burrwood (BRJ), Louisiana: Potential temperature (^{o}K, solid and long-dashed lines), and relative humidities (per cent, short-dashed lines. "A" indicates "motorboating"). Stable layers and tropopause are marked by heavy dashed and solid lines (DEN = Denver, Colorado; DDC = Dodge City, Kansas; OKC = Oklahoma City, Oklahoma; SHV = Shreveport, Louisiana).

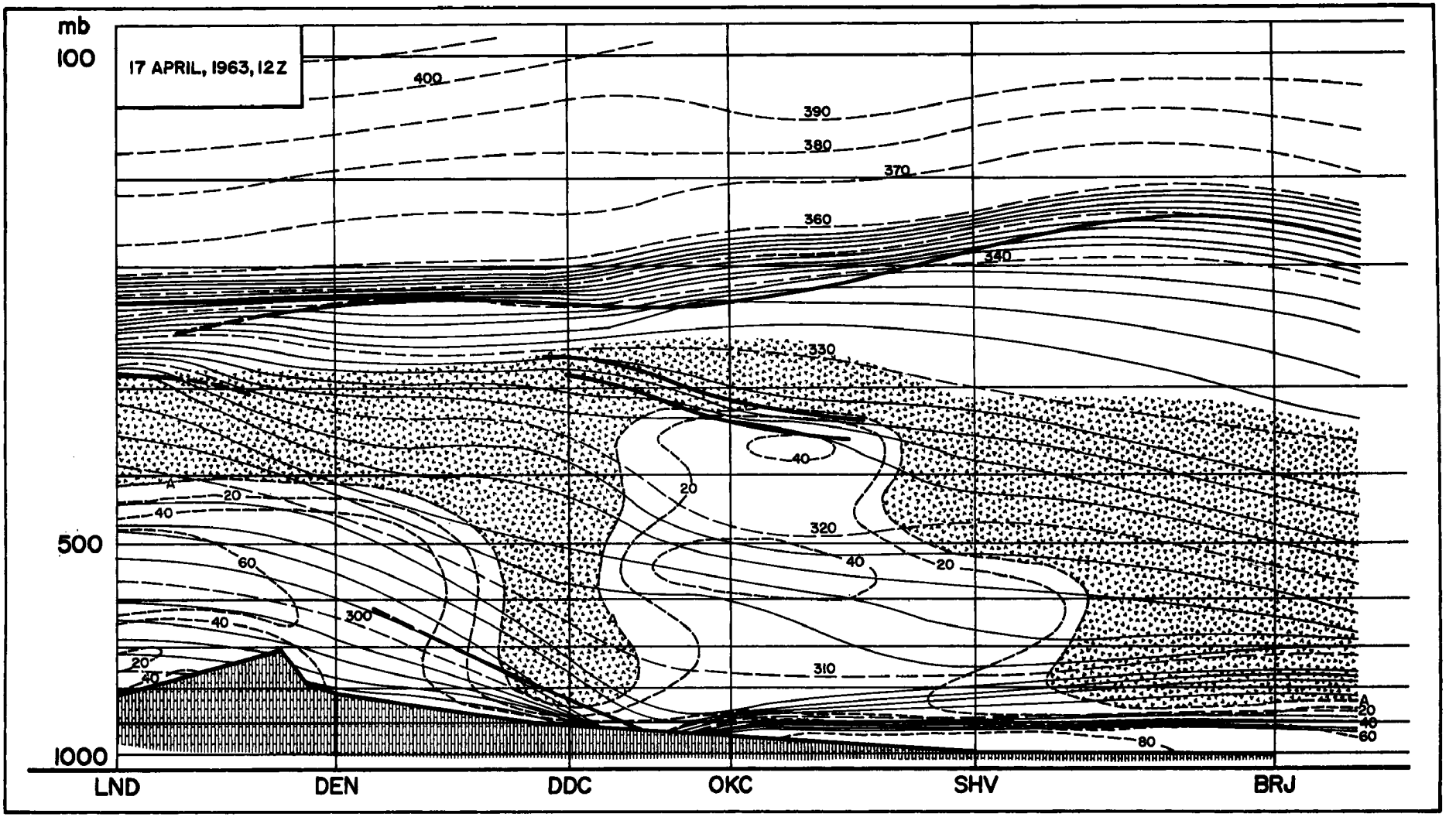

Fig. 22 b: Cross section through the atmosphere, from Lander (LND), Wyoming, to Burrwood (BRJ), Louisiana: Potential temperature (^{o}K, solid and long-dashed lines), and relative humidities (per cent, short-dashed lines. "A" indicates "motorboating"). Stable layers and tropopause are marked by heavy dashed and solid lines (DEN = Denver, Colorado; DDC = Dodge City, Kansas; OKC = Oklahoma City, Oklahoma; SHV = Shreveport, Louisiana).

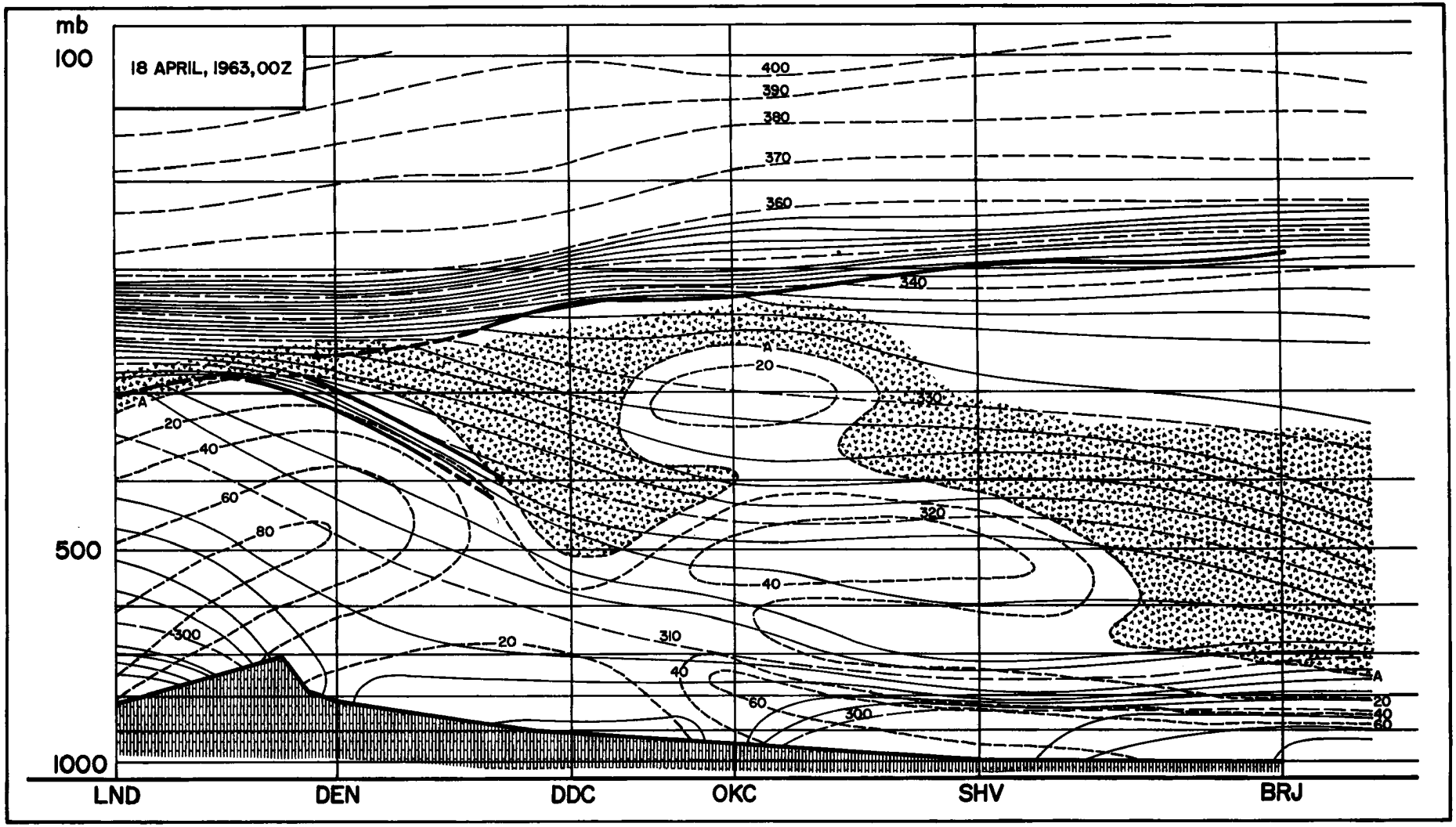

Fig. 22 c: Cross section through the atmosphere for dates and observation times as indicated. (LND = Lander, Wyoming; DEN = Denver, Colorado; DDC = Dodge City, Kansas; OKC = Oklahoma City, Oklahoma; SHV = Shreveport, Louisiana; BRJ = Burrwood, Louisiana.) Potential temperatures: ^{o}K, solid and long-dashed lines; relative humidities: per cent, short-dashed lines. "A" indicates "motorboating". Stable layers and tropopause are marked by heavy dashed and solid lines.

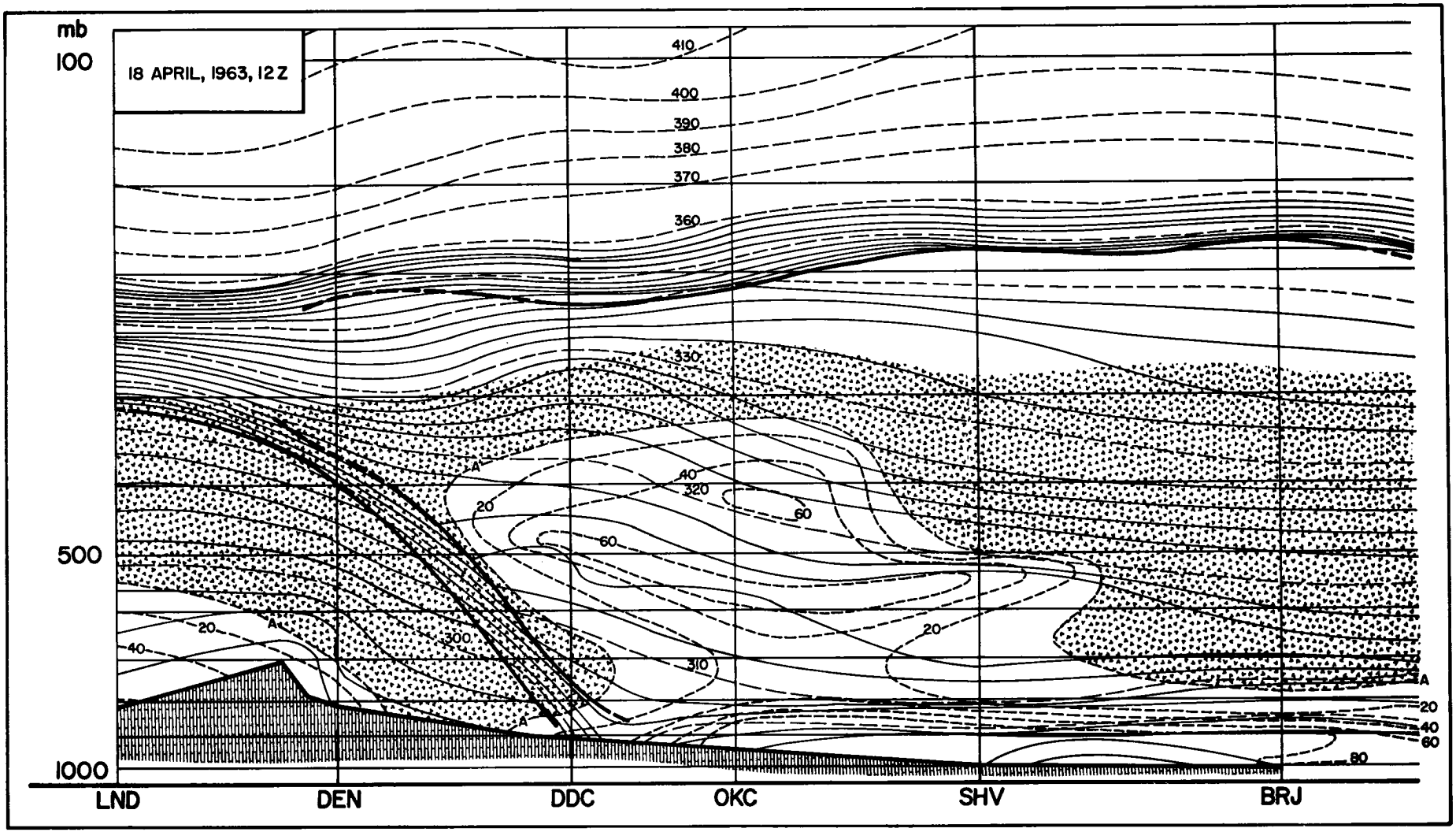

Fig. 22 d: Cross section through the atmosphere for dates and observation times as indicated. (LND = Lander, Wyoming; DEN = Denver, Colorado; DDC = Dodge City, Kansas; OKC = Oklahoma City, Oklahoma; SHV = Shreveport, Louisiana; BRJ = Burrwood, Louisiana.) Potential temperatures: ^{o}K, solid and long-dashed lines; relative humidities: per cent, short-dashed lines. "A" indicates "motorboating". Stable layers and tropopause are marked by heavy dashed and solid lines.

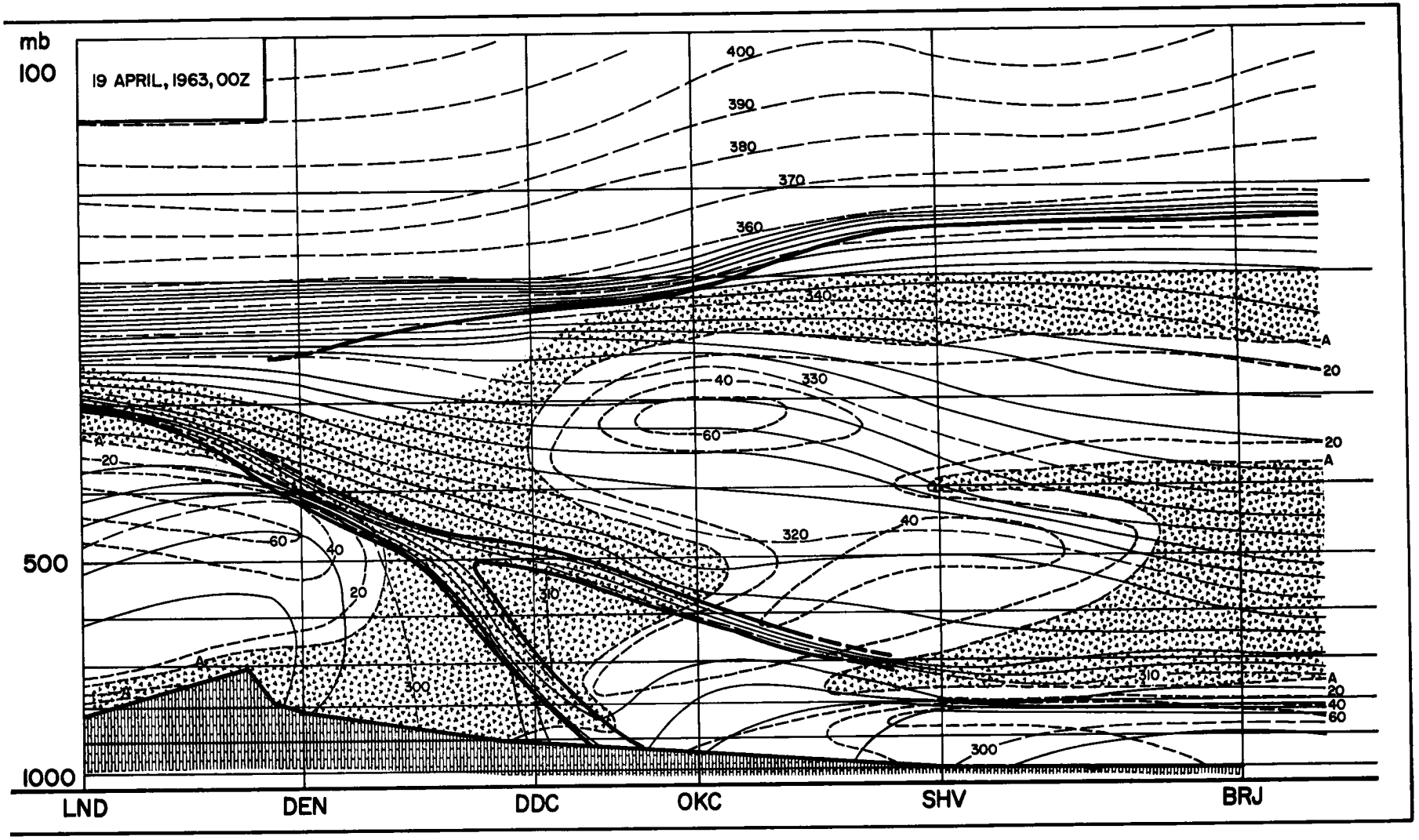

Fig. 22 e: Cross section through the atmosphere for dates and observation times as indicated. (LND = Lander, Wyoming; DEN = Denver, Colorado; DDC = Dodge City, Kansas; OKC = Oklahoma City, Oklahoma; SHV = Shreveport, Louisiana; BRJ = Burrwood, Louisiana.) Potential temperatures: °K, solid and long-dashed lines; relative humidities: per cent, short-dashed lines. "A" indicates "motorboating". Stable layers and tropopause are marked by heavy dashed and solid lines.

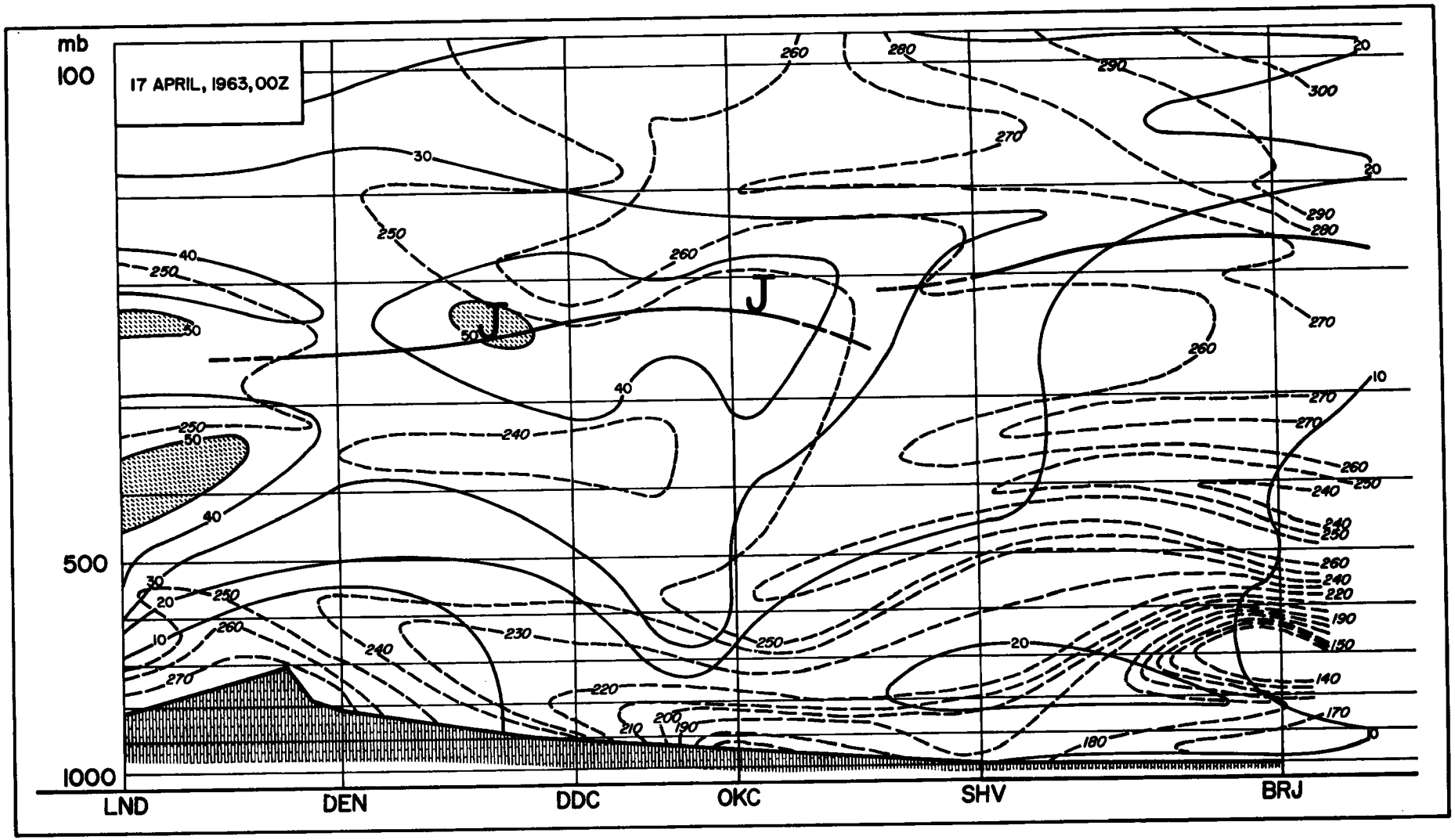

Fig. 23 a: Cross section through the atmosphere, from Lander (LND), Wyoming, to Burrwood (BRJ), Louisiana: wind speeds (mps, solid lines) and wind directions (degrees, dashed lines). Regions with speeds > 50 mps are shaded. (For station abbreviations see legend to Fig. 22 a).

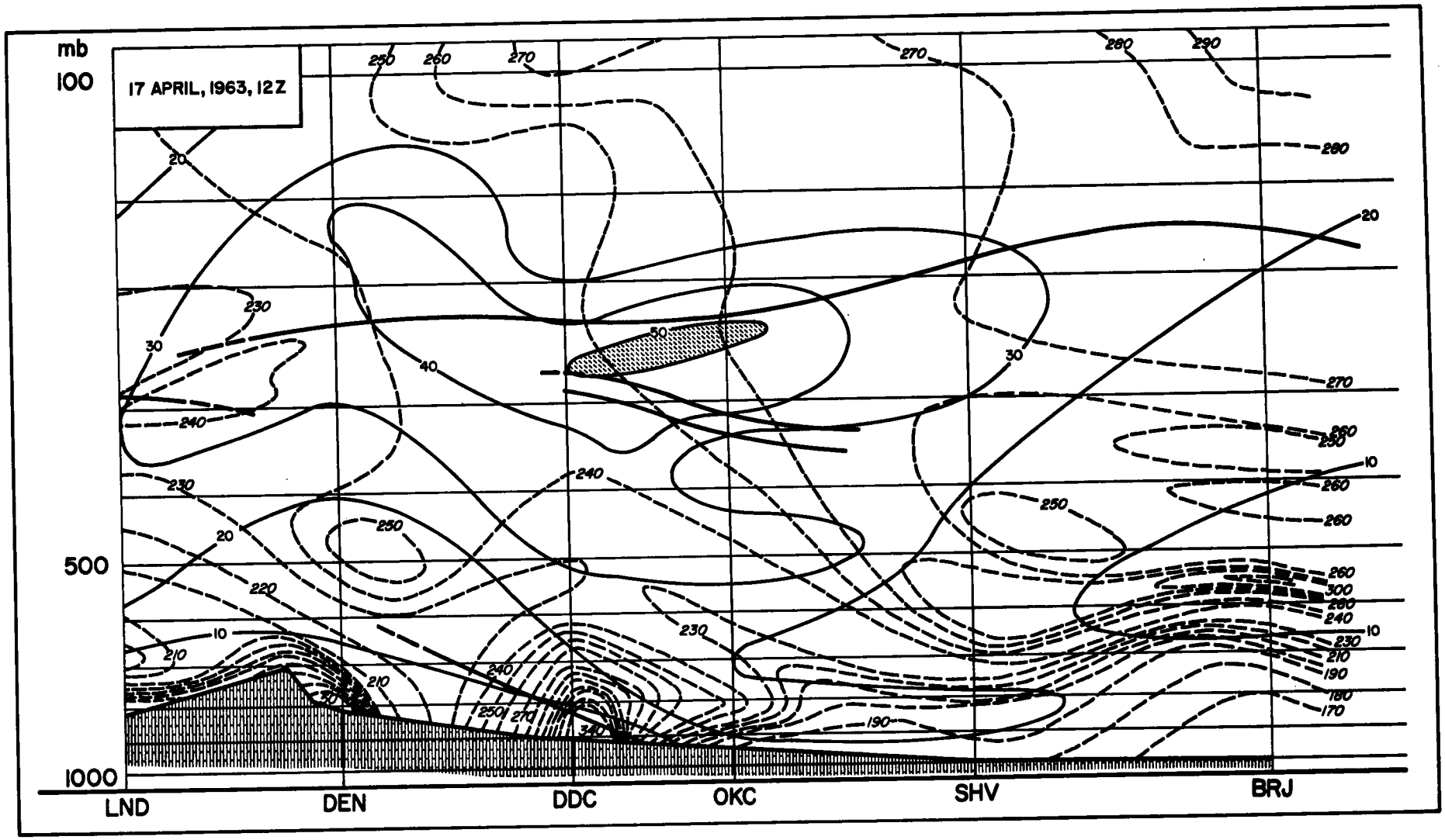

Fig. 23 b: Cross sections through the atmosphere, from Lander (LND), Wyoming to Burrwood (BRJ), Louisiana: wind speeds (mps, solid lines) and wind directions (degrees, dashed lines).

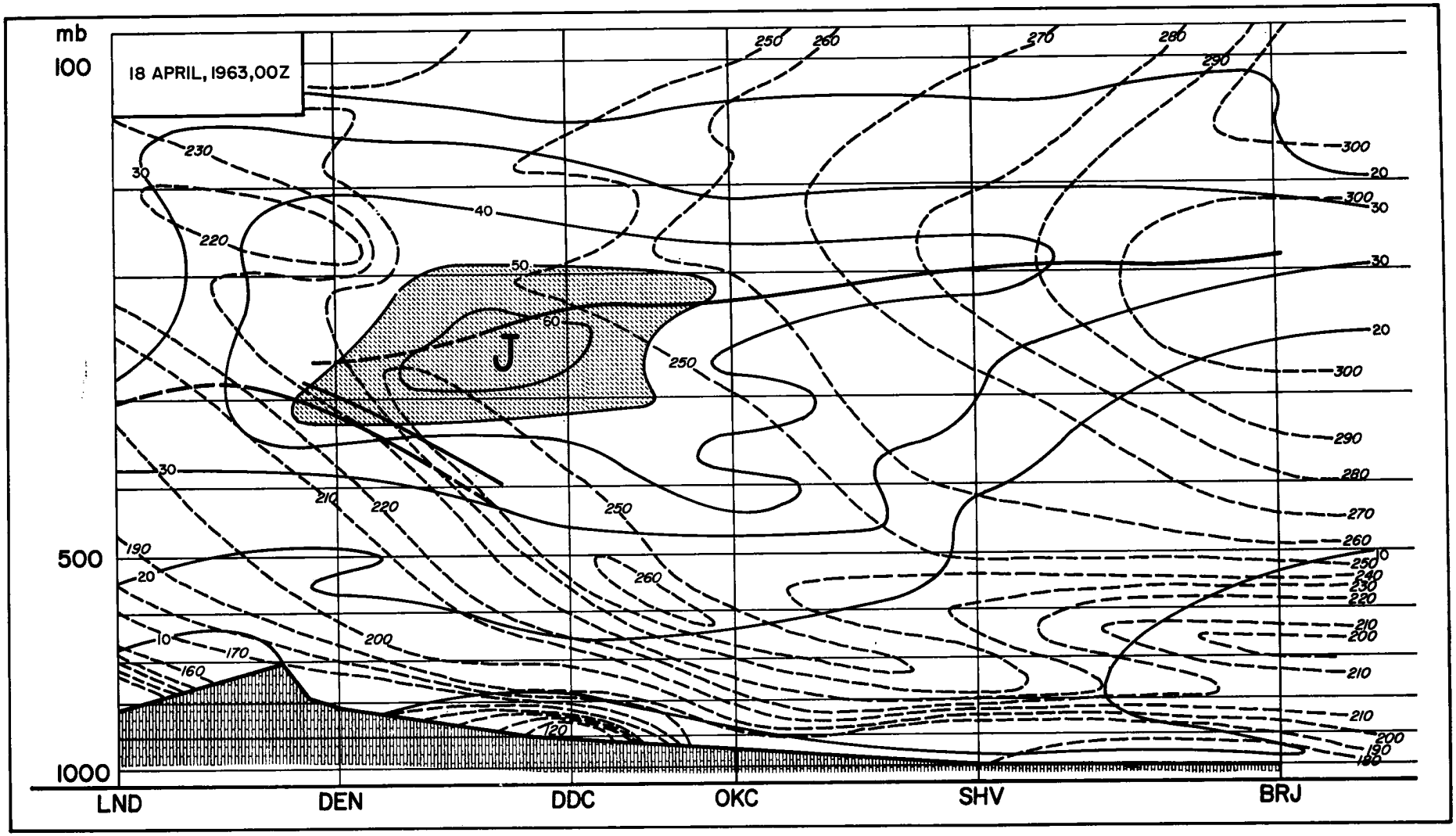

Fig. 23 c: Cross sections through the atmosphere, from Lander (LND), Wyoming, to Burrwood, Louisiana: wind speeds (mps, solid lines) and wind directions (degrees, dashed lines).

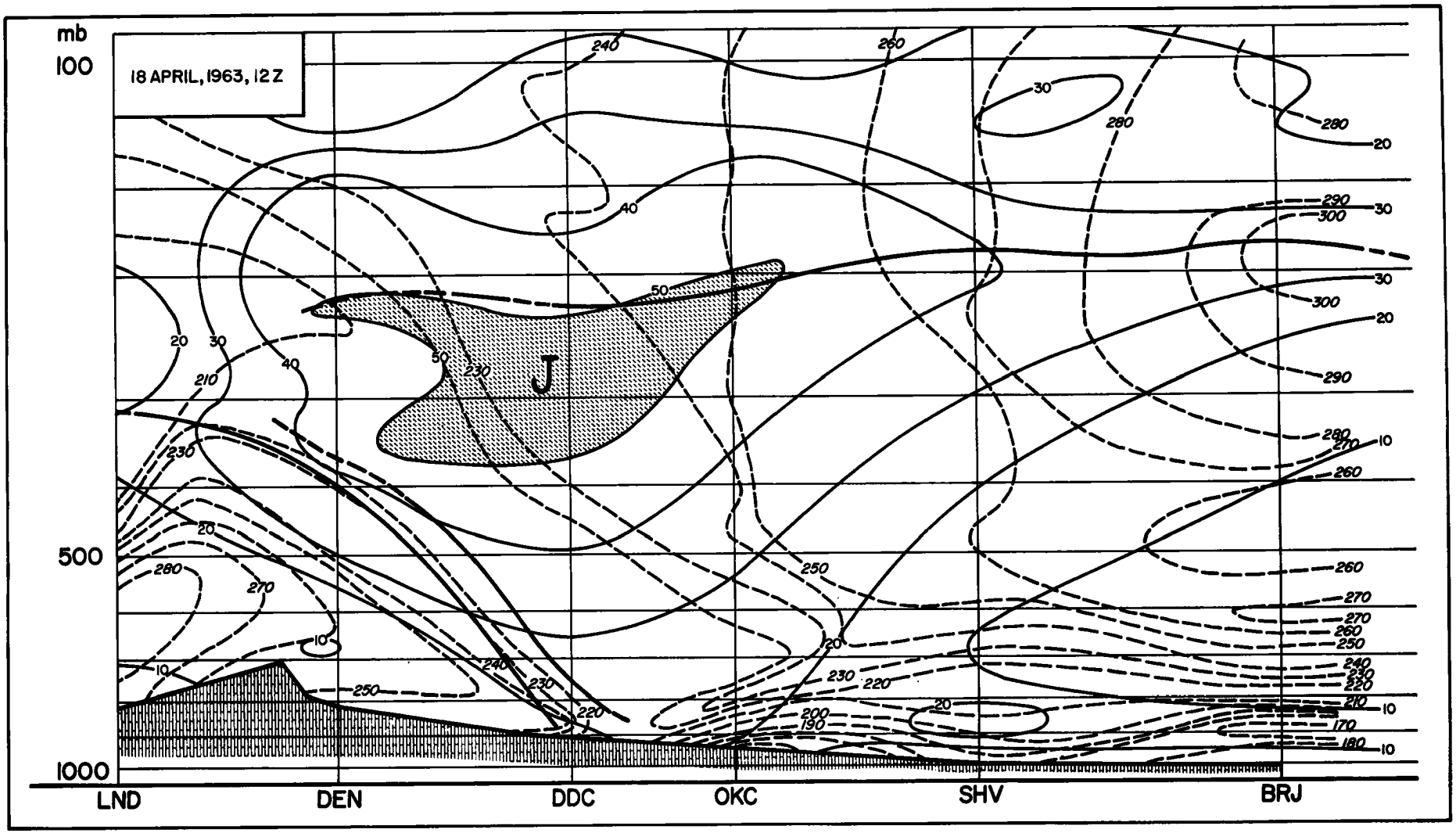

Fig. 23 d: Cross sections through the atmosphere, from Lander (LND), Wyoming, to Burrwood (BRJ), Louisiana: wind speeds (mps, solid lines) and wind directions (degrees, dashed lines).

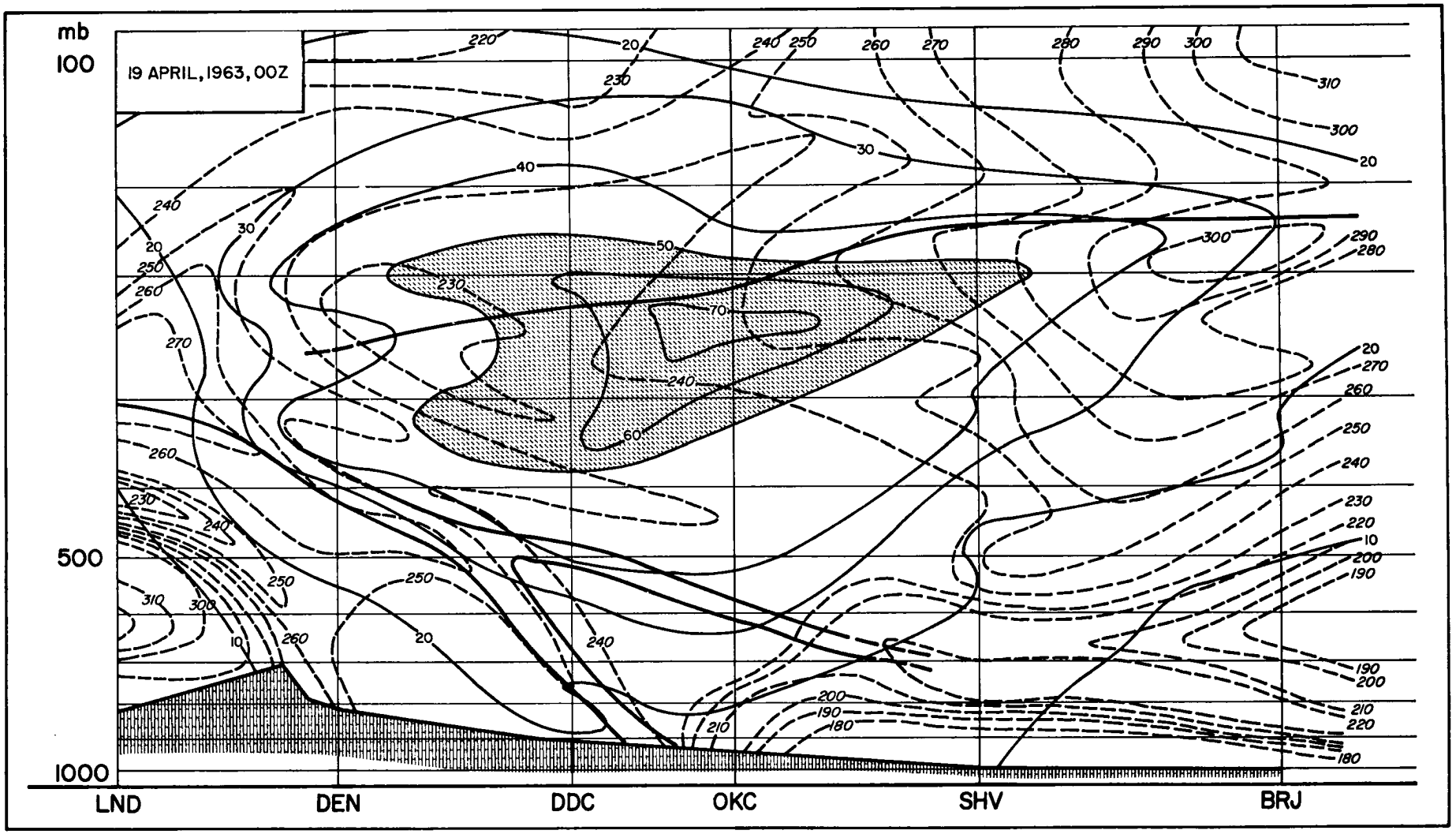

Fig. 23 e: Cross sections through the atmosphere, from Lander (LND), Wyoming, to Burrwood (BRJ), Louisiana: wind speeds (mps, solid lines) and wind directions (degrees, dashed lines).

On the TIROS photograph (Fig. 19) the low level broken clouds appear as a gray area slightly to the south of the cold front between OKC and CBI. After 21 GMT on 16 April, OKC reports only broken clouds at high levels, in all probability thin cirrus, as reported by several stations located behind the cold front on the 18 GMT surface map.

The extremely brilliant cloud band in Fig. 19 extending from Fort Worth (FTW), Texas, northeastward is made up by cumulo-nimbus clouds, in agreement with the following Area Forecast issued in the Aviation Weather Reports by the Kansas City Fore-Cast Center:

"Tornado Forecast: Along and 60 miles either side of a line from Mineral Wells, Texas (close to FTW), to 30 miles southeast of Fort Smith, Arkansas. Valid 1700 to 2300 GMT." It is this area of bright clouds in Fig. 19 that gives the first indication of baroclinic wave formation. Cumulo-nimbus tops in the area were expected to reach 50,000 ft. Since the tropopause was reported at 201 mb (ca. 36,500 ft) over Oklahoma City (OKC), only violent convective activity could account for such deep penetration of clouds into the stratosphere.

From the expression

$$D = \frac{\partial V}{\partial s} + V \frac{\partial \phi}{\partial n}$$

divergence values have been computed at the 250-mb level (s and n indicate natural coordinates along, and normal to, the stream lines; ϕ is the angle between stream lines and a certain reference stream line). The divergence and convergence patterns for this pressure surface are shown in Fig. 24 for 16 April 12 GMT and 17 April 00 GMT.

Apparently the frontal wave starts forming as a region of divergence in the upper troposphere (Fig. 24) becomes super-imposed upon the surface front. This, again, is in agreement with cyclone theories. The cirrus clouds between Pueblo (PUB) and Omaha (OMA), shown in Fig. 19 agree well with a region of

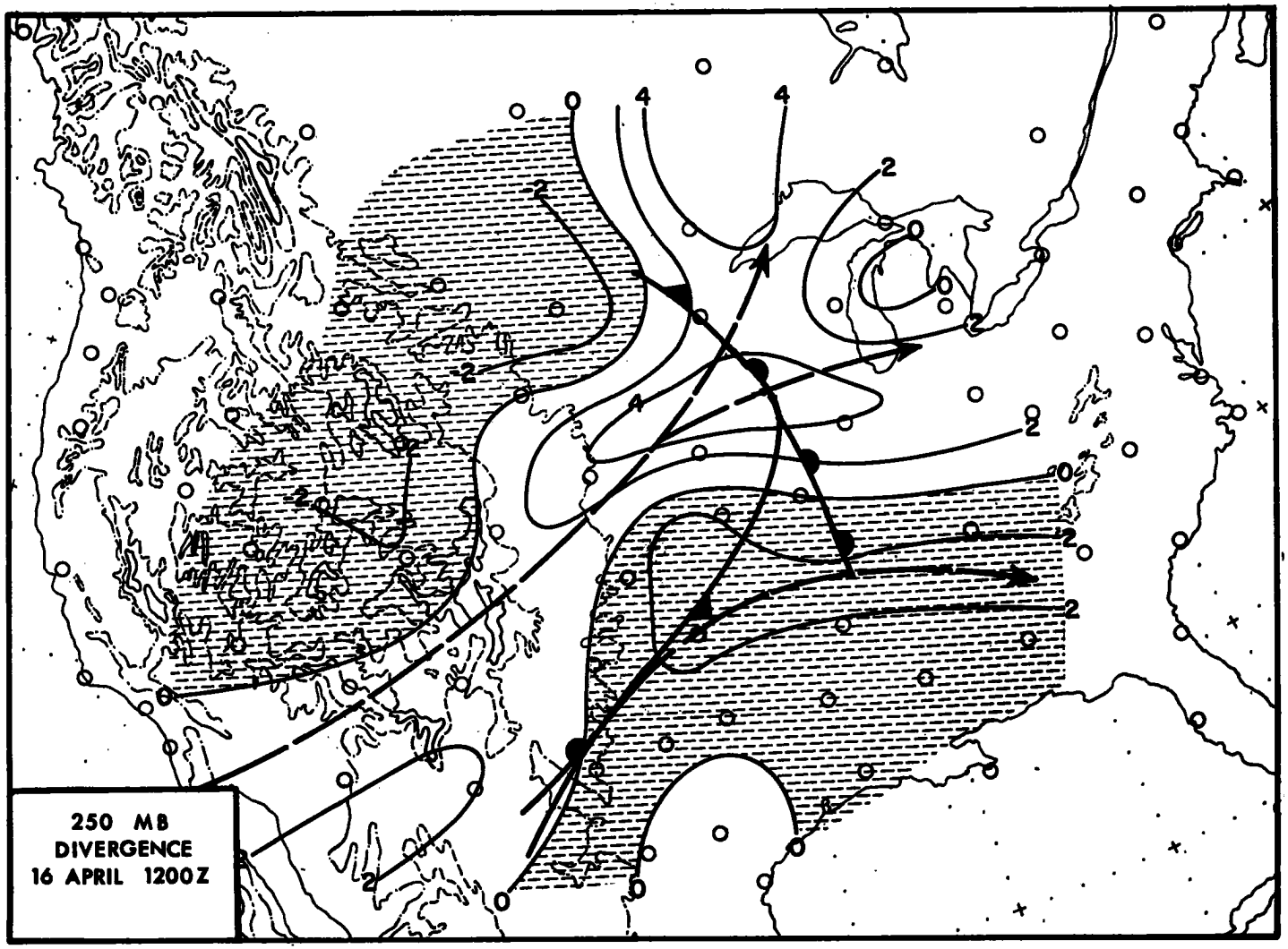

Fig. 24 a: Divergence (10^{-5} sec^{-1}) (solid lines) and jet streams (long dashed lines) on 250-mb surface. Frontal positions from surface map. Valid at 16 April, 1963, 12 GMT. Convergent areas are shaded.

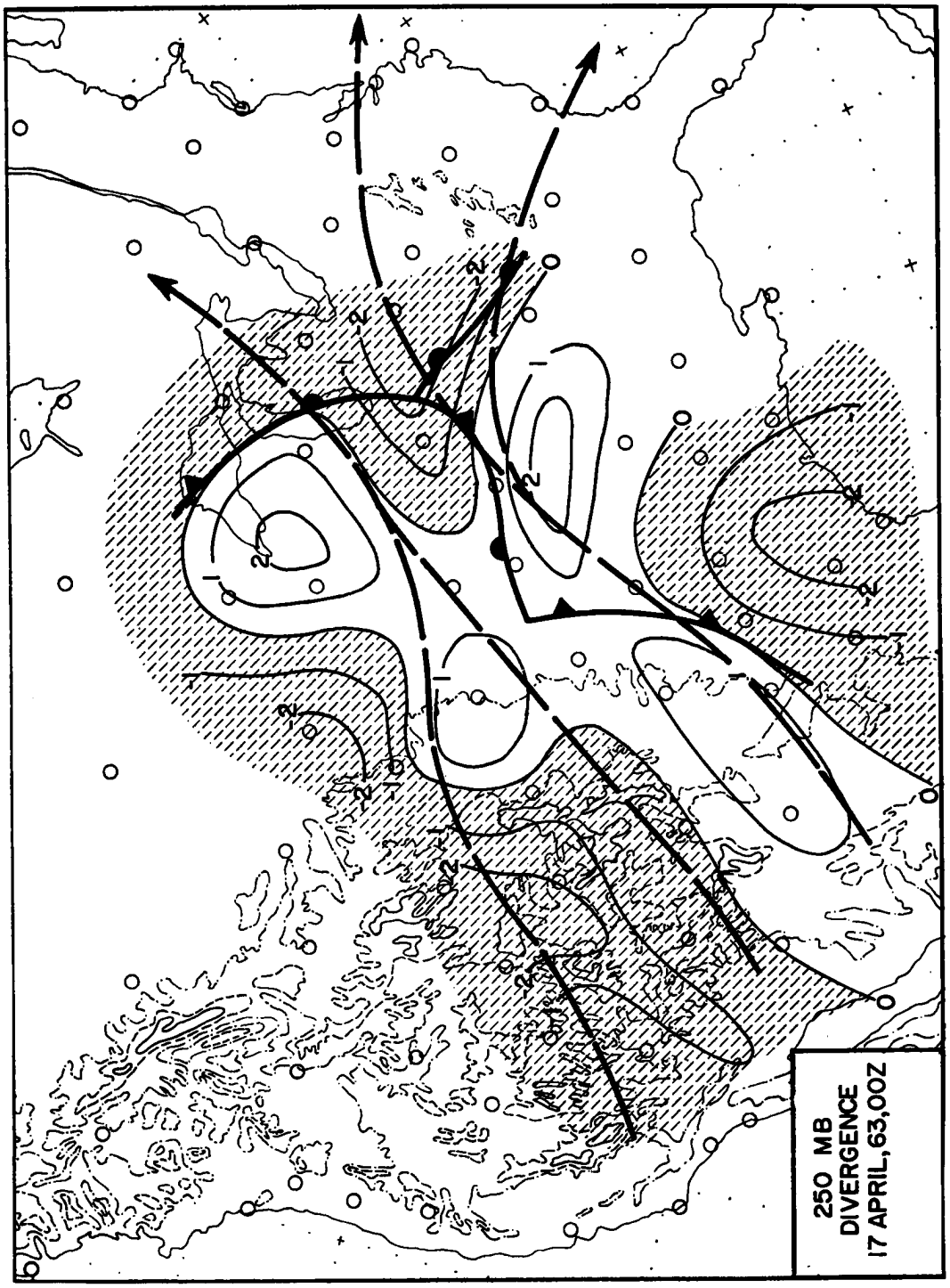

Fig. 24 b: Divergence (10^{-5} sec^{-1}) (solid lines) and jet streams (long dashed lines) on 250-mb surface. Frontal positions from surface map. Valid at 17 April, 1963, 00 GMT.

upper divergence. The region of dense cumulonimbus clouds east of Oklahoma City (OKC) appears to coincide with an area in which upper convergence (Fig. 24 a) is replaced by upper divergence (Fig. 24 b).

Surface pressure tendencies between 16 April 21 GMT and 17 April 00 GMT associated with the wave formation are shown in Fig. 25 in a relative coordinate system, moving with the occlusion point of the newly-forming wave. Strongest pressure falls are measured in the wave itself, corroborating the observed deepening tendency. Again, there is good agreement with the divergence pattern aloft.

More detailed studies on the correlation between observed cloud distributions and flow patterns near the incipient wave and the multiple jet streams will be undertaken.

(5) Cloud Bands and Jet Streams.

It has already been mentioned in the previous section that cirrus clouds between Pueblo (PUB) and Omaha (OMA) in Fig. 19 are oriented along a jet stream branch.

A more pronounced cloud band is shown on TIROS V frame No. 14, orbit 4349 (Tape) taken at 1955:30GMT on 18 April, 1963 (Fig. 3) extending along but not quite parallel to the cold front, which has been superimposed on this photograph. Fig. 5 c shows the 250 mb isotachs and isotherms of 19 April,1963, 00 GMT.

The jet axes from this analysis have been entered in Fig. 26, together with the surface frontal positions of 18 April 21 GMT, and the position of the cloud band as seen from the TIROS photograph shown in Fig. 3. It may be noted from this diagram that the cloud band is neither strictly parallel to the surface front, nor to the jet axes. It appears to part from the southern-most jet branch near Midland (MAF), Texas, and joins with the center branch of the jet not far from Topeka (TOP), Kansas. Such alignment of clouds seems to indicate the crossing-over of air masses from one jet branch to another. A similar but more pronounced case has been described by Reiter and Whitney (1965).

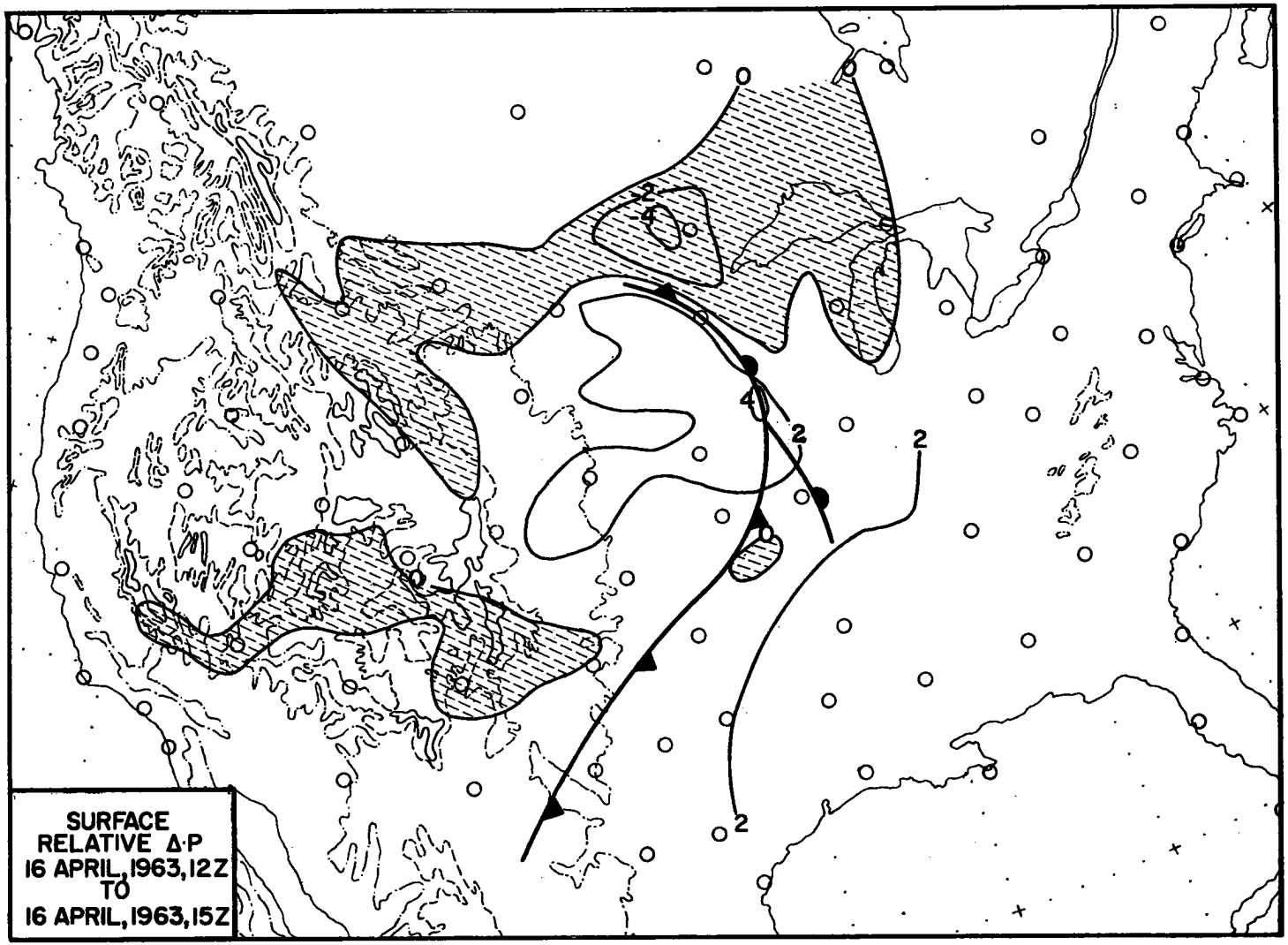

Fig. 25 a: Relative surface pressure tendencies (mb/ 3 hours) between 16 April, 1963, 12 GMT and 16 April, 1963, 15 GMT. Coordinate system moving with occlusion point of developing wave on cold front. Areas with pressure falls are shaded.

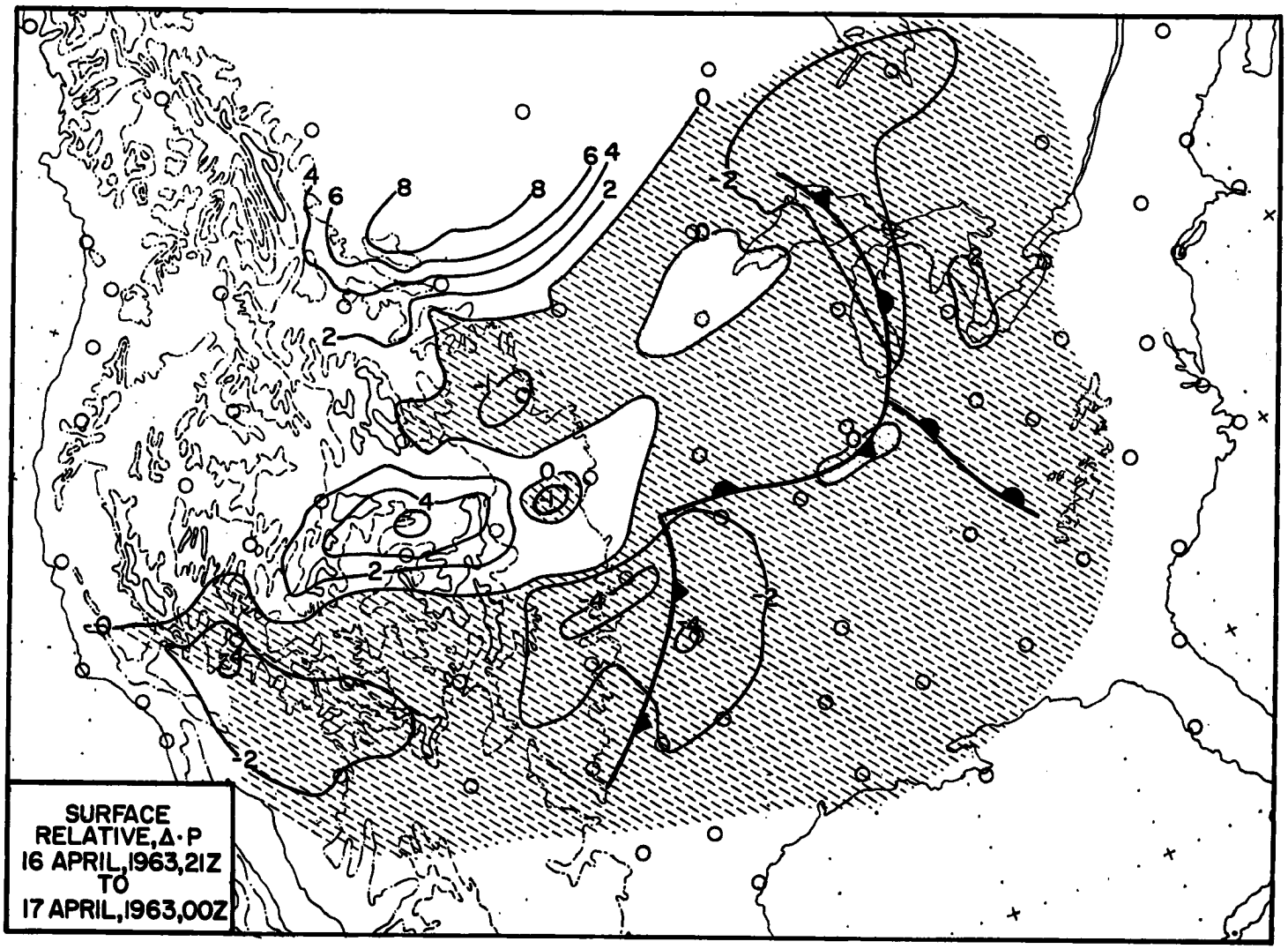

Fig. 25 b: Relative surface pressure tendencies (mb/ 3 hours) between 16 April, 1963, 21 GMT and 17 April, 1963, 00 GMT. Coordinate system moving with occlusion point of developing wave on cold front. Areas with pressure falls are shaded.

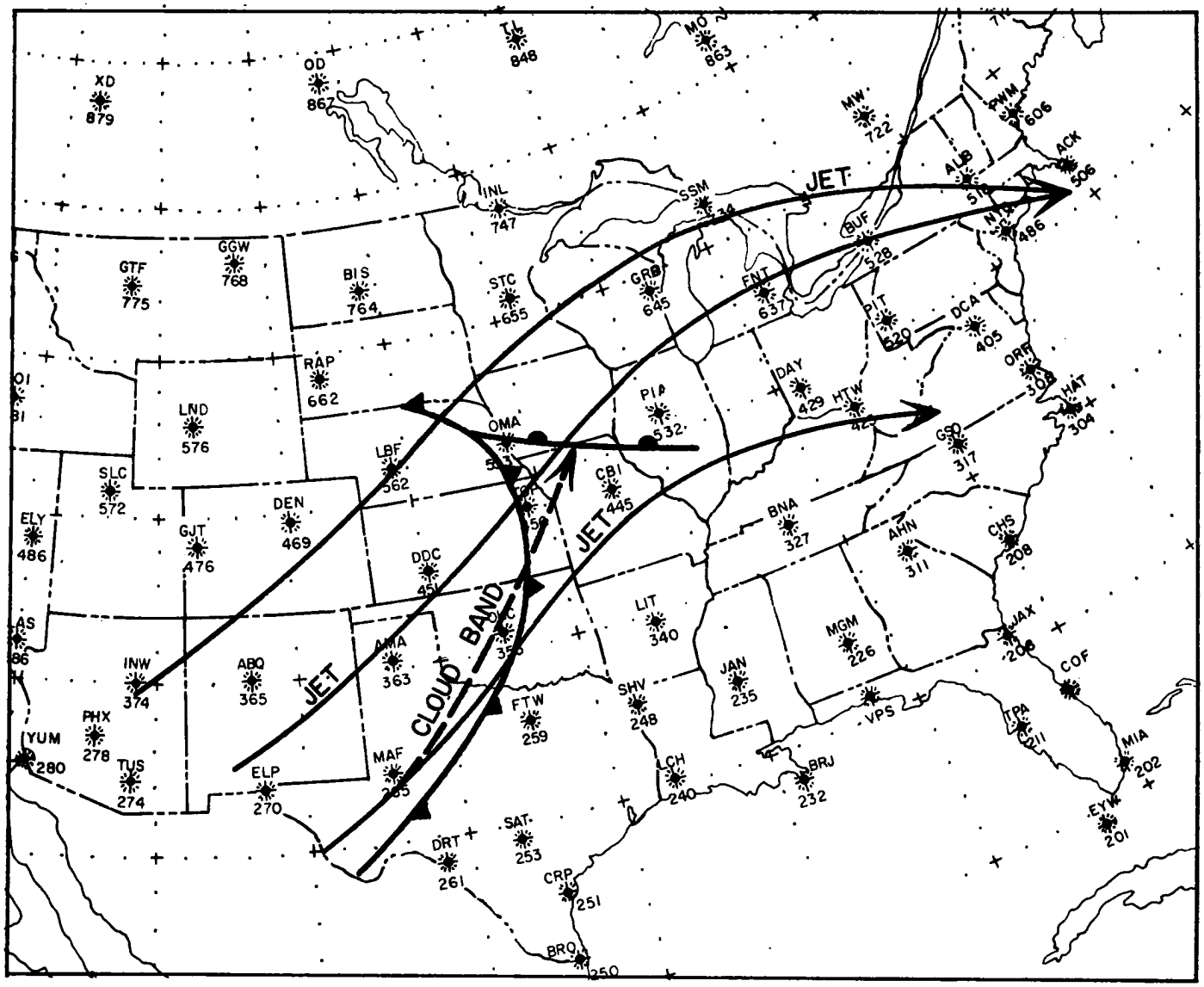

Fig. 26: Jet axes of 19 April, 1963, 00 GMT surface frontal positions of 18 April 21 GMT and location of cloud band (taken from Fig. 3) of 18 April 1955 GMT.

The existence of the cloud band observed from the TIROS photograph, Fig. 3, is corroborated by cloud observations at the surface. Aviation Weather Reports from Oklahoma City on 18 April 20 GMT indicate scattered clouds at 4000 and 12000 ft, and a thin overcast at higher levels. Tulsa, Oklahoma, reports scattered clouds at 3000 ft and overcast skies with unknown cloud height (two hours earlier the base of the overcast layer was estimated at 16,000 ft). San Antonio, Texas, to the east of the cloud band shown in Fig. 3 reports scattered clouds at 3500 and 12000 ft.

Fig. 22 shows cross sections from Lander (LND), Wyoming, to Burrwood (BRL), Louisiana, from 17 April, 1963,00 GMT to 19 April, 00 GMT. A stable baroclinic zone appears in the upper troposphere on 18 April 00 GMT over Denver. Within the next 12 hours this frontal layer intensifies and reaches the ground near Dodge City (DDC), Kansas. Dry ("motorboating") conditions in the vicinity of this frontal layer indicate subsiding air motions. Ahead of the front the air is relatively humid. By the 19th at 00 GMT over Oklahoma City a moist layer appears near the 300-mb level. It probably is this layer which contains the high-level overcast mentioned in the Aviation Weather Reports, and which shows as a cloud band in the TIROS photographs.

Trajectories on the 330°K isentropic surface (not reproduced in this report), which intersects the jet core over Oklahoma City, reveal a rising motion of air parcels as they move from southwestern Texas into the region of the cloud band. Following an air parcel originally located near the 290-mb level on this isentropic surface over the Mexican border region, one finds that it rises by approximately 10 to 20 mb as it passes near Oklahoma City, and reaches the 240-mb level over Kentucky.

More detailed analyses of this cloud band and its association with the high-tropospheric flow pattern will be described in a future report.

(6) The Structure of a Cyclone.

Fig. 27 shows cloud formations in a large cyclone whose center is located over Minnesota. The surface pressure pattern and cloud observations for 19 April 18 GMT are given in Fig. 28.

Several interesting features characterize this TIROS frame and others taken from the same orbit and contributing to a mosaic of large area coverage (not reproduced in this report).

(a) A bright and elongated cloud band parallels and precedes the cold front south of the tip of Lake Michigan similar to the band described for April 16 and 17. From there on southward it is associated with a squall line (Fig. 28). The western edge of this band is rather sharply developed while its eastern edge seems to be more diffuse. This may in part be due to perspective viewing of the band close to the horizon. There may be other reasons, however, which will be indicated later. Over Lake Michigan the western edge of the cloudy region is less sharply developed. Here the clouds extend over and to the rear of the cold front. Only in this region, therefore, are the "classical" cold-frontal clouds formed as described by the Norwegian cyclone model. Comparing Fig. 27 with Fig. 28 one finds that the pre-frontal squall line starts to develop in the region where the cloud band crosses the surface cold front.

(b) This cloud band, together with bright cloud masses to the north, west, and southwest of the cyclone center, and with a cloud-free wedge to the rear of the cold front, generates the impression of a spiral. This spiral pattern seems to be quite characteristic of cyclones in the process of occlusion (Wiegman et al., 1964).

(c) Cloud patterns to the southwest of the cyclone center show distinctive striations. These are especially evident on frame 16 (not reproduced here) of the same TIROS orbit as Fig. 22. A schematic indication of these striations, and of the cloud distribution evaluated from TIROS photographs is given in Fig. 25.

A preliminary investigation has been made of the flow pattern leading to the observed cloud formations. Fig. 29 contains an

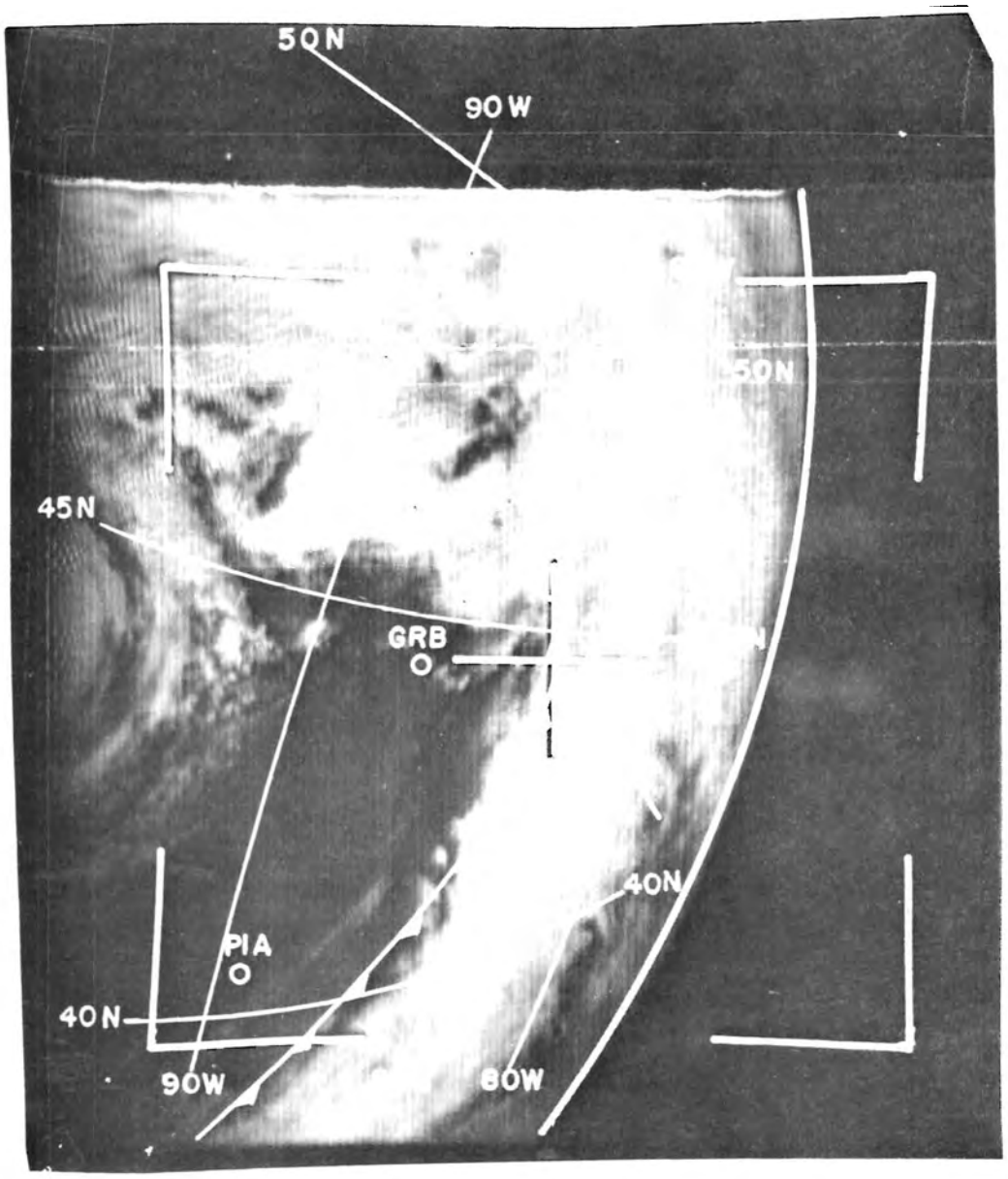

Fig. 27: Cloud photograph TIROS V orbit 4363 (tape) Frame 10, 19 April, 1963, 1925:30 GMT.

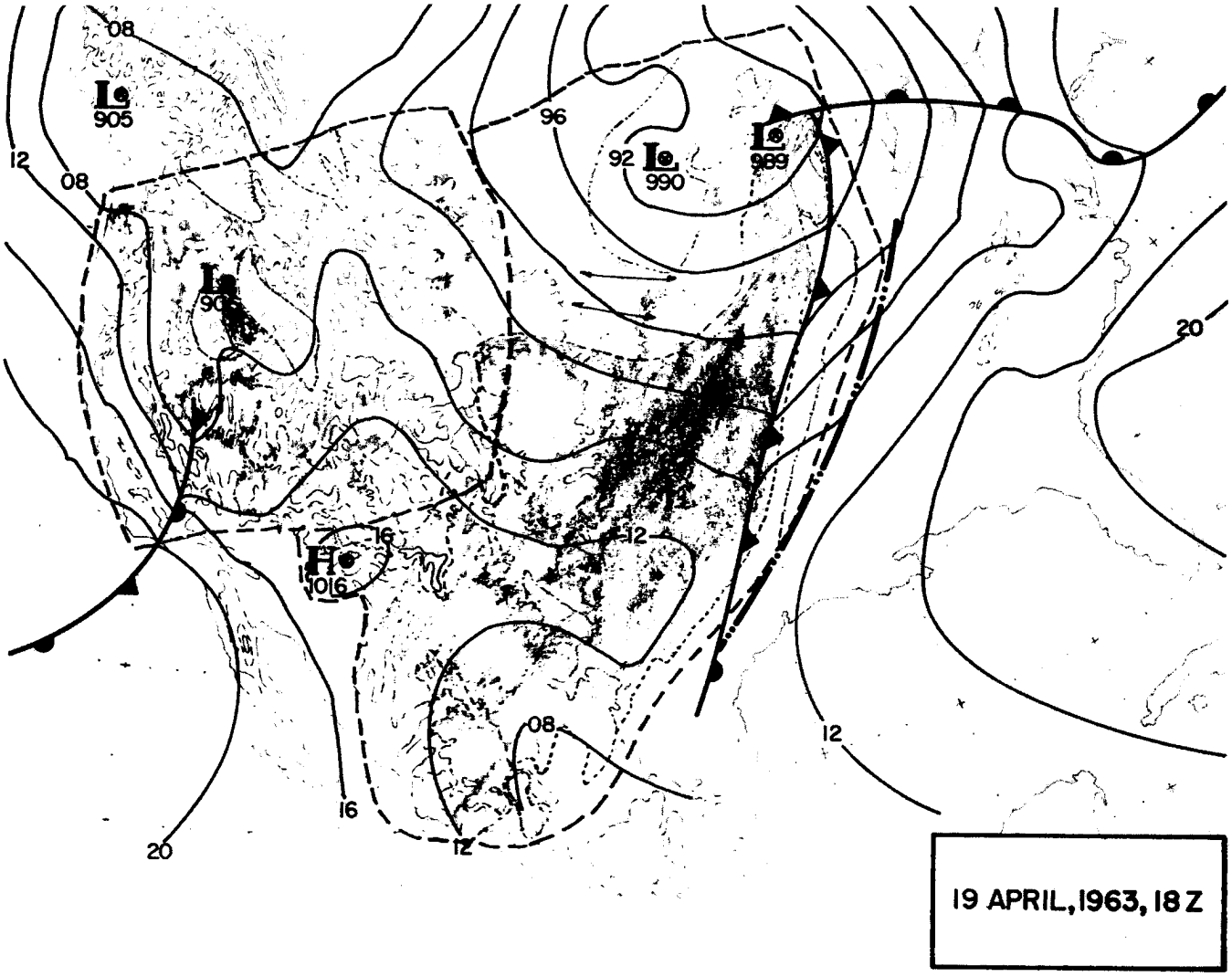

Fig. 28: Surface pressure distribution and frontal positions with squall line (long dash and two dots). Area enclosed by heavy dashed line is covered by TIROS nephanalysis, dark areas are cloud free, white areas are overcast. Thin lines with arrows indicate orientation of cloud bands.

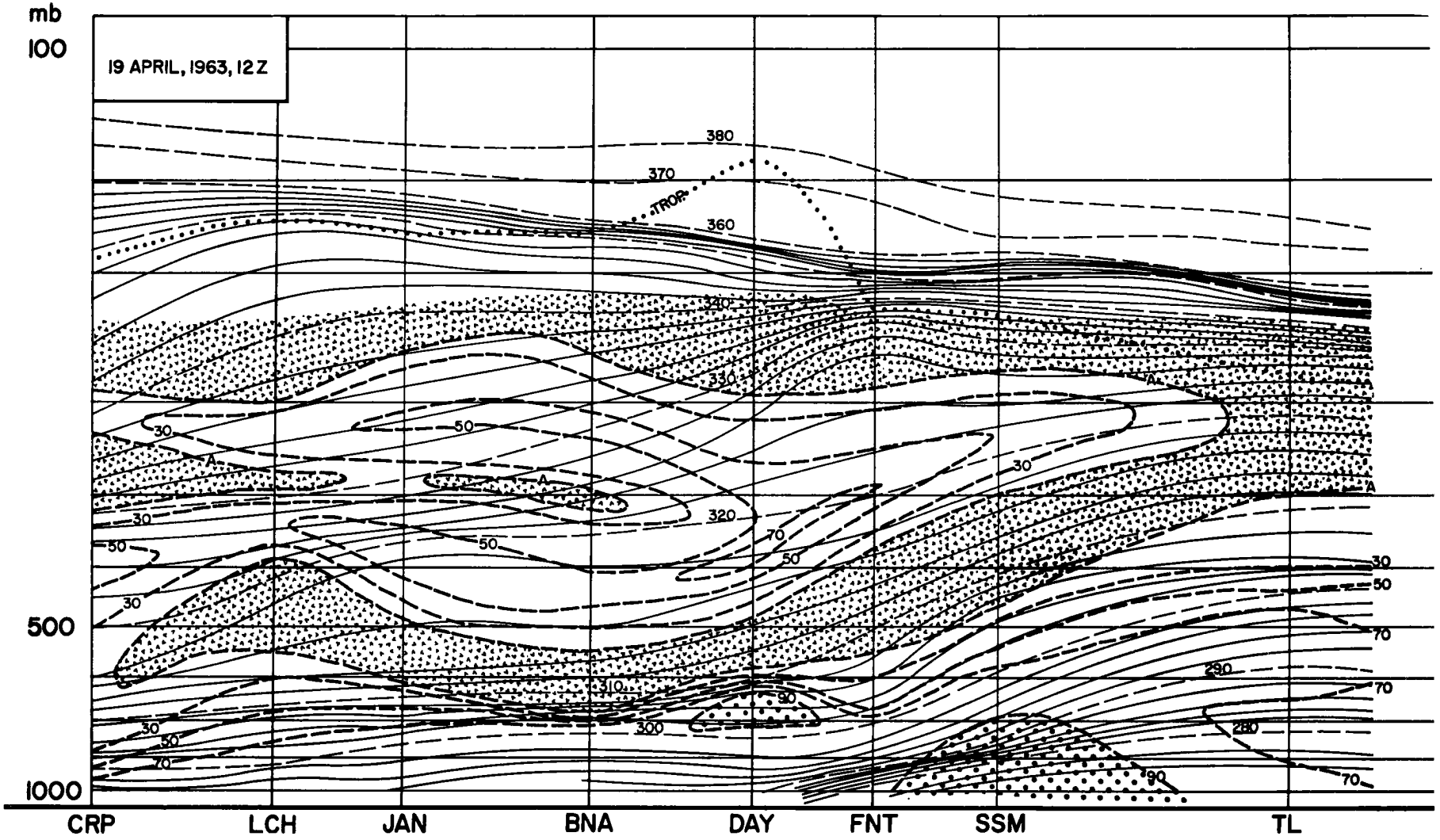

Fig. 29: Cross section through the atmosphere from Corpus Christi (CRP), Texas, to Trout Lake (TL), Ontario: Potential temperatures (°K, solid and long-dashed lines) and relative humidities (per cent, short-dashed lines; "A" indicates "motorboating"). Coded tropopause is marked by dotted line. Moist (>90% relative humidity) and dry layers ("A") are indicated by different shading (LCH = Lake Charles, Louisiana; JAN = Jackson, Mississippi; BNA = Nashville, Tennessee; DAY = Dayton, Ohio; FNT = Flint, Michigan; SSM = Sault St. Marie, Michigan).

analysis of relative humidities and potential temperatures in a cross-section from Corpus Christi (COR), Texas, to Trout Lake, (TL), Ontario. The plane of this section runs approximately parallel to the cold front shown in the surface map Fig. 28. The flow characteristics within the lower moist layer evident from this cross section are adequately portrayed by the 300 K isentropic surface. A dry layer with relative humidities less than 20 per cent exists above this bottom layer. It is characterized by potential temperatures of approximately 310 K. Above this we find again an abundance of moisture. The isentropic surfaces 320 K and 330 K describe conditions in this upper layer.

Trajectories near the isentropic surface 300 K between 19 April, 1963, 00 GMT and 20 April 00 GMT are shown in Fig. 30 together with a schematic nephanalysis obtained from rectified TIROS pictures of orbit 4363. These trajectories are indicative of air motions within the lower moist layer evident from the cross-section in Fig. 24. Aviation Weather Reports indicate extensive cloudiness in this layer. Over Fargo, North Dakota, for instance, broken clouds are observed at 3000 ft, overcast at 8000 ft.

In view of these cloud observations, indicating the presence of moist-adiabatic processes, standard procedure of isentropic trajectory calculation had to be abandoned. These calculations are based upon conservation of potential temperature, and of potential vorticity which, in itself, is valid only for dry-adiabatic processes. Trajectories shown in Fig. 30, rely on dry-adiabatic motions only in first approximation. In a careful iterative computation process they were adjusted to conserve equivalent-potential temperature (θ_E) as closely as possible.

From a comparison of Fig. 30 with Fig. 31 it may be seen that the striations in the cloud pattern observed by TIROS to the southwest of the cyclone center are aligned parallel to the trajectories of flow in the lower cloud layer. Meso-structural cloud rows of wave-lengths of

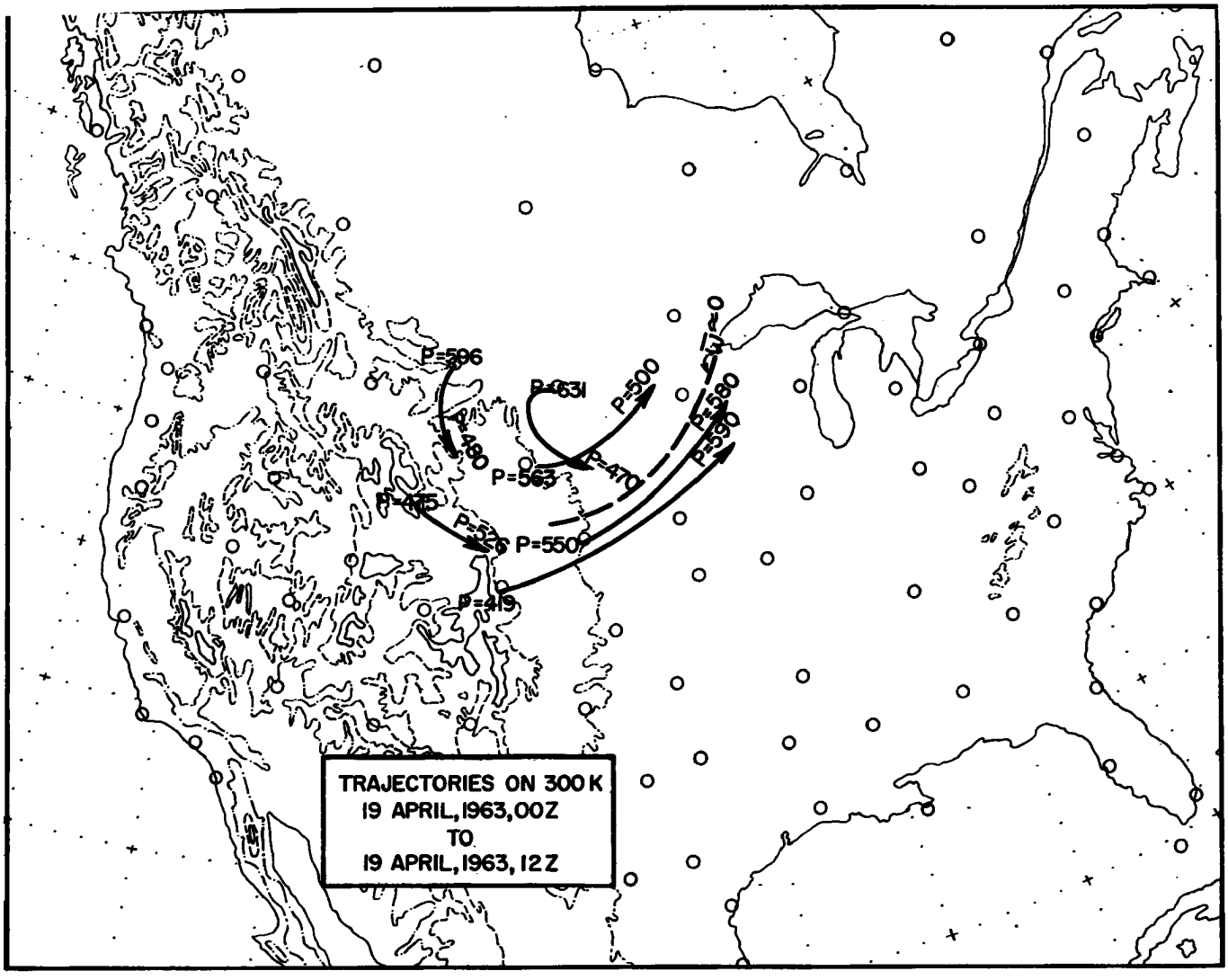

Fig. 30 a: Trajectories on 300 K isentropic surface. $\bar{w} \approx o$ (dashed line) indicates line of zero vertical velocity. Pressure values are given at beginning and end of trajectories.

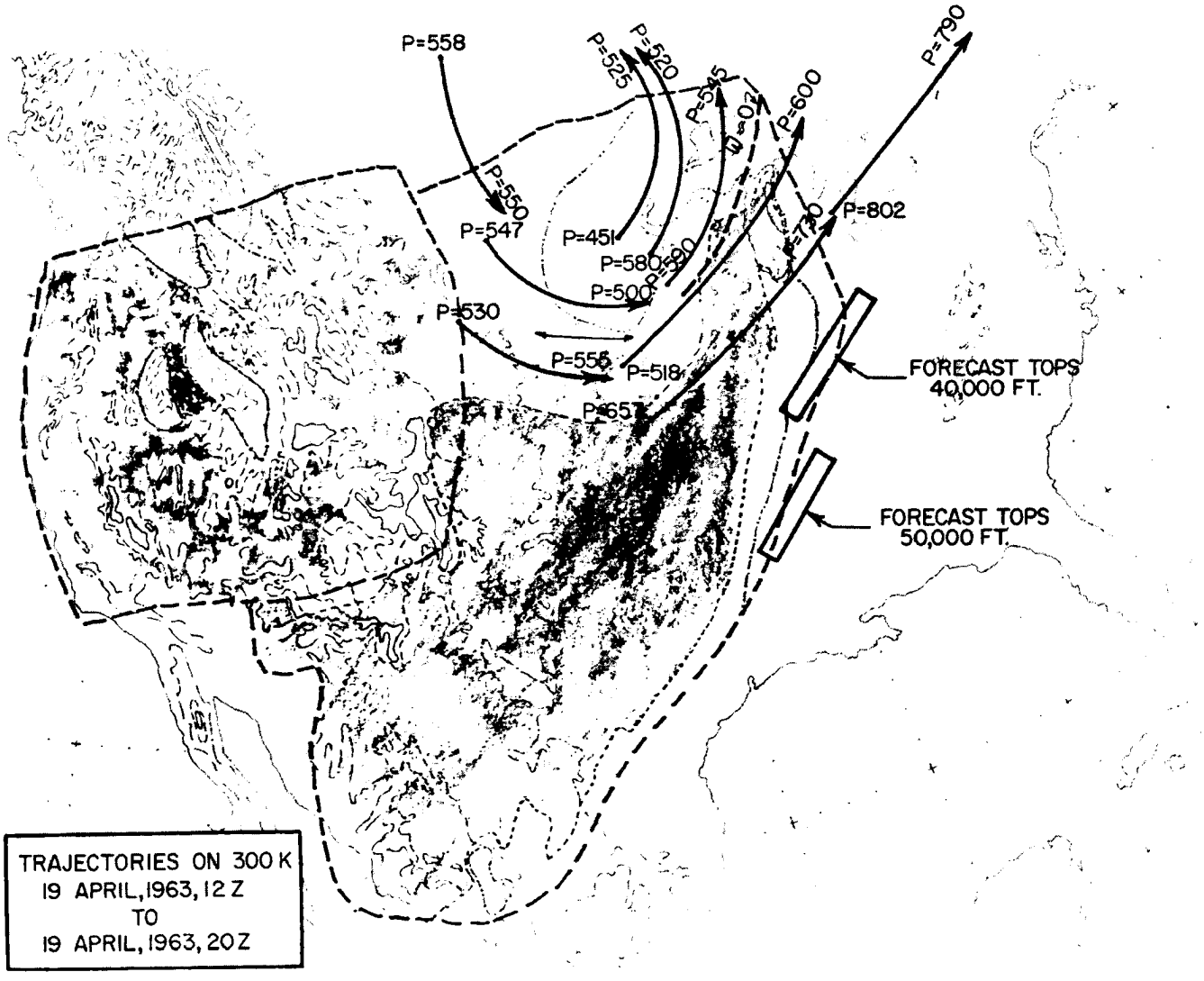

Fig. 30 b: Trajectories on 300 K isentropic surface. $\overline{w} \approx o$ (dashed line) indicates line of zero vertical velocity. Pressure values are given at beginning and end of trajectories. Boxes indicate cloud top height forecasts. Thin line with arrows shows orientation of cloud bands. Large areas enclosed by heavy dashed lines depict TIROS picture coverage. The shaded areas are cloud free. Areas between short dashed lines and dash-dot lines are broken clouds. Areas enclosed by dash-dot lines are overcast.

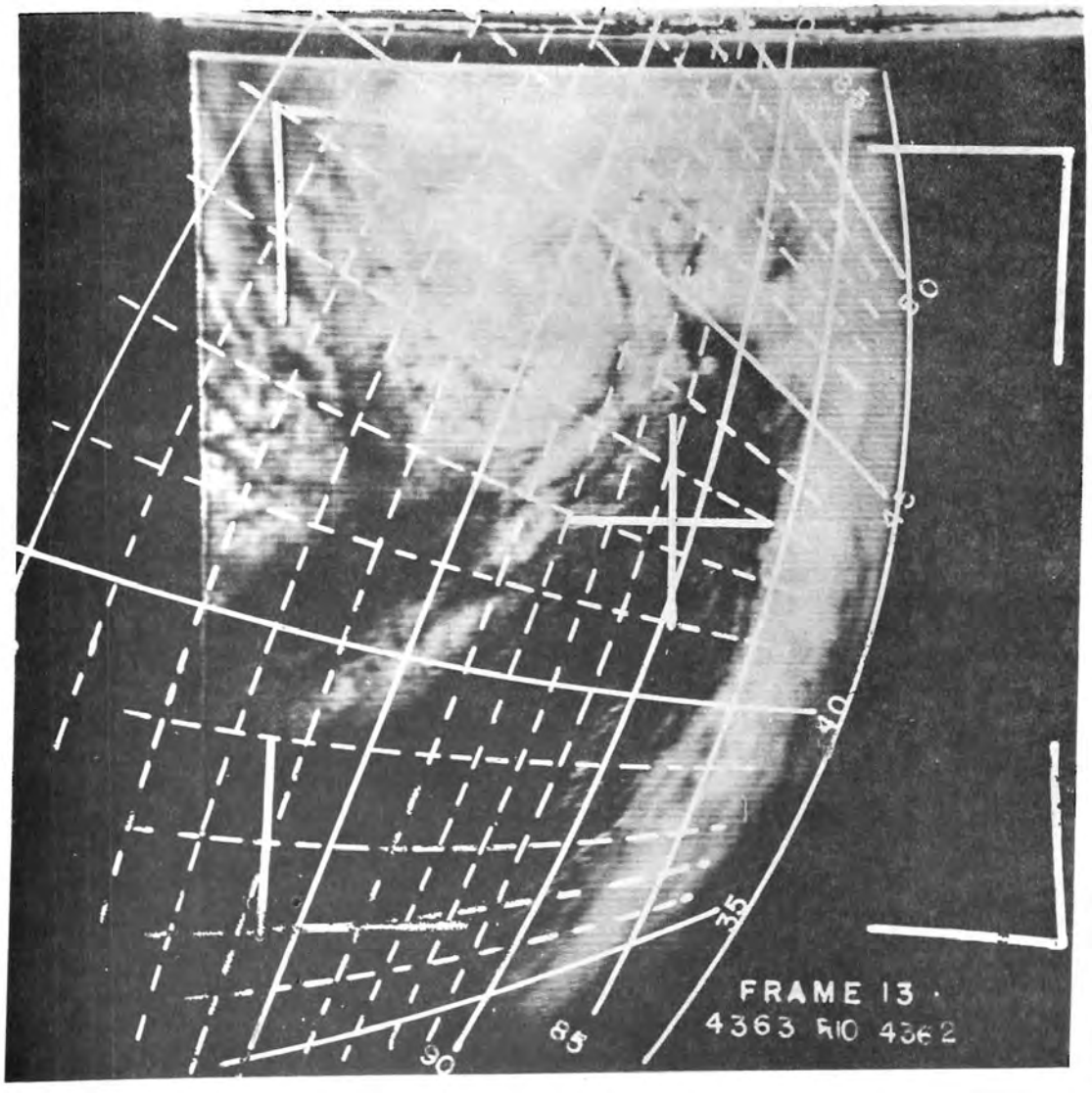

Fig. 31: Cloud photograph TIROS V orbit 4363 (tape), Frame 13, 19 April, 1963, 1924 GMT.

approximately 15 n. miles, measured normal to the direction of flow, are observed in this region. These rows seem to combine into brighter and less bright regions, also oriented parallel to the trajectories of Fig. 25, with a characteristic wave length normal to the current of approximately 60 to 80 n. miles (Fig. 31).

Pressure values have been plotted along the trajectories in Fig. 30. From these it may be seen that strong rising motions--as much as 160 mb in twelve hours in one instance of a strongly curved trajectory segment--prevail in the region of bright clouds. A dashed line, labelled w = o has been entered in Fig. 30. It separates rising from sinking trajectory segments for the period 19 April 12 GMT to 20 April 00 GMT. With sinking motions potential temperatere, θ, and potential vorticity are well conserved. The separation line, w = o, is in good agreement with the western border of the cloud-free "wedge" which apparently "spirals" into the cyclone. The trajectories of Fig. 30 do not indicate a spiral motion, however. A strong divergence of flow seems to take place near the separation line, w = o. The rising trajectories curve northward around the cyclone while the sinking trajectories follow an almost straight path towards the northeast.

Air motions in the pre-frontal squall line, which appears as a bright cloud band in Fig. 27 follow an altogether different pattern. A cross-section from Grand Junction (GJT), Colorado, to Washington (DCA), D. C., of 19 April 12 GMT, is shown in Figs. 32 and 33. The location of the squall line is characterized by a large vertical column in which equivalent potential temperatures remain nearly constant and relative humidities are close to saturation. Wind speeds change only little between 700 and 350 mb, indicating that in this tropospheric layer rising air masses tend to conserve their horizontal momentum. The dry air in the vicinity of the cold front, indicative of sinking motions, is also clearly evident from this cross-section.

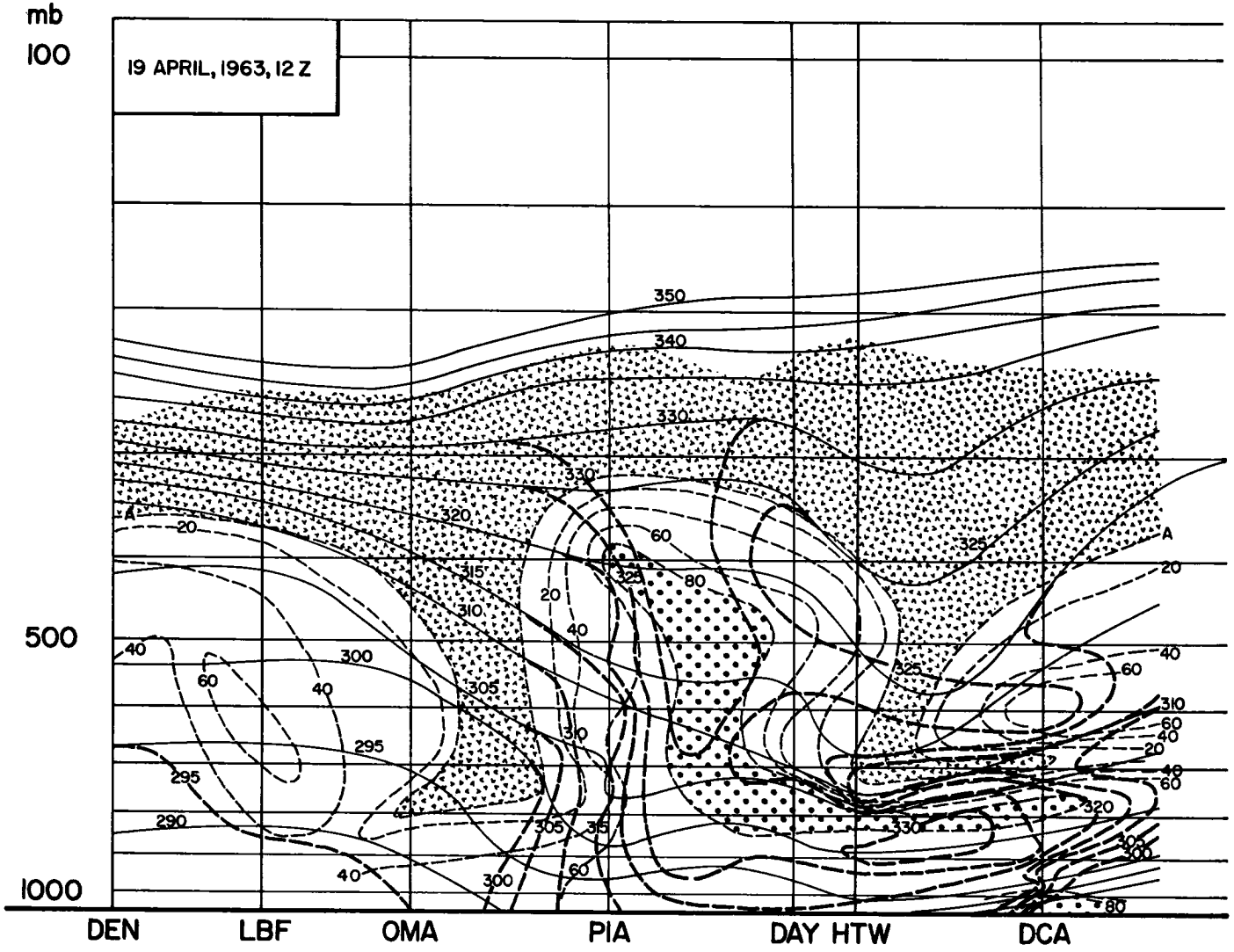

Fig. 32: Cross section through the atmosphere from Denver (DEN), Colorado, to Washington (DCA), D. C. Equivalent potential temperature (^{o}K, heavy dashed lines) potential temperature (^{o}K, solid lines) relative humidity (per cent, dashed lines). Boundary of "motorboating" area is marked by letter "A", the area itself is indicated by irregular shading. The dotted area shows moist regions with humidities > 80 % (LBF = North Platte, Nebraska; OMA = Omaha, Nebraska; PIA = Peoria, Illinois; DAY = Dayton, Ohio; HTW = Huntington, West Virginia).

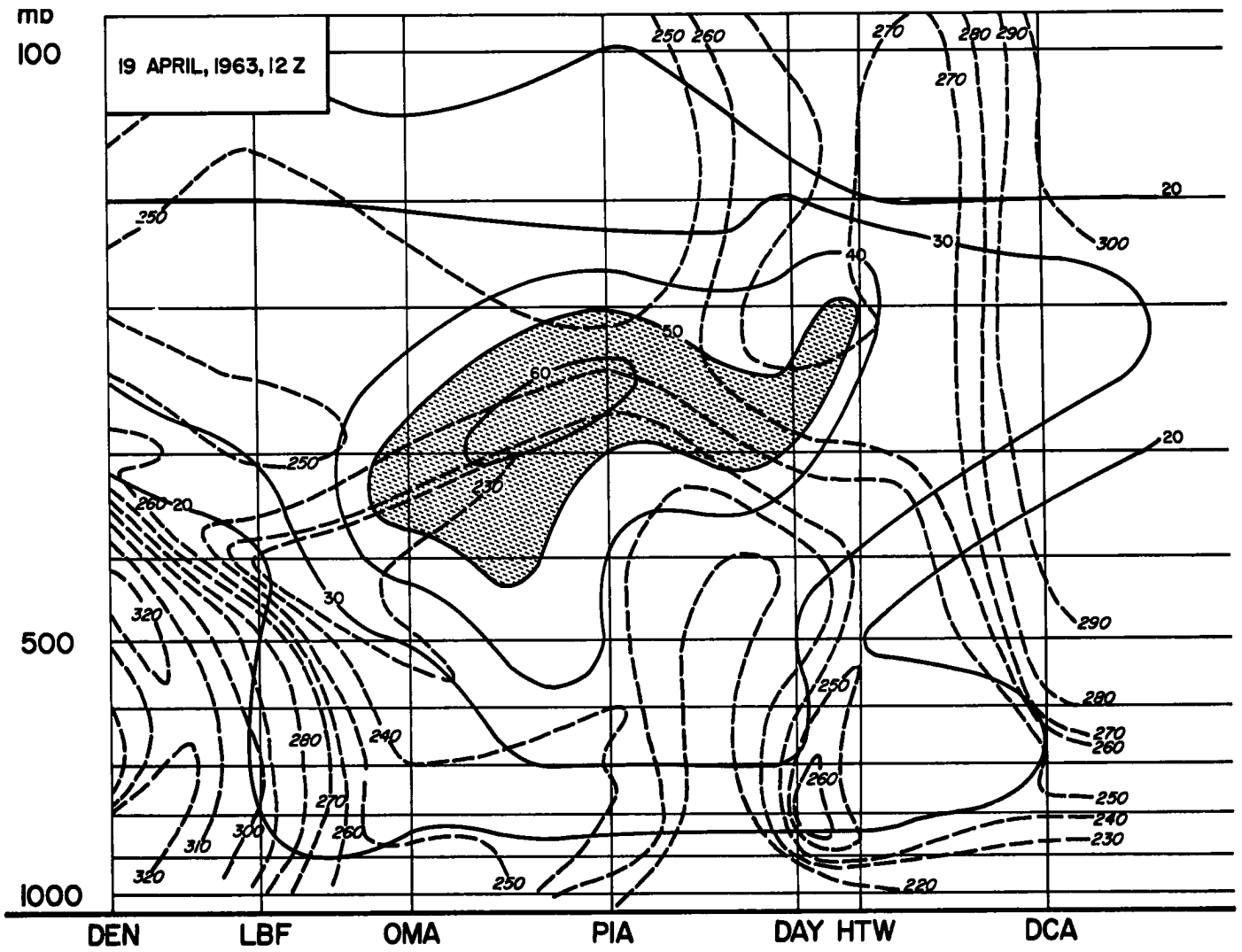

Fig. 33: Cross section through the atmosphere from Denver (DEN), Colorado, to Washington (DCA), D. C. Wind speeds (mps, solid lines) wind directions (degrees, short dashed lines). Areas with speeds > 50 mps are shaded.

Fig. 34 a shows isotachs and wind directions on the isentropic surfaces 320 K for 19 April 12 GMT. A striated jet-stream pattern, as we have observed it earlier, appears again in this analysis. The stream-lines in the southwesterly flow on the 320 K surface at this observation time are almost exactly parallel to the squall-line orientation. A small, secondary wind maximum appears at this isentropic level over the southern portions of the squall line on 20 April 00 GMT (Fig. 34 b). The northern portion of the squall-line location, however, is characterized by a wind speed minimum. This should be expected from the transport of low-momentum, low-tropospheric, air to high levels within the convective cloud systems.

Whereas the 320 K stream lines on 19 April 12 GMT are parallel to the squall line in its vicinity, the 330 K stream lines at the same observation time run from a more westerly direction (Fig. 35). From the cross-section of Fig. 32 we see that in the squall-line region the 330 K isentropic surface still is expected to lie within clouds. Aviation weather reports forecast cloud tops at 40,000 to 50,000 ft, well above the 330 K surface. This means that the cirrus tops of the cumulo-nimbi within the squall line are blown off towards the northeast, causing a broadening of the cloud band observed by TIROS and a diffuse appearance of its eastern edge. Such veering of winds with height in the upper troposphere is quite frequently observed near squall-lines.

From the evidence collected so far in this case study we arrive at the schematic diagram shown in Fig. 36. In the vicinity and to the rear of the cold front air is sinking in the cloud free region. Some of this air may be of stratospheric origin (Reiter and Mahlman, 1965). Trajectories in, and to the north of, the occlusion point reveal ascending motions, giving rise to cloud decks in the middle and lower troposphere and to precipitation.

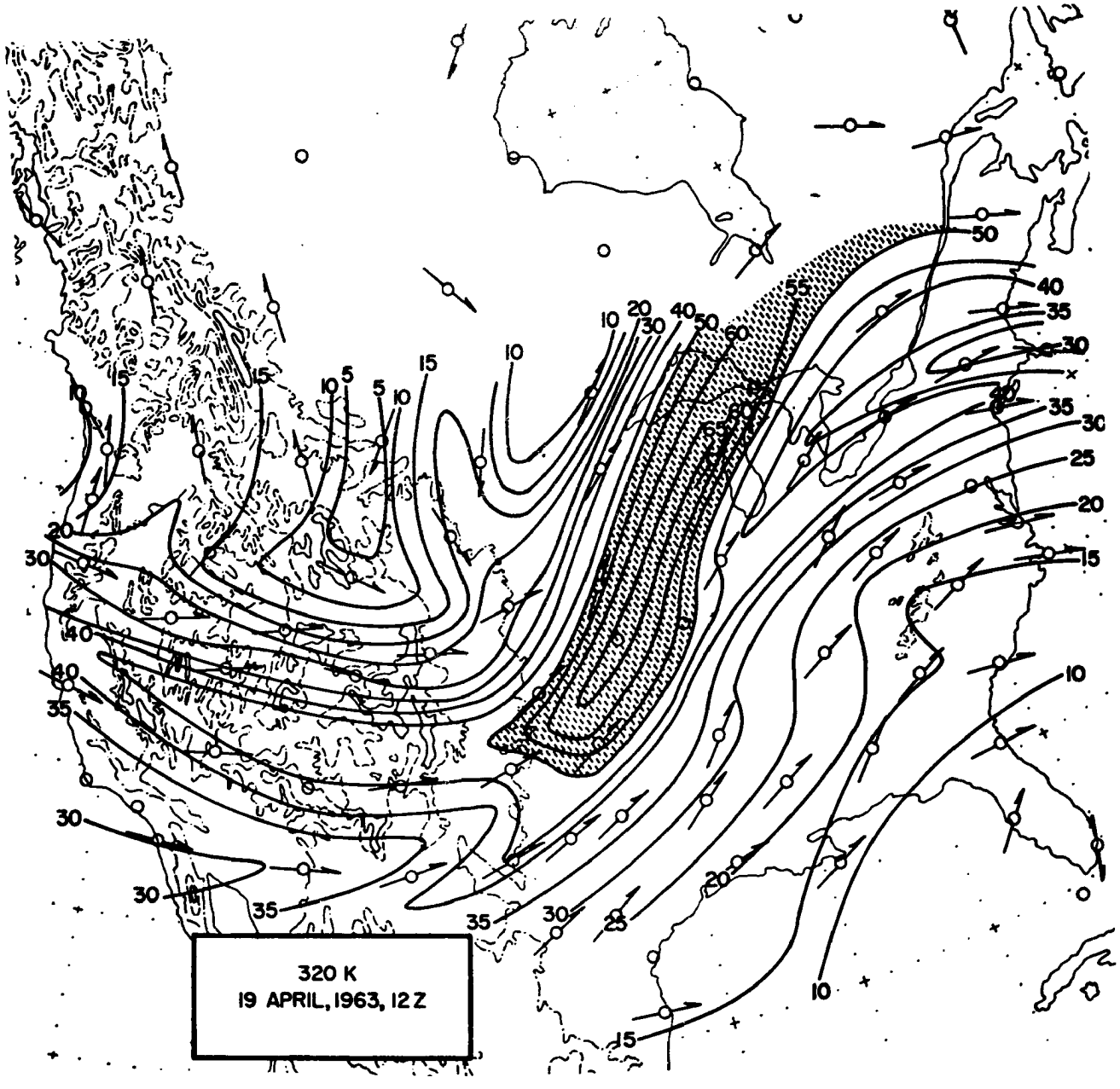

Fig. 34 a: Isotachs (mps) on isentropic surface 320 K. Regions with speeds > 50 mps are shaded. Arrows indicate observed wind direction.

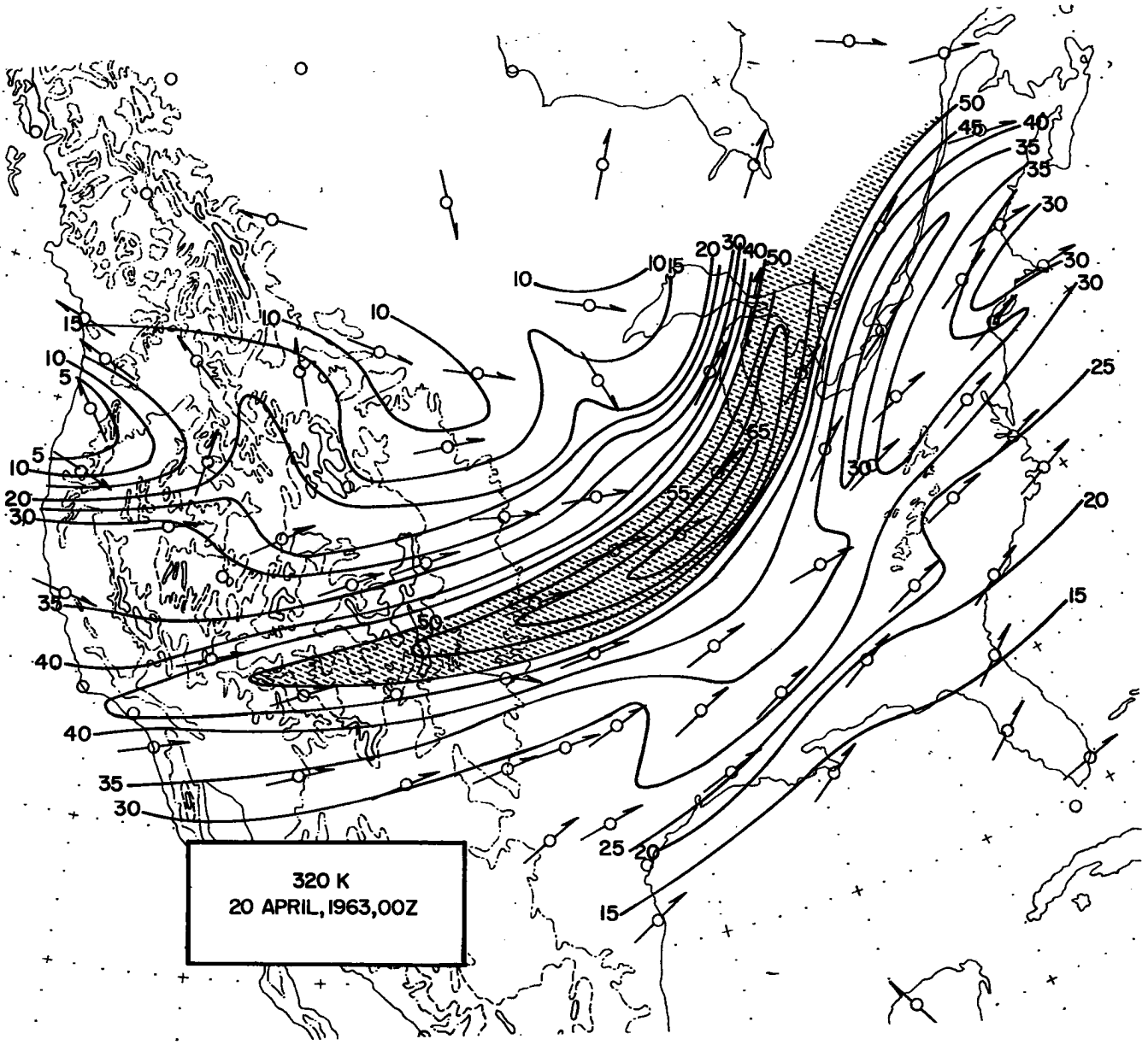

Fig. 34b: Isotachs (mps) on isentropic surfaces 320 K. Regions with speeds > 50 mps are shaded. Arrows indicate observed wind direction.

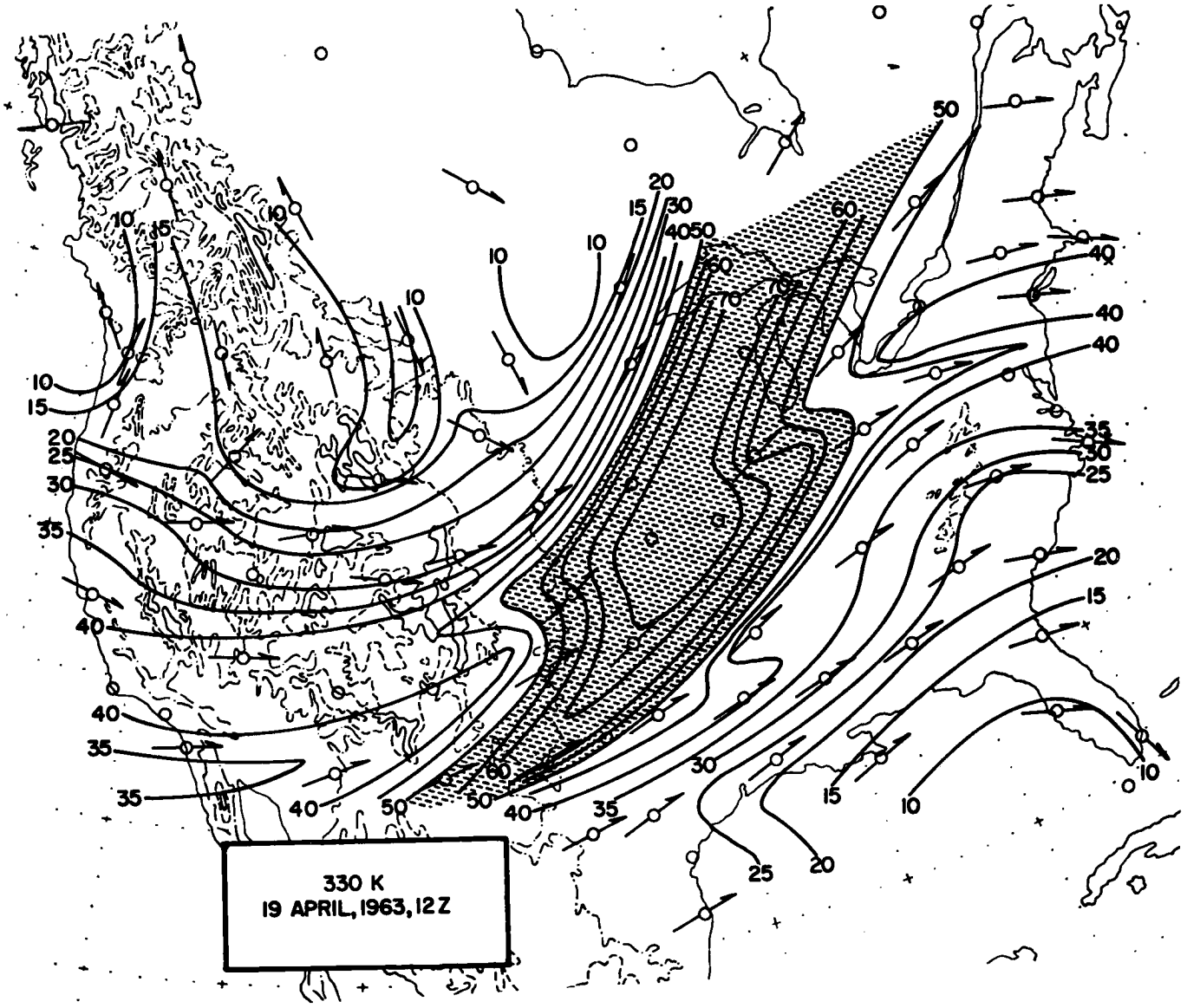

Fig. 35: Isotachs (mps) on isentropic surface 330 K. Regions with speeds > 50 mps are shaded. Arrows indicate observed wind direction.

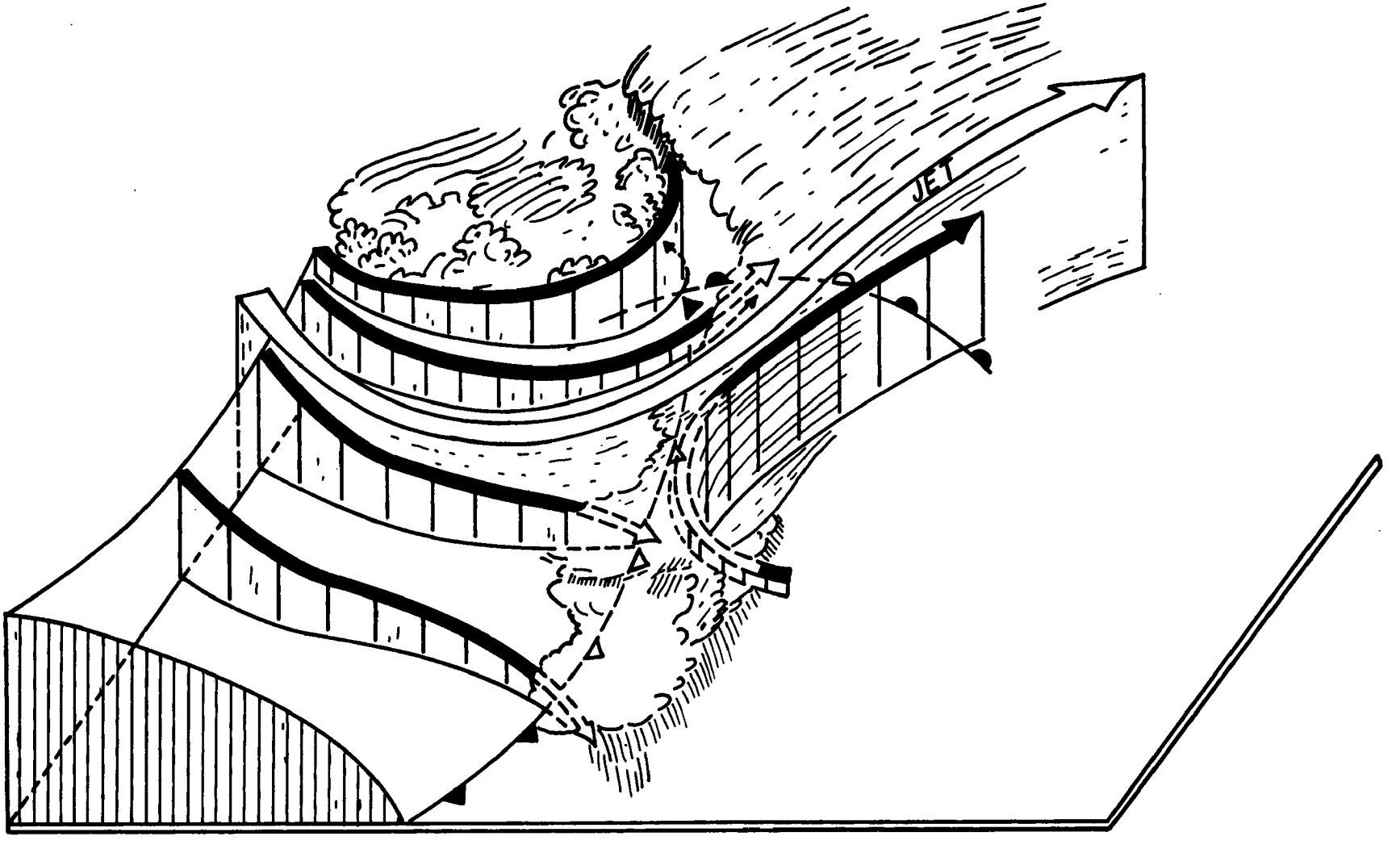

Fig. 36: Schematic diagram showing trajectories and clouds around low and over the cold front and squall line.

Warm and moist air from the south is entrained into the prefrontal squall line, rising rapidly within the convective cloud systems and merging with the jet-stream flow aloft. The import of low tropospheric air causes a retardation in this flow aloft, leading to the formation of a wind-speed minimum embedded in faster winds. The dry layer of subsiding air near the cold front is destroyed by convective currents in the squall-line region. The large-scale spiral-shaped cloud pattern of an occluding cyclone, thus, is produced by the superposition of moist, dry, and again moist layers. The meso-scale striations, which are observed frequently in the low-level clouds near the occlusion point (see Fig. 31) support the impression of a spiraling flow. Such flow is, however, confined to the low troposphere.

(7) Merging of Jet Streams.

The merging of a "polar front jet" with a "subtropical jet stream" on 20 November, 1962, produced a cirrus-cloud distribution which is characteristic for such flow patterns (Kadlec, 1963). The northern edge of the deck of high-tropospheric clouds appeared very distinctly on TIROS photographs, as it generated a shadow band on the lower clouds (Oliver et al., 1964).

It could be shown in detailed analysis (Reiter and Whitney, 1965), that the flow in the so-called "subtropical jet stream" crossed over the air moving in the "polar-front jet". Furthermore it appeared that the present nomenclature of "subtropical" and "polar-front" jet stream may be a misnomer, since, at least in the present case study, the latter was not associated with a low-tropospheric front, whereas the former was.

IV. Conclusions and Outlook:

This report contains preliminary results obtained from a number of case studies of details in atmospheric flow, using TIROS photographs as indicators of such details. The interpretation of cloud patterns and their formation necessitates careful three-dimensional analyses of atmospheric structure. These have been facilitated by

the development of electronic computer programs, calculating Montgomery stream functions on isentropic surfaces, and plotting radiosonde data to the scale of a tephigram. In spite of these computing aids detailed analysis of available data still remains a time-consuming task. The full details of such analyses, and the conclusion drawn from them, will be published in separate reports pertaining to individual case studies.

From the evidence presented in the foregoing section we may state that TIROS satellites present a powerful tool in revealing atmospheric meso-structure and macro-structure of scale lengths larger than ca. 8 km. Although disturbances of smaller scale lengths are not directly visible from TIROS cloud patterns, there is evidence--as for instance shown by power-spectrum measurements--that meso-scale disturbances provide an energy input for smaller atmospheric eddies. Certain correlations between meso- and micro-scale, therefore, should be expected.

So far, the dynamics of atmospheric meso- and micro-structure are poorly understood. Especially the processes of energy transfer from larger to smaller disturbances--outside the inertial subrange--still need exploration. TIROS photographs give evidence of a wide scale range of atmospheric disturbances, but only from supporting data on atmospheric structure may we obtain insight into the physical nature of these disturbances. The present radiosonde system is not capable of rendering information on meso- or micro-structure. Special measurement programs are needed to penetrate this data gap.

Mountain regions, such as the Rocky Mountain area, are known to generate atmospheric turbulence over the whole spectrum range. Detailed analysis of flow patterns over, and in the vicinity of, the mountains--implemented by additional measurements--will provide means of correlating TIROS data with the dynamic properties of atmospheric disturbances over a wide scale range.

V. Acknowledgements:

The authors wish to acknowledge the technical assistance of Mrs. G. Wooldridge and Mr. W. Ehrman in preparing the raw data and Mr. J. White who drafted the figures. Mrs. S. Olson typed the manuscript.

The rectification of TIROS photographs used in this report was done by Mr. G. Wooldridge. The meteorological analysis work was mainly carried out by D. W. Beran and E. R. Reiter. J. D. Mahlman computed air parcel trajectories.

REFERENCES

Bolin, B., 1950: On the influence of the earth's orography on the general character of the westerlies. Tellus.2 (3): 184-195.

Clodman, J., G. M. Morgan, Jr., and J. T. Ball, 1961: High level turbulence. Air Weather Service, Tech. Report 158.

Colson, DeVer, 1963: Analysis of clear air turbulence data for March, 1962. Monthly Weather Rev. 91 (2): 73-82.

Conover, J. H., 1960: Cirrus patterns and related air motions near the jet stream as derived by photography. J. Meteorol. 17 (5): 532-546.

Cook, A. W., and A. G. Topil, 1952: Some examples of chinooks east of the mountains in Colorado. Bulletin Amer. Meteorol. Soc. 33 (2): 42-47.

Endlich, R. M., and G. S. McLean, 1957: The structure of the jet-stream core. J. Meteorol. 14: 543-552.

Fujita, T., 1961: Outline of a technique for precise rectification of satellite cloud photographs. Univ. of Chicago, Mesometeorology Project, Research Paper No. 3.

_____, 1963: A technique for precise analysis of satellite photographs. Univ. of Chicago, Mesometeorology Project, Research Paper No. 17.

_____, 1964: Evaluation of errors in the graphical rectification of satellite photographs. Univ. of Chicago, Satellite and Mesometeorology Research Project, Research Paper No. 30.

Godske, C. L., T. Bergeron, J. Bjerknes, and R. C. Bundgaard, 1957: Dynamic meteorology and weather forecasting. Amer. Meteor. Soc. and Carnegie Institution, 800 pp.

Harrison, H. T., 1956: Synoptic features of the mountain wave at Denver, Colorado. United Air Lines, Meteorology Circular No. 41.

_____, 1957: Mountain wave zones in the United States. United Air Lines, Meteorology Circular No. 43.

Kadlec, P. W., 1963: An in-flight study of the relation between jet streams , cirrus, and wind shear turbulence. Final Report, U. S. Weather Bureau Contract Cwb - 10356.

Kao, S. -K., and H. D. Woods, 1964: Energy spectra of meso-scale turbulence along and across the jet stream. J. of Atmosph. Sci. 21 (5): 513-519.

Kuettner, J., 1959: The rotor flow in the lee of mountains. USAF Cambridge Research Laboratories, Research Notes No. 6.

McClain, E. P., 1952: Synoptic investigation of a typical chinook situation in Montana. Bulletin Amer. Meteorol. Soc. 33 (2): 87-96.

Newton, C. W., 1959: Axial velocity streaks in the jet stream: ageostropic "inertial" oscillations. J. Meteorol. 16 (6): 638-645.

Oliver, V. J., R. K. Anderson, and E. W. Ferguson, 1964: Some examples of the detection of jet streams from TIROS photographs. Monthly Weather Rev. 92 (10): 441-448.

Panofsky, H. A., and J. C. McLean, Jr., 1964: Physical mechanism of clear-air turbulence, Dept. of Meteorology, Pennsylvania State Univ., Research Report to U. S. Weather Bureau.

Reiter, E. R., 1963:Jet-Stream Meteorology. Univ. of Chicago Press, 515 pp.

_____, 1964: The effect of large mountain ranges on atmospheric flow patterns as seen from TIROS satellites. Progress Report on Contract Cwb - 10879, 15 December 1964.

_____, 1965 a: The fine-scale structure of the atmosphere. Colorado State University, Atmosph. Sci. Miscellaneous Report.

_____, 1965 b: Tropospheric circulation and jet streams. To be published: Vol. III of "World Survey of Climatology". Elsevier Publishing Co.

_____, and A. Burns, 1965: Atmospheric structure and clear-air turbulence. Colorado State University, Atmosph. Sci. Tech. Paper No. 28.

_____, and J. D. Mahlman, 1964: Heavy radioactive fallout over the southern United States, November 1962. Colorado State University, Atmosph. Sci. Tech. Paper No. 58.

_____, and J. D. Mahlman, 1965: A case study of mass transport from stratosphere to troposphere, not associated with surface fallout. Colorado State University, Atmosph. Sci. Tech. Paper No. 70.

Reiter, E. R. and L. F. Whitney, 1965: Subtropical or polar-front jet stream? Colorado State University, Atmosph. Sci. Tech. Paper No. 66.

Stinson, J. R., and A. I. Weinstein, and E. R. Reiter, 1964: Details of wind structure from high-resolution balloon soundings. NASA TM X - 53115.

Vinnichenko, N. K., N. Z. Pinus, and G. M. Shur, 1965: Some results of the experimental turbulence investigations in the troposphere. Paper presented at International Colloquium on the Fine-Scale Structure of the Atmosphere, Moscow, 15-22 June, 1965.

Weinstein, A. I., E. R. Reiter, and J. R. Scoggins, 1965: Meso-scale structure of 11-20 km winds with applications to missile operations. Meteorology Research, Inc. Report MRI 65 FR-213. To be published, J. of Applied Meteorol.

Wiegman, E. J., 1965: The distribution of clear-air turbulence reports and cloud patterns as seen in satellite photographs. Stanford Research Institute, Final Report, Contract Cwb - 10791.

Wiegman, E. J., R. G. Hadfield, and S. M. Serebreny, 1964: Atlas of cloud vortex patterns observed in satellite photographs. Stanford Research Institute, Final Report, Contract Cwb-10627.

Wooldridge, G., 1965: A modified method of TIROS photograph rectification suitable for research purposes. Colorado State University, Atmosph. Sci. Tech. Paper No. 71.

APPENDIX

DEVELOPMENT OF COMPUTER PROGRAMS FOR COMPUTATION OF MONTGOMERY STREAM FUNCTIONS AND PLOTTING OF THERMODYNAMIC DIAGRAMS *

by

J. D. Mahlman and W. Kamm

* Developed jointly under Weather Bureau Contract Cwb - 10879 and U. S. Atomic Energy Commission Contract AT (11-1)-1340.

ABSTRACT

Machine procedures are developed for computation of isentropic analysis parameters and for plotting of tephigrams, both in terms of derived basic equations. Computation flow charts and program copies are included from both programs.

I. Introduction:

In detailed analyses of atmospheric structure it is generally necessary that three-dimensional motions of the air be known to a high degree of reliability. It was demonstrated by Danielsen (1959) that this three-dimensional character of the flow may be adequately represented on isentropic surfaces provided that great care is taken in the computation of the Montgomery stream function (M). Especially the height of the chosen isentropic (θ) surface (Z_θ) must be determined accurately, and also the temperature (T_θ) and pressure (P_θ) on the θ - surface must satisfy Poisson's equation ($\theta = T\,(1000/P)^{R/c_p}$). By following this procedure one arrives at an expression for M (see section II). It is possible to compute M from this expression by hand with the aid of a plotted thermodynamic diagram but the calculation is very laborious and time consuming. To avoid this difficulty a computer program was written and tested which determines M and other desirable meteorological parameters on a given θ surface from the initial radiosonde data cards (see flow chart 1 and program 1). This program has also been expanded to plot mechanically the thermodynamic diagrams (tephigrams) from these data cards (see flow chart 2 and program 2). It is thus possible to generate data for isentropic analysis in a completely objective manner.

II. Mathematical Development:

For an isentropic representation the stream function on this surface is given by

$$M = c_p T_\theta + g Z_\theta \qquad (1)$$

where c_p is the specific heat of air at constant p and g is the acceleration of gravity (980.6 cm sec^{-2}).

If the height of the θ surface (Z_θ) is expressed as the height of a nearby isobaric level (Z_p) plus the height difference between the θ and p surfaces, Eqn. 1 may be written as

$$M = c_p T_\theta + gZ_p + g(Z_\theta - Z_p). \tag{2}$$

By integrating the hydrostatic equation to find the height difference between the p and θ surfaces, one obtains

$$Z_\theta - Z_p = \frac{-R\overline{T}}{g} \left(\frac{P_\theta}{P_p}\right) \tag{3}$$

where $\overline{T}$ is the mean temperature of the layer under consideration. Combining Eqns. 2 and 3,

$$M = c_p T_\theta + gZ_p + R\overline{T} \ln \left(\frac{P_p}{P_\theta}\right) . \tag{4}$$

However, as noted in the previous section, to minimize computational errors P_θ and T_θ should not be determined independently from the radiosonde data. This may be circumvented by solving Poisson's equation for P_θ to obtain

$$P_\theta = 1000 \left(\frac{T_\theta}{\theta}\right)^{c_p/R} \tag{5}$$

where R is the gas constant for dry air. By substitution of Eqn. 5 into Eqn. 4 one obtains

$$M = c_p T_\theta + gZ_p + R\overline{T} \ln \left[\frac{P_p}{1000} \left(\frac{\theta}{T_\theta}\right)^{c_p/R}\right] . \tag{6}$$

This expression for M is now in a form which can be readily computed by machine methods from the original radiosonde cards. Other significant parameters which can be easily obtained from the input data are the height of the θ surface (Z_θ) and the static stability ($-\partial\theta / \partial p$).

III. Explanation of the Montgomery Stream Function Program:

The input cards used in this program were purchased from the National Weather Records Center at Asheville, North Carolina. In order to insure sufficiently accurate input data it was necessary to combine two different formats, the 645 WBAN RAOBS CONST PRESSURE and 505 RAOB SIGNIFICANT LEVELS. These are contained in the Climatic Center, USAF, Air Weather Service, (MATS), NWRC, Office of Climatology, U. S. Weather Bureau Reference Manuals. This program was extensively tested and operated on an IBM 1620 computer processing only card input and output capabilities. To avoid the difficulties presented by the limited input capabilities and mixed formats, it was necessary to insert a blank card between each input station to be read into the computer.

After the data are read into the machine, they are arranged in order of descending pressure so that at any given pressure, a corresponding temperature and height is also defined at that level. At this point the machine is instructed to compute the potential temperature ($\theta = T(1000/p)^{R/c_p}$) for all pressure levels. At pressures lower than 800 mb the data were checked for superadiabatic lapse rates in the soundings by noting the sign of the static stability ($-\partial\theta/\partial p$). If this parameter becomes negative ($-\partial\theta/\partial p > 0$) the machine prints out the discrepancy and continues without modifying the calculation in any way. The calculation of M in a region which possesses a very unstable lapse rate is not seriously affected because under dry adiabatic conditions $\partial M/\partial Z = 0$. Thus the only serious difficulty which arises is the indeterminacy in finding the pressure or height of the θ surface of interest. By noting the lapse-rate discrepancy in the machine print-out, the analyst is aided in his evaluation of the topography of the isentropic surface.

In proceeding to calculate the Montgomery stream function at an isentropic surface of interest, it is necessary to find the temperature at this level (T_θ) by linear interpolation from the input data. This is obtained by employing the formula

$$T_\theta = T_b + (T_t - T_b) \left(\frac{\theta - \theta_b}{\theta_t - \theta_b} \right) \tag{7}$$

where the subscripts t and b indicate values of T and θ from the nearest input data above and below the θ level of interest.

The pressure (P_θ) at this θ level is then calculated from Eqn. 5 and the standard pressure values are scanned to find the nearest value of P_p larger than P_θ . The parameter Z_p in Eqn. 6 is now defined from the data at level P_p . To determine all parameters necessary to calculate from Eqn. 6, an expression for $\overline{T}$ between P_p and P_θ must be found in terms of the input data. This is accomplished by summing the weighted (linear) mean temperatures between all data points from P_p to P_θ as given in the formula

$$\overline{T} = \sum_{i=1}^{N} \left[\left(\frac{T_i + T_{i \pm 1}}{2} \right) \left(\frac{P_i - P_{i \pm 1}}{P_p - P_\theta} \right) \right]$$

$$\overline{T} = \frac{1}{2(P_p - P_\theta)} \sum_{i=1}^{N} \left[(T_i + T_{i \pm 1}) (P_i - P_{i \pm 1}) \right] \tag{8}$$

where $T_1 = T_\theta$, $T_N = T_p$, $P_1 = P_\theta$, and $P_N = P_p$. The direction of summation is determined by the sign of $P_p - P_\theta$.

The calculation of M is now performed from Eqn. 6 with the three terms on the right hand side of the equation (abbreviated as M_1 , M_2 and M_3), and their sum (M) being printed out separately.

At this point the wind direction and speed are linearly interpolated from the winds on the nearest standard pressure levels above and below the chosen isentropic surface. In the 645 WBAN RAOBS CONST PRESSURE format the standard pressures are given every 50 mb. This type of interpolation is justified in view of the closeness of standard pressures to any given isentropic level. The wind speed at the chosen θ surface is computed from the formula

$$FF_\theta = FF_b + (FF_t - FF_b)\left(\frac{P_b - P_\theta}{50}\right) . \qquad (9)$$

Computation of the wind direction is considerably more complicated because of the difficulty in interpolation when the two wind reports are on opposite sides of the $0^o = 360^o$ direction. This problem is circumvented by a series of tests in the program which act to eliminate the "discontinuity" at the $0^o \equiv 360^o$ point.

The static stability $(-\partial\theta / \partial p)$ is evaluated from the expression

$$-\frac{\partial\theta}{\partial p} = \frac{\theta_t - \theta_b}{P_b - P_t} . \qquad (10)$$

After all these computations have been completed for a specific level, a new θ level is defined, and the entire calculation is then performed at this new level. The whole procedure is then continuously recycled until the calculations at all θ surfaces of interest have been completed. The machine then reads in a new station and the entire process is repeated until completion.

IV. Explanation of the Plotting Program:

The program for plotting tephigrams is designed for the same type of input data utilized in the Montgomery stream function program. Its purpose is to mechanically plot radiosonde soundings on tephigrams in the same manner that has been traditionally done

by hand. The use of this program proved to be of great advantage because of the large increases in speed and accuracy of plotting.

This program was tested and run on an IBM 1620 computer coupled with a California Computer Products x-y continuous-roll plotter. It is designed to plot soundings to the same scale as the University of Chicago Pressure-Altitude Tephigram Chart No. 3. As before, the input data are arranged by the machine in order of descending pressure.

Because this plotter is only capable of linear representation, it is necessary to convert the tephigram coordinates to meet this specification. The tephigram is an area-conserving thermodynamic diagram which is linear in the centigrade temperature (T) and the entropy (ϕ). The entropy, however, is expressed on the diagram in terms of the potential temperature and does not appear explicitly as a coordinate. The differential relationship between entropy and potential temperature is given by

$$d\phi = c_p d \ln\theta \quad . \tag{12}$$

On this tephigram, the zero entropy point is defined to be at the intersection of the T = -90 C and θ = 230 K lines. Under this condition, upon integration the entropy is given by

$$\phi = c_p \ln(\theta / 230) \quad . \tag{13}$$

However, in the input data the only thermodynamic variables given are T and P. Thus from Poisson's equation

$$\phi = c_p \left[\ln \left(\frac{T + 273.16}{230} \right) - \chi \ln \left(\frac{P}{1000} \right) \right] \tag{14}$$

where χ = 0.2857, and T is given in centigrade. In terms of the computer plotter a scale factor must be introduced so that the

tephigram specifications are satisfied. This gives

$$y\,(\text{sounding}) = \text{scale factor}\left[\ln\left(\frac{T + 273.16}{230}\right) - 0.2857 \ln\left(\frac{P}{1000}\right)\right] . \tag{15}$$

From the linear equation above and comparisons with the actual tephigram, the scale factor gives equation (15) the following form:

$$y\,(\text{sounding}) = \frac{595}{50 \ln \frac{500}{230}}\left[\ln\left(\frac{T + 273.16}{230}\right) - 0.2857 \ln\left(\frac{P}{1000}\right)\right] . \tag{16}$$

This now defines completely the y coordinate.

The x coordinate (T) on the tephigram is linear and thus is easily determined by measurement to be

$$x = 0.0709\ T . \tag{17}$$

This now completely specifies the sounding. It is then plotted as a continuous line which is linear between data points. When a humidity reading is available at a given point a small x is plotted (see sample sounding, Fig. 1). To save time the pressure, height, temperature, and humidity values are printed out by the machine and attached to the sounding at a later time. It is equally simple to instruct the plotter to write out these values, but with the present machine this is very time consuming.

This program has produced tephigram soundings which are considerably more accurate than those obtained by hand-plotting. A disadvantage arises if certain computations necessitate the use of a tephigram underlay with the machine-plotted sounding. In principle this problem could be circumvented by using computer plotting paper which contains printed tephigram coordinates. It is, of course, possible to adapt this approach to any other thermodynamic diagram and to a computer plotter of almost any specification.

ACKNOWLEDGEMENT

This publication was prepared and funded jointly with the Department of Commerce, U. S. Weather Bureau, Contract No. Cwb - 10879. Mrs. S. Olson typed the manuscript.

REFERENCE

Danielsen, E. F., 1959: The laminar structure of the atmosphere and its relation to the concept of a tropopause, Archiv für Meteorologie, Geophysik und Bioklimatologie, A 11, 293-332.

SYMBOL CORRESPONDENCE TABLE

TEXT	PROGRAM	DESCRIPTION
---	ISTA	Station
---	IYR	Year
---	IMØ	Month
---	IDA	Day
---	IHR	Hour
dd	DD	Wind speed
ff	FF	Wind direction
Z	HGT	Height
T	T	Temperature
P	P	Pressure
θ	TH	Potential temperature
θ	TH1	Isentropic level of computation
P_p	PP	Standard level closest to TH1
M	F	Montgomery stream function = $M_1 + M_2 + M_3$
M_1	F1	$c_p T_\theta$
M_2	F2	gZp
M_3	F3	$RT \ln \left[\frac{P_p}{1000} \left(\frac{\theta}{T_\theta} \right)^{c_p/R} \right]$
$\overline{T}$	TBAR	Average temperature of the layer between P_p and P_θ
Z_p	HGT (M)	Height at P_p
$\frac{-\partial\theta}{\partial P}$	STAB	Static stability
---	HUM	Relative humidity

The following symbols, when added to a previously defined symbol, indicate the following:

T = value above TH1
B = value below TH1
TH = value at the surface TH1
i.e., TB = temperature at the nearest level below TH1
PPT = nearest standard level above TH1
DDTH = wind direction at TH1

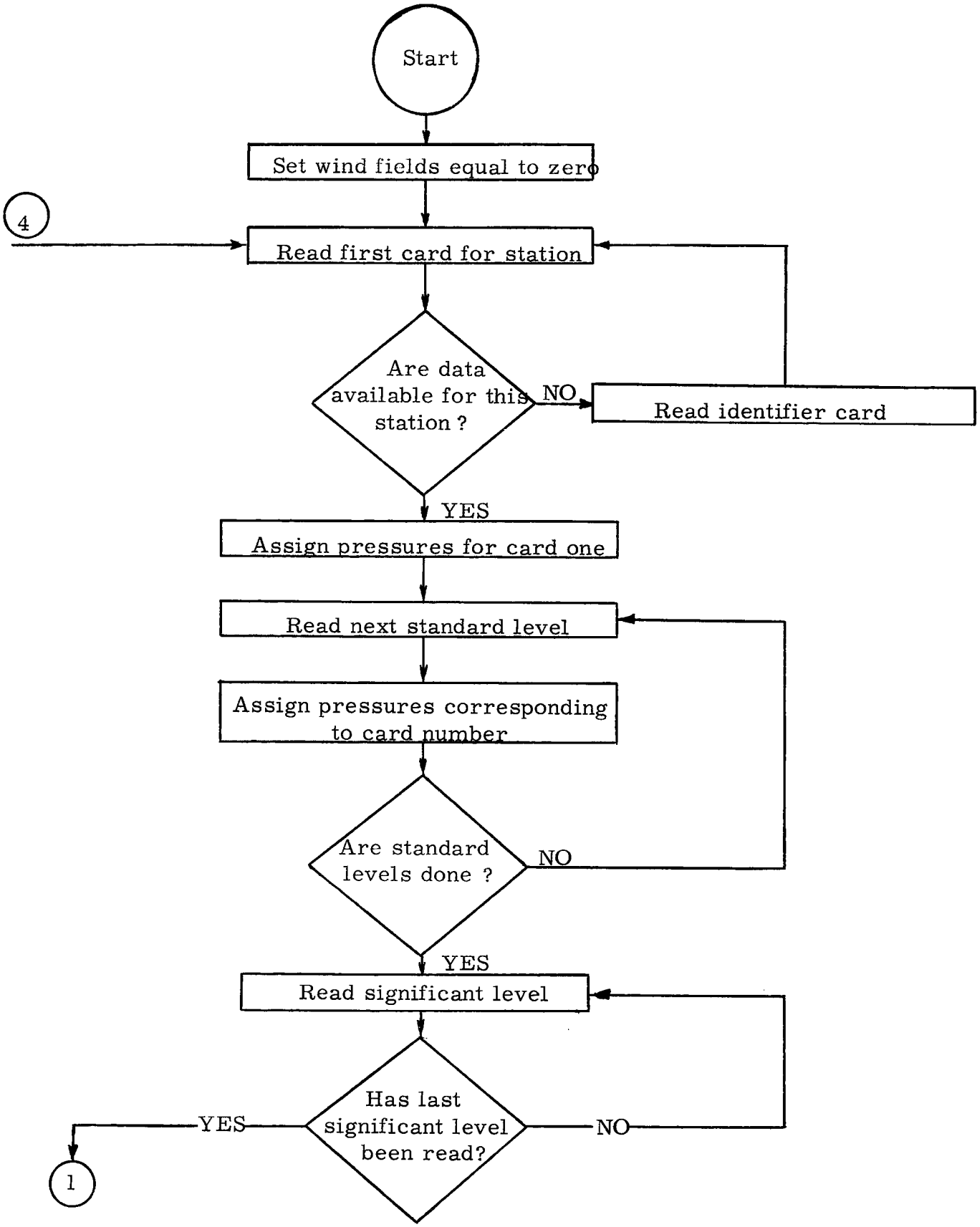
Start
Set wind fields equal to zero
4
Read first card for station
Are data available for this station ?
NO
Read identifier card
YES
Assign pressures for card one
Read next standard level
Assign pressures corresponding to card number
Are standard levels done ?
NO
YES
Read significant level
Has last significant level been read?
YES
NO
1

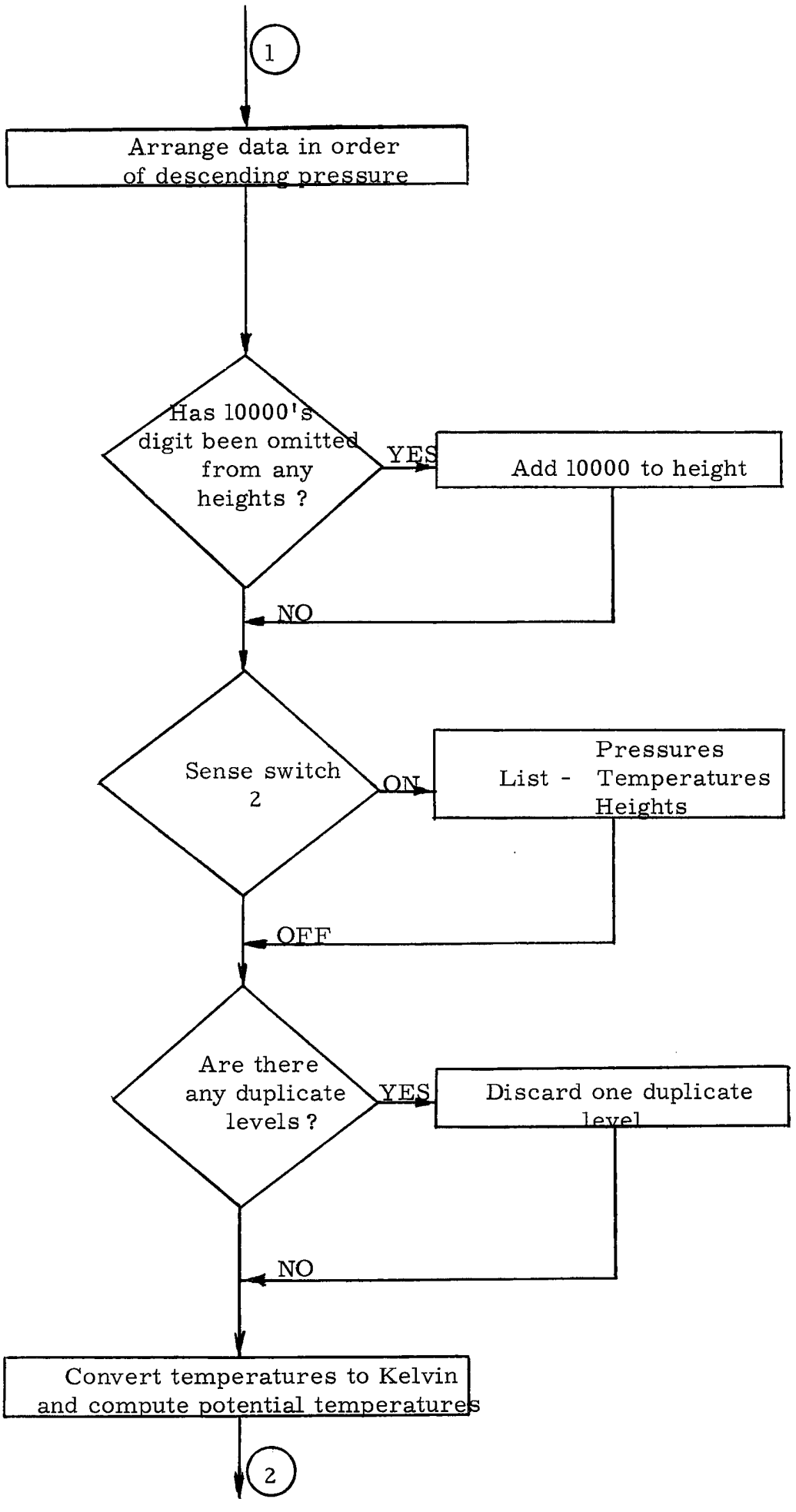
1
Arrange data in order of descending pressure
Has 10000's digit been omitted from any heights ?
YES
Add 10000 to height
NO
Sense switch 2
ON
List - Pressures Temperatures Heights
OFF
Are there any duplicate levels ?
YES
Discard one duplicate level
NO
Convert temperatures to Kelvin and compute potential temperatures
2

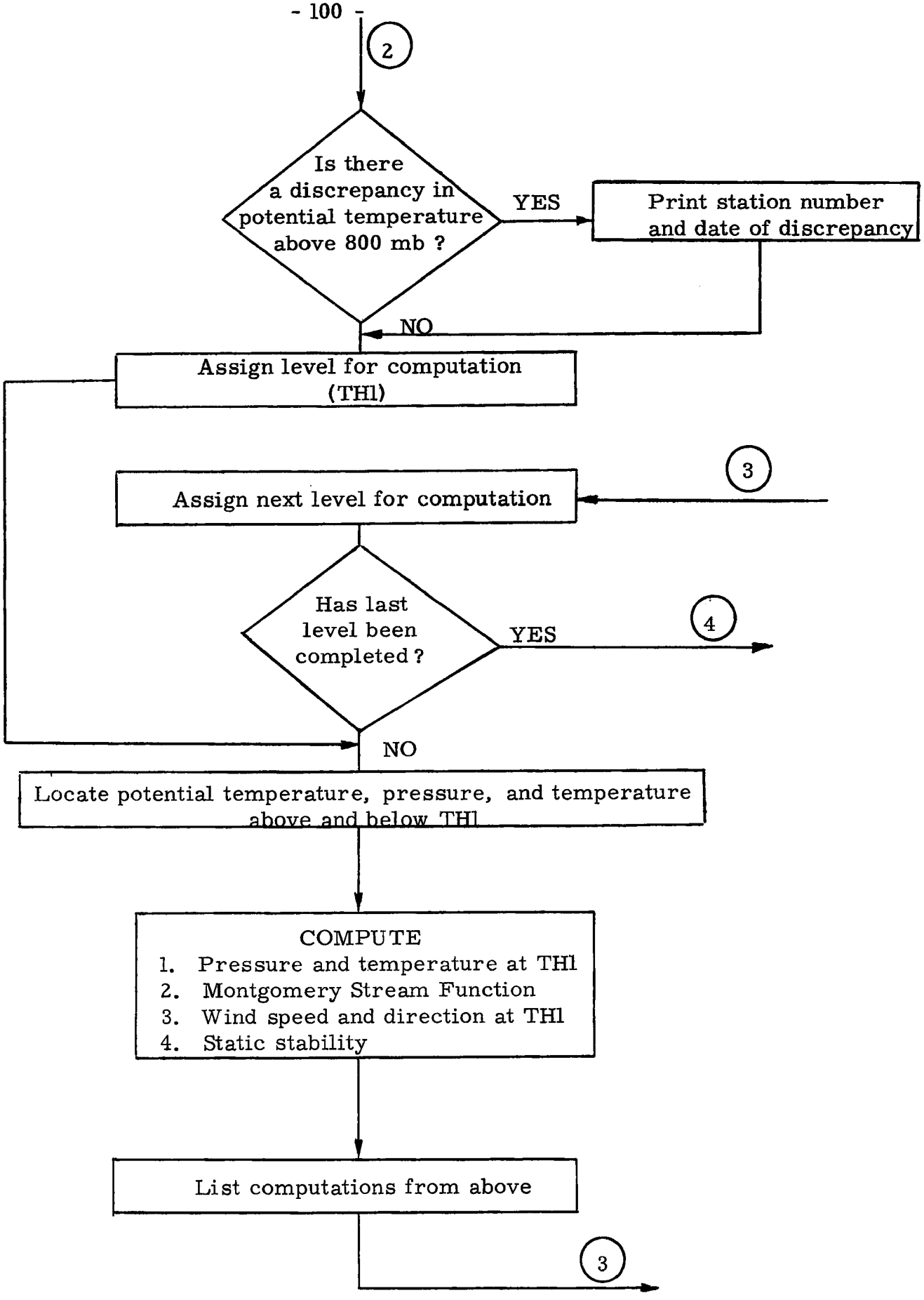

NOTE: Program will terminate when all data has been completed, rather than from a normal exit.

MONTGOMERY STREAM FUNCTION PROGRAM

```
C     COMPUTE MONTGOMERY STREAM FUNCTIONS WITH WINDS NUMBER ONE 1620
      DIMENSION T(50),P(50),HGT(50),       TH(50),FP(50),FT(50),FHGT(50)
     1,DD(50),FF(50),FDD(50),FFF(50)
C     ZERO OUT WIND FIELDS
      DO 711 I=1,50
      DD(I)=0
  711 FF(I)=0
C     READ FIRST STANDARD LEVEL
  904 READ 900,ISTA,IYR,IMO,IDA,IHR,JJ,(HGT(I),T(I),DD(I),FF(I),I=1,3),N
     1C
  900 FORMAT(I5,4I2,I1,15X,3(F4.0,F4.1,2X,F3.0,F2.0),I1)
      KK1=-1
      KSTA=ISTA
      J=0
      NN=0
C     CHECK FOR MISSING STATION DATA
      IF(NC)914,914,905
  914 READ 916,JUNK
  916 FORMAT(I2)
      GO TO 904
C     ASSIGN PRESSURES FOR CARD ONE
  905 P(1)=1000.
      DO 924 I=2,3
  924 P(I)=P(I-1)-50.
      IF (NC-5)901,901,902
  902 N=4
      GO TO 903
  901 N=NC-1
  903 J=J+4
      K=J+3
C     READ REMAINDER OF STANDARD LEVEL CARDS
  906 READ 907,JJ,(HGT(I),T(I),DD(I),FF(I),I=J,K)
  907 FORMAT(13X,I1,4(F4.0,F4.1,2X,I3,I2))
C     ASSIGN PRESSURES FOR CARD TWO THROUGH FIVE
      GO TO (908,909,910,911      ),JJ
  908 P(J)=850.
      GO TO 912
  909 P(J)=650.
      GO TO 912
  910 P(J)=450.
  912 M=J+1
      MM=K
      DO 913 I=M,MM
  913 P(I)=P(I-1)-50.
      GO TO 9112
  911 P(J)=250.
      J=J+1
      P(J)=200.
      J=J+1
      P(J)=175.
      J=J+1
      P(J)=150.
C     STANDARD LEVELS HAVE BEEN READ IN
      K=J
 9112 NN=NN+1
      IF(NN-N)903,925,925
  925 I=K+1
C     READ SIGNIFICANT LEVELS
  915 READ 917,ISTA,P(I),T(I),HGT(I)
  917 FORMAT(15,13X,F4.0,F4.1,3X,F5.0)
```

```
      IF (ISTA)918,918,919
  919 I=I+1
      GO TO 915
  918 N=I-1
      J=1
  923 I=1
C     ARRANGE DATA IN ORDER OF DECENDING PRESSURE
      K=1
      DUMP=P(1)
      DO 920 I=2,N
  922 IF(DUMP-P(I))921,920,920
  921 DUMP=P(I)
      K=I
  920 CONTINUE
      FFF(J)=FF(K)
      FDD(J)=DD(K)
      FP(J)=DUMP
      FT(J)=T(K)
      FHGT(J)=HGT(K)
      P(K)=0.0
      J=J+1
      IF(J-N)923,923,926
  926 CONTINUE
      DO 927 I=1,N
      DD(I)=FDD(I)
      FF(I)=FFF(I)
      T(I)=FT(I)
      HGT(I)=FHGT(I)
  927 P(I)=FP(I)
      I=2
C     CHECK FOR HEIGHTS WITH 10000 DIGIT DROPPED
  779 IF(HGT(I)-HGT(I-1))778,777,777
  777 I=I+1
      IF(I-N)779,781,781
  778 II=I
      DO 782 K=II,N
  782 HGT(K)=HGT(K)+10000.
  781 CONTINUE
C     IF SS2 PUNCH DATA FOR CHECK ON ORDER
      IF(SENSE SWITCH 2)831,832
  831 PUNCH 950,(P(I),I=1,N)
  950 FORMAT(16F5.0)
      PUNCH 951,(T(I),I=1,N)
  951 FORMAT(16F5.1)
      PUNCH 952,(HGT(I),I=1,N)
  952 FORMAT(13F6.0)
  832 I=1
C     CHECK FOR DUPLICATE DATA AND DISCARD ONE
  704 IF(P(I)-P(I+1))701,702,701
  701 I=I+1
      IF(I-N)704,703,703
  702 K=I+1
      N=N-1
      DO 705 I=K,N
      P(I)=P(I+1)
      DD(I)=DD(I+1)
      FF(I)=FF(I+1)
      T(I)=T(I+1)
  705 HGT(I)=HGT(I+1)
      I=K
```

```
      GO TO 704
  703 CONTINUE
C     CONVERT TEMPERATURES AND COMPUTE POTENTIAL TEMPERATURES
      DO 30 I=1,N
      T(I)=T(I)+273.2
   30 TH(I)=T(I)*(1000./P(I))**.2857
      I=1
C     CHECK FOR DISCREPANCIES IN POTENTIAL TEMPPERATURES ABOVE 800 MB
  802 IF(P(I)-800.)800,800,801
  801 I=I+1
      GO TO 802
  800 KI=I+1
      DO 803 I=KI,N
      IF(TH(I)-TH(I-1))805,803,803
  803 CONTINUE
      GO TO 804
  805 PUNCH 806,KSTA,IYR,IMO,IDA,IHR
  806 FORMAT(62HTHERE IS A DISCREPANCY IN THE THETA VALUES FOR STATION N
     1UMBER I5,4I2)
C     ASSIGN POTENTIAL TEMPERATURES FOR COMPUTATION
  804 TH1=290.
      GO TO 40
  210 IF(TH1-320.)211,212,212
  211 TH1=TH1+5.
      GO TO 40
  212 IF(TH1-350.)213,904,904
  213 TH1=TH1+10.
   40 I=1
      FFTH=0.0
      DDTH=0.0
C     SEARCH LIST FOR VALUES ABOVE AND BELOW LEVEL BEING COMPUTED
  220 IF(TH(I)-TH1)50,60,70
   50 GO TO 80
   60 TTH=T(I)
      GO TO 90
   70 THB=TH(I)
      TB=T(I)
      PPB=P(I)
      IF(I-1)210,210,71
   71 THT=TH(I-1)
      TT=T(I-1)
      PPT=P(I-1)
      GO TO 100
   80 I=I+1
      GO TO 220
C     COMPUTE PRESSURE AND TEMPERATURE AT LEVEL OF INTEREST
C     FIND NEAREST STANDARD LEVEL
  100 TTH=TB+(TT-TB)*((TH1-THB)/(THT-THB))
   90 PTH=1000.*(TTH/TH1)**3.5001
      IPP=PTH/100.
      AAA=IPP*100
      DIF=PTH-AAA
      IF(DIF-50.)400,400,410
  400 PP=AAA+50.
      GO TO 132
  410 PP=AAA+100.
  132 I=1
  130 IF(ABSF(PP-P(I))-.01)120,120,110
  110 I=I+1
      IF(I-N)130,131,131
```

```
  131 CONTINUE
  120 J=I
      AA=0.0
  160 IF(PTH-P(J+1))162,161,161
  161 CCC=P(J+1)
      P(J+1)=PTH
  162 AA=AA+ (T(J)+T(J+1))*(P(J)-P(J+1))
      IF(PTH-P(J+1))150,140,140
  150 J=J+1
      GO TO 160
  140 TBAR=(1.0/(2.0*(PP-PTH)))*AA
C     COMPUTE MONTGOMERY STREAM FUNCTION IN THREE SEGMENTS
      P(J+1)=CCC
      Z=10.**6
      F1=10.046*TTH*Z
      F2=9.806*HGT(I)*10000.
      M=I
      F3=2.8704*Z*TBAR*LOGF(PP/PTH)
      PP=PP-50.
      I1=M
      I=1
  812 IF(ABSF(PP-P(I))-.01)811,811,809
  809 I=I+1
      IF(I-N)812,812,500
  500 IF(SENSE SWITCH 1)501,823
C     ERROR ONE-DATA LIST EXCEEDED,CANNOT COMPUTE WIND
  501 PUNCH 502
  502 FORMAT(7HERROR 1)
      GO TO 823
  811 I2=I
      IF(FF(I1))505,505,808
  808 IF(FF(I2))505,505,807
  505 IF(SENSE SWITCH 1)503,823
C     ERROR TWO-WIND SPEED IS NEGATIVE
  503 PUNCH 504
  504 FORMAT(7HERROR 2)
      GO TO 823
C     INTERPOLATE WIND DIRECTION AND WIND SPEED
  807 FFTH=FF(I1)+((FF(I2)-FF(I1))*((P(I1)-PTH)/50.))
      DD1=DD(I2)-DD(I1)
      IF(DD1-180.)818,816,816
  816 DD1=DD1-360.
      GO TO 819
  818 IF(DD1+180.)817,819,819
  817 DD1=DD1+360.
  819 DDTH=DD(I1)+DD1*((P(I1)-PTH)/50.)
      IF(DDTH)821,823,822
  821 DDTH=DDTH+360.
      GO TO 823
  822 IF(DDTH-360.)823,824,824
  824 DDTH=DDTH-360.
  823 CONTINUE
C     COMPUTE STABILITY FACTOR
      PP=PP+50.
      STAB=(THT-THB)/(PPB-PPT)
      F=F1+F2+F3
      ISTA=KSTA
C     PUNCH RESULTS AND PROCEED TO NEXT LEVEL
      PUNCH 10,IYR,IMO,IDA,IHR,ISTA,N,F1,F2,F3,F
   10 FORMAT(4I2,1X,I5,1X,I2,2X,4E15.5)
```

```
    KK1=KK1+1
    IF(KK1)678,678,737
678 PUNCH 190,(TH(I),I=1,N)
190 FORMAT(10F8.2)
    PUNCH 677,(P(I),I=1,N)
677 FORMAT(13F6.0)
737 PUNCH 739,FFTH,CDTH
739 FORMAT(12HWIND SPEED =F5.1,4X,16HWIND DIRECTION =F7.1)
738 PUNCH 741,TBAR,THB,THT,TB,TT
741 FORMAT(5HTBAR=F6.1,3X,4HTHT=F6.1,3X,4HTHB=F6.1,3X,3HTT=F6.1,3X,3HT
   1B=F6.1)
    PUNCH 734,PTH,HGT(M),TH1,PP,STAB
734 FORMAT(4HPTH=F7.1,3X,4HHGT=F8.0,3X,4HTH1=F7.1,3X,3HPP=F7.1,6H STAB
   1=F6.3)
    GO TO 210
    END
```

FLOW CHART 2

MACHINE PLOTTING OF THERMODYNAMIC DIAGRAMS

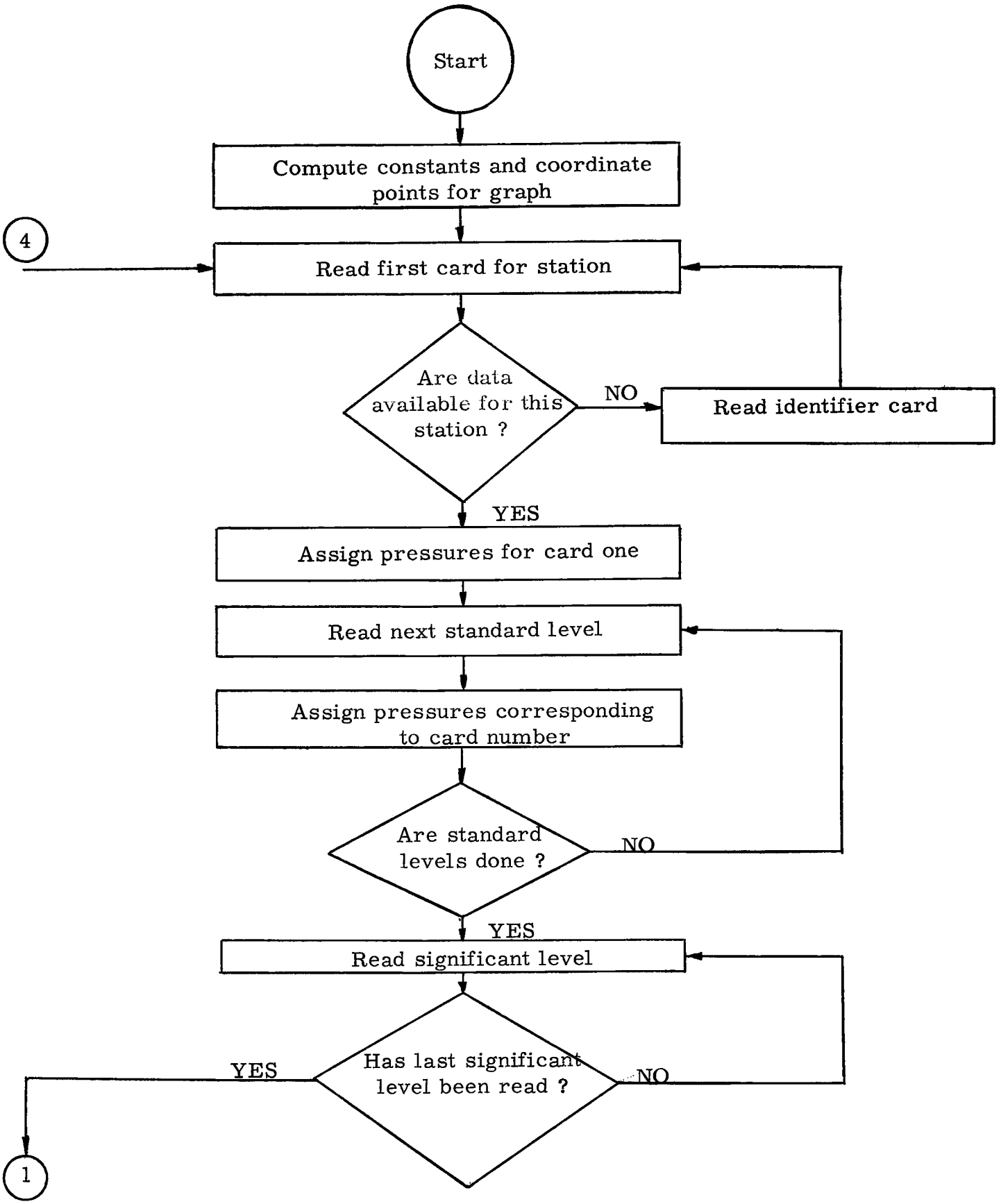

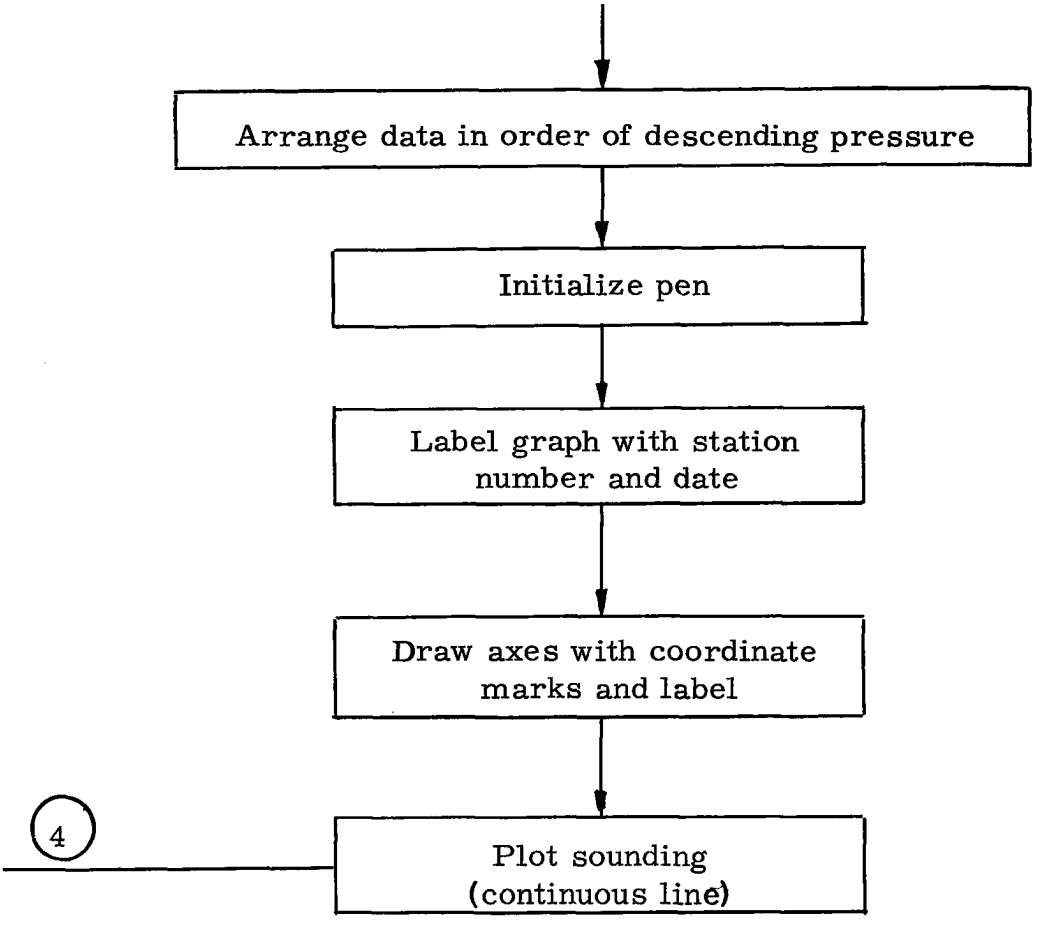
Arrange data in order of descending pressure
Initialize pen
Label graph with station number and date
Draw axes with coordinate marks and label
4
Plot sounding (continuous line)

TEPHIGRAM SOUNDING PROGRAM

```
C       PROGRAM  PLOT SOUNDINGS
        DIMENSION P(50),T(50),FP(50),FT(50)
        DIMENSION TM(6),TTM(17)
C       CALCULATE TIC MARK VALUES
        CC=595./(50.*LOGF(50./23.))
        TM1=20.0
        DO 17 I=1,6
        TM(I)=.0709*TM1
   17   TM1=TM1-20.
        TTM1=400.
        DO 18 I=1,17
        TTM(I)=LOGF(TTM1/230.)*CC
   18   TTM1=TTM1-10.0
        L=0
        FK=2./7.
C       READ FIRST STANDARD LEVEL
   40   READ 900,ISTA,IYR,IMO,IDA,IHR,JJ,(T(I),I=1,3),NC
        KK1=1
        KSTA=ISTA
  900   FORMAT(I5,4I2,I1,15X,3(4X,F4.1,7X),I1)
        J=0
        NN=0
C       CHECK FOR MISSING STATION DATA
        IF(NC)914,914,905
  914   READ 916,JUNK
  916   FORMAT(I2)
        GO TO 40
C       ASSIGN PRESSURES FOR CARD ONE
  905   P(1)=1000.
        DO 924 I=2,3
  924   P(I)=P(I-1)-50.
        IF (NC-5)901,901,902
  902   N=4
        GO TO 903
  901   N=NC-1
  903   J=J+4
        K=J+3
C       READ REMAINDER OF STANDARD LEVEL CARDS
  906   READ 907,JJ,(T(I),I=J,K)
  907   FORMAT(13X,I1,4(4X,F4.1,7X))
C       ASSIGN PRESSURES FOR CARD TWO THROUGH FIVE
        GO TO (908,909,910,911),JJ
  908   P(J)=850.
        GO TO 912
  909   P(J)=650.
        GO TO 912
  910   P(J)=450.
  912   M=J+1
        MM=K
        DO 913 I=M,MM
  913   P(I)=P(I-1)-50.
        GO TO 9112
  911   P(J)=250.
        J=J+1
        P(J)=200.
        J=J+1
        P(J)=175.
        J=J+1
        P(J)=150.
C       STANDARD LEVELS HAVE BEEN READ IN
```

```
      K=J
 9112 NN=NN+1
      IF(NN-N)903,925,925
  925 I=K+1
C     READ SIGNIFICANT LEVELS
  915 READ 917,ISTA,P(I),T(I)
  917 FORMAT(I5,13X,F4.0,F4.1)
      IF(ISTA)918,918,919
  919 I=I+1
      GO TO 915
  918 N=I-1
      J=1
  923 I=1
      K=1
C     ARRANGE DATA IN ORDER OF DECENDING PRESSURE
      DUMP=P(I)
      DO 920 I=2,N
  922 IF(DUMP-P(I))921,920,920
  921 DUMP=P(I)
      K=I
  920 CONTINUE
      FP(J)=DUMP
      FT(J)=T(K)
      P(K)=0.0
      J=J+1
      IF(J-N)923,923,926
  926 CONTINUE
      DO 927 I=1,N
      T(I)=FT(I)
  927 P(I)=FP(I)
      L=L+1
C     ZERO PEN
      Z=PLOTF(11111.)
      Y=0.0
      X=0.0
      Z=PLOTF(Y)
      Z=PLOTF(60000.)
       Y=-.3
      X=0.0
      Z=PLOTF(Y)
      Z=PLOTF(50000.)
C     LABEL GRAPH WITH DATE AND STATION
      CALL CHAR(5,.1,0,KSTA,IYR,IMO,IDA,IHR)
   11 FORMAT(I5,1X,4I2)
      Z=PLOTF(60000.)
C     DRAW X AXIS WITH TIC MARKS
      Y=0.0
      X=.0709*40.
      Z=PLOTF(Y)
      Z=PLOTF(50000.)
      DO 13 I=1,6
        Y=0.0
      X=TM(I)
      Z=PLOTF(Y)
      Y=.1
      X=TM(I)
      Z=PLOTF(Y)
      Y=0.0
      X=TM(I)
      Z=PLOTF(Y)
```

```
   13 CONTINUE
      Y=0.0
      X=.0709*(-90.)
      Z=PLOTF(Y)
      Z=PLOTF(60000.)
C     DRAW Y AXIS WITH TIC MARKS
      Y=LOGF(400./230.)*CC
      X=.0709*(-90.)
      Z=PLOTF(Y)
      Z=PLOTF(50000.)
      DO 14 I=1,17
      Y=TTM(I)
      X=.0709*(-90.)
      Z=PLOTF(Y)
      Y=TTM(I)
      X=.0709*(-90.)-.1
      Z=PLOTF(Y)
      Y=TTM(I)
      X=.0709*(-90.)
      Z=PLOTF(Y)
   14 CONTINUE
      Y=LOGF(1.0)*CC
      X=.0709*(-90.)
      Z=PLOTF(Y)
      Z=PLOTF(60000.)
C     PLOT SOUNDING
      Y=(LOGF((T(1)+273.16)/230.)-FK*LOGF(P(1)/1000.))*CC
      X=.0709*T(1)
      Z=PLOTF(Y)
      Z=PLOTF(50000.)
      DO 30 I=2,N
      Y=(LOGF((T(I)+273.16)/230.)-FK*LOGF(P(I)/1000.))*CC
      X=.0709*T(I)
   30 Z=PLOTF(Y)
      Z=PLOTF(60000.)
C     CONTINUE TO NEXT SET OF DATA
      GO TO (50,50,70),L
   50 Y=9.5
      X=0.0
      Z=PLOTF(Y)
      GO TO 40
   70 Y=-19.0
      X=10.0
      Z=PLOTF(Y)
      L=0
      GO TO 40
      END
```

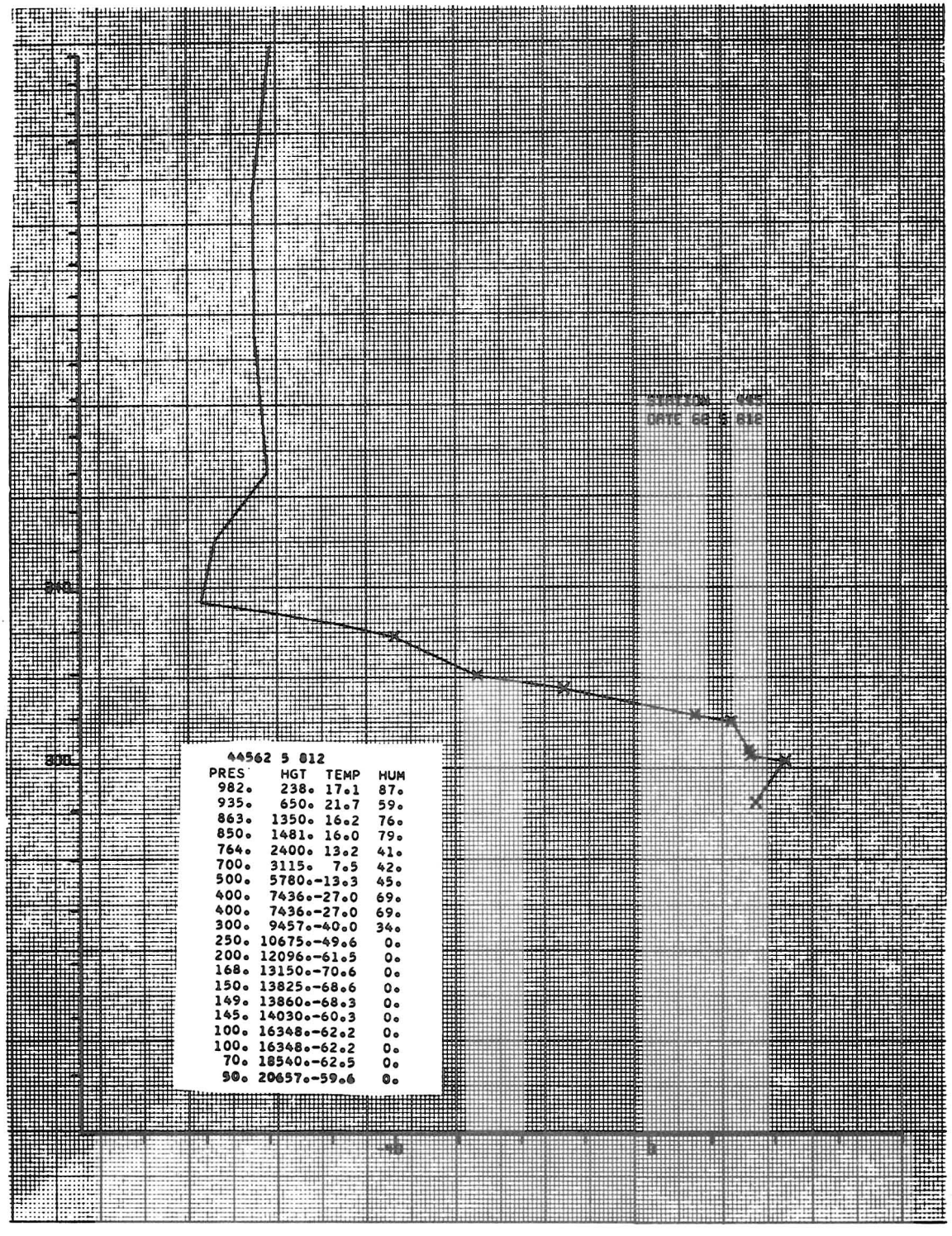

Fig. 1: Example of sounding plotted to the scale of a tephigram (Columbia, Missouri, 8 May 1962, 12 GMT). Sounding points with humidity reports are indicated by "X." The ordinates of diagram are temperature (^{o}C) and potential temperature (^{o}K).